Kinetic and Thermodynamic Characterization of

Matrix Metalloproteinase-3, Stromelysin,

and

Its Effect in an Ocular

Anterior Segment Organ Culture System

by

Christine Mie Colvis

A DISSERTATION

Presented to the Department of

Biochemistry and Molecular Biology

and the

Oregon Health Sciences University

School of Medicine

in partial fulfillment of

the requirements for the degree of

Doctor of Philosophy

March 1998

School of Medicine
Oregon Health Sciences University

_____

CERTIFICATE OF APPROVAL

_____

This is certify that the Ph.D. thesis of

Christine M. Colvis

has been approved

█████████████████████████████

_____

█████████████████████████

_____
Stephen R. Planck, Ph.D.

████████████████████████
_____
Thomas R. Shearer, Ph.D.

██████████████████████
_____
Nicholas P. Morris, Ph.D.

_____
Associate Dean for Graduate Studies
Richard Mauer, Ph.D.

This dissertation is lovingly dedicated to my parents,
Louis Jack and Chie Colvis

and to my grandparents,
Louis Jack and Jacqueline B. Colvis
And
Masashige and Yae Oteki

TABLE OF CONTENTS

LIST OF FIGURES

LIST OF TABLES

LIST OF EQUATIONS

ABBREVIATIONS

AMPA..............Aminophenylmercuric acetate

D-MEM............Dulbecco's modified Eagle medium

DNP.................Dinitrophenyl

FITC................Fluorescein isothiocyanate

HEPES.............N-(2-hydroethyl)piperazine-N'-(2-ethanesulfonic acid)

Mca.................Methoxycoumarin

MES.................2-(N-morpholino)ethanesulfonic acid

MMP................Matrix metalloproteinase

NFF3................Nagase Fields & Fields-3 (Mca-R-P-K-P-V-E-[Nva]-W-R-K[DNP]-NH$_2$)

Nva..................Norvaline

PAGE...............Polyacrylamide gel electrophoresis

PMSF...............Phenylmethylsulfonyl fluoride

SDS..................Sodium dodecyl sulfate

TIMP...............Tissue inhibitor of matrix metalloproteinases

Tris...................Tris(hydroxymethyl)aminomethane

Standard single letter and three letter abbreviations were used for all L-amino acids

ACKNOWLEDGMENTS

I am also very grateful to my advisory committee and my defense committee members, Drs. Dick Brennan, Nick Morris, Mike Riscoe, Steve Planck and Tom Shearer for all of their support, advice and encouragement.

My acknowledgments would not be complete without thanking the National Eye Institute for providing not only financial support, but also outstanding opportunities to better myself as a scientist. A special thank you to Dr. James Rosenbaum who has made the OHSU contingent of the NEI training grant the most successful in the country.

My warm and loving thanks to all of those who made my life outside of graduate school (and sometimes in graduate school) so very wonderful. I am particularly thankful to my husband, Michael Kennedy, my family and my very dear friend of 7 years, Canis Sapien, for all of their love and support. It is because of them that I have never felt that any task was insurmountable.

ABSTRACT

Matrix metalloproteinase-3, stromelysin, is a member of the metalloproteinase family of endopeptidases. As with all of the family members, stromelysin binds both calcium and zinc, presumably using a zinc atom to ligate the water molecule that will be used in the hydrolysis of a peptide bond. Also like the other family members, stromelysin is secreted into the extracellular matrix in a latent, pro-enzyme form. The metalloproteinases are activated upon cleavage of a propeptide at the amino terminus of the protein. Once activated, stromelysin can activate other family members (interstitial collagenase and gelatinase B), degrade extracellular matrix molecules, or be inhibited by tissue inhibitors of metalloproteinases.

Presented in the first results section of this dissertation is a protocol established for the separation of matrix metalloproteinase-2 from stromelysin isolated from cell culture medium. Matrix metalloproteinase-2 has relatively high proteolytic activity toward casein. Therefore, the removal of matrix metalloproteinase-2 from stromelysin preparations was important before conducting kinetic assays using FITC-conjugated casein. In the same chapter, the conditions for activating stromelysin with heat in a standard Tris buffer are also presented. This method allowed for activation without the addition of any other proteinases or chemical activating agents to the preparation. Unlike other methods of matrix metalloproteinase activation, heat activation would not activate matrix metalloproteinase-2.

The MMPs have been implicated in many physiologic states. Among these is their putative role in the trabecular meshwork of the eye. It is our hypothesis that in cases of primary open angle glaucoma which is accompanied by an increase in intraocular pressure,

the homeostatic balance between the tissue inhibitors of metalloproteinases and MMPs in the trabecular meshwork has been disrupted. A portion of my dissertation is dedicated to evaluating this putative role. These studies were conducted by testing various agents for their ability to inhibit matrix metalloproteinase activity and examining their effect on an anterior segment organ culture system in which fluid outflow through the trabecular meshwork is measured. Conversely, the addition of matrix metalloproteinases or interleukin-1 (a known inducer of matrix metalloproteinases) was also evaluated. The data show convincing evidence that treatment that enhances MMPs in the trabecular meshwork results in an increase in fluid outflow through the trabecular meshwork while matrix metalloproteinase inhibitors cause a decrease in outflow.

The matrix metalloproteinases (MMPs) have also been implicated in disease states such as cancer metastasis, osteoarthritis, rheumatoid arthritis, periodontal disease and angiogenesis. In these diseases, MMP activity is abnormally high. An effective method to control pathology may be to decrease the level of MMP activity. Inhibition of the enzymes with synthetic inhibitors is a viable option. The most effective enzyme inhibitors are generally those which resemble the transition state of the substrate/enzyme interaction. Determining what the transition state structure is, can be accomplished through a detailed understanding of the kinetic mechanism by which the catalyzed reaction takes place. The last chapter of this dissertation focuses on using thermodynamics to gain information about the kinetics of MMP-3, stromelysin. By examining Arrhenius and Eyring plots of k_{cat} at three proton concentrations, we have been able to gain significant information regarding the mechanistic pathway of stromelysin catalysis. The Arrhenius and Eyring plots show non-linear plots at

pH 7.5 with a significant decrease in non-linearity at pH 6.0 and 8.0. While the non-linear behavior at pH 7.5 might be explained by $\Delta H^{\ddagger}$ temperature dependence, collectively, the thermodynamic data from all three proton concentrations would be difficult to reconcile with that explanation.

The data are, however, in agreement with a complex, parallel mechanism in which two protonation states of stromelysin correspond to active enzyme forms, and two protonation states correspond to inactive enzyme forms. These four states of the enzyme are separated by three acid dissociation constants. We conclude, therefore, that the non-linearity of Arrhenius and Eyring plots observed at pH 7.5 is due, at least in part, to the complex mechanism. These data also suggest that two, not one, transition states exist for stomelysin which would have to be a consideration in designing inhibitor molecules.

INTRODUCTION

MATRIX METALLOPROTEINASES: AN INTRODUCTION

The matrix metalloproteinases (MMPs), are a family of proteinases that degrade extracellular matrix molecules such as collagens, fibronectins, laminin, proteoglycan core proteins, and others. The current family members, their EC numbers and their common names are presented in Table 1.

Stromelysin, MMP-3, as well as many of the other family members have been the subject of investigation on several fronts. Their activation, kinetic mechanisms, protein structure, interaction with each other as well as their endogenous inhibitors, and the regulation of their expression have all been focal points of many studies in recent years.

Much of the reason for such great interest in these proteinases is that they have been implicated in several disease states among which are: cancer growth and metastasis (Chen 1992, Lin et al. 1997, Lochter et al. 1997, Polette et al. 1993, Stetler-Stevenson et al. 1993), arthritis (Hiraoka et al. 1992, Ishiguro et al. 1996, Lohmander et al. 1993, Mort et al. 1993, Van Meurs et al. 1997), angiogenesis (Schnaper et al. 1993) and periodontal disease (Ingman et al. 1994, Reynolds et al. 1994). They also have a role in normal physiology during growth and development (Boudreau et al. 1995, Southgate et al. 1992), wound healing (Agren et al. 1992, Schultz et al. 1992, Stricklin et al. 1993, Wysocki et al. 1993), and matrix turnover in trabecular meshwork (Alexander et al. 1991, Ando et al. 1993, Snyder et al. 1993).

Our hypothesis is that in primary open angle glaucoma the homeostatic balance between the tissue inhibitors of metalloproteinases (TIMPs) and MMPs in the trabecular meshwork has been disrupted. A portion of this dissertation is dedicated to evaluating this

2

putative role, while the remainder focuses on the kinetics and thermodynamics of MMP-3, stromelysin.

DOMAIN STRUCTURE OF MMPs

Description of the Domains of the MMPs

Members of the MMP family have very similar structural organization. Figure 1 shows the primary structure domains of a "prototype" MMP as well as several individual MMPs. In the prototype, the amino-terminus begins with a signal peptide which is present in all of the MMPs. The next domain is the propeptide, which is responsible for maintaining latency. The third commonly shared domain is the catalytic domain, also called the amino-terminal domain. This domain contains the active site zinc and probably a second zinc as well. The second zinc atom is a likely possibility in all of the MMPs, although it has been shown by structural analysis in only stromelysin, MMP-1, and MMP-8 (Becker et al. 1995, Bode et al. 1994, Borkakoti et al. 1994, Gooley et al. 1994, Lovejoy et al. 1994, Stams et al. 1994, Van Doren et al. 1995a, Van Doren et al. 1993). In these MMPs, the second zinc atom binds residues in the catalytic domain amino-terminal to the zinc site indicated in Figure 1. The next domain is called the hinge region, and it is the domain which separates the catalytic domain and the pexin-like domain. The hinge region varies in length and sequence among the MMPs, but is proline-rich in all of the MMPs. The pexin-like domains, also called the carboxy-terminal domain, contain a cysteine residue at the beginning of the domain and another at the end of the protein. These two residues come together to form a disulfide bond in the native proteins. Deviating from the prototype, both MMP-2 and MMP-9 have three

3

fibronectin type II domains amino terminal to the active site zinc binding domain while MMP-7 has neither the fibronectin domains nor the carboxyl- terminal domain.
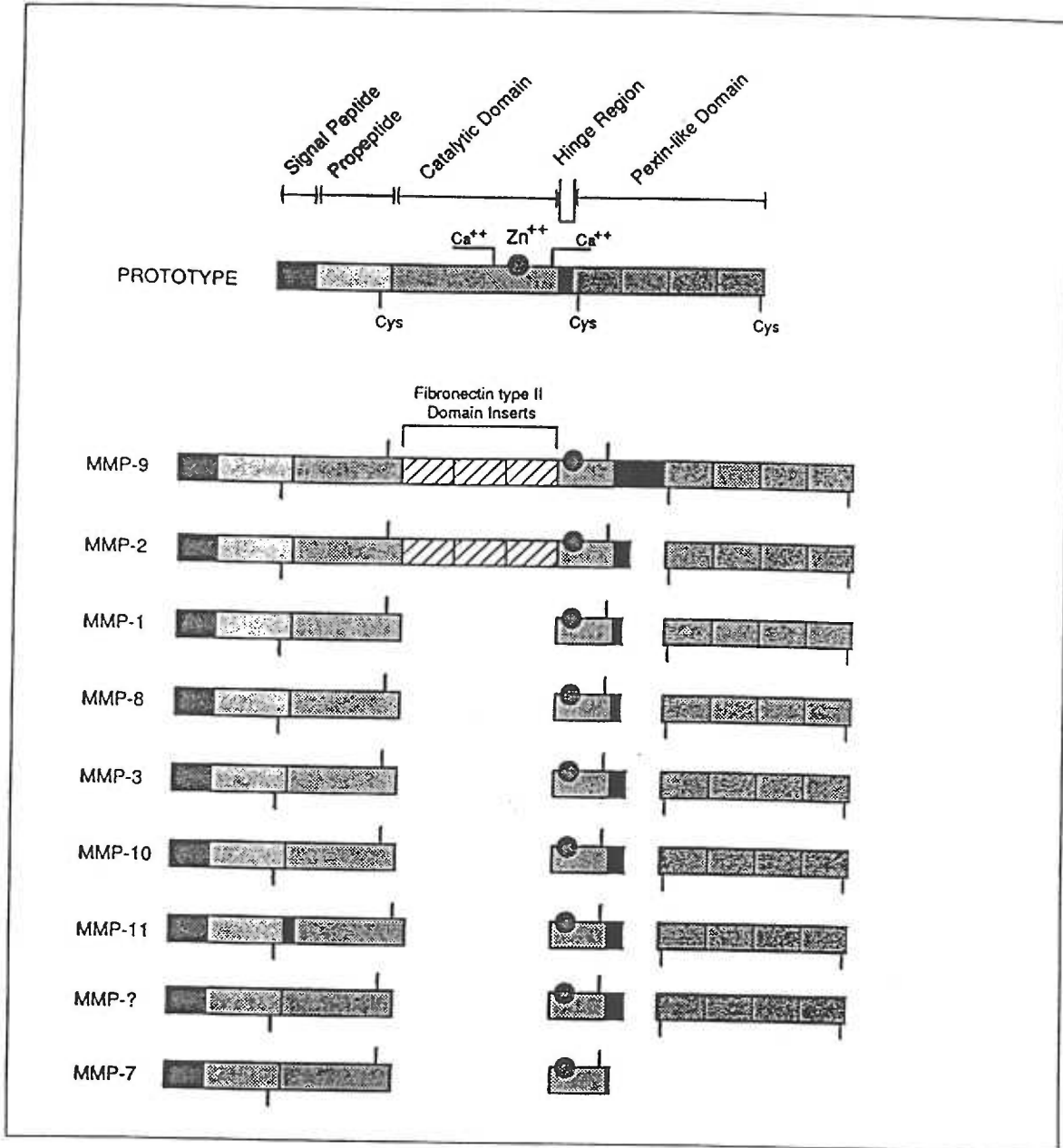
Figure 1
Domain structures of MMPs. See *Table 1* for MMP names. (From: Birkedal-Hansen et. al., "Matrix Metalloproteinases: A Review," *Critical Reviews in Oral Biology and Medicine* Vol.4, No. 2, page 202, 1993).

TABLE 1: MMP FAMILY MEMBERS

MMP No.	EC No.	Common name
MMP-1	EC 3.4.24.7	Interstitial collagenase, Tissue collagenase, Fibroblast collagenase
MMP-2	EC 3.4.24.24	72 kD Gelatinase, type IV collagenase, Gelatinase A, TBE-1
MMP-3	EC 3.4.24.17	Stromelysin-1, SL-1, STR1 protein, Transin-1
MMP-7	EC 3.4.24.23	Matrilysin, Matrin, PUMP-1 protease, Uterine metalloproteinase
MMP-8	EC 3.4.24.34	PMNL Collagenase, Neutrophil collagenase
MMP-9	EC 3.4.24.35	92 kD Gelatinase, type IV collagenase, Gelatinase B
MMP-10	EC 3.4.24.22	Stromelysin-2, SL-2, Transin-2
MMP-11	EC 3.4.24.	Stromelysin-3, ST3, SL-3
MMP-12	EC 3.4.24.65	Macrophage Metalloelastase, HME
MMP-13		Collagenase-3
MMP-19		
MMP-14		Membrane-type-1 MMP
MT-2 MMP		Membrane-type-2 MMP
MT-3 MMP		Membrane-type-3 MMP
MT-4 MMP		Membrane-type-4 MMP

TIMPs

The TIMPs are a family of specific, slow-tight binding inhibitors of the MMPs. K_i values in the nanomolar to sub-nanomolar range have been reported for TIMP/MMP interactions (Baragi et al. 1994, Bodden et al. 1994, Cawston et al. 1983). To date, there have been four human TIMPs identified (TIMP-1, TIMP-2, TIMP-3 and TIMP-4) (Apte et al. 1995 , Carmichael et al. 1986, Greene et al. 1996, Stetler-Stevenson et al. 1990). All four of the TIMPs have 12 cysteine residues, which in TIMPs 1 and 2 form 6 disulfide bonds (Miyazaki et al. 1993, Murphy et al. 1991b, Williamson et al. 1993), and presumably do the same in TIMPs 3 and 4. In the primary structure, the 6 disulfide bonds result in the formation of 6 loops, Figure 2. The residues which make up the first three loops are regarded as the amino terminal domain of the protein, while loops 4, 5 and 6 make up the carboxy-terminal domain.
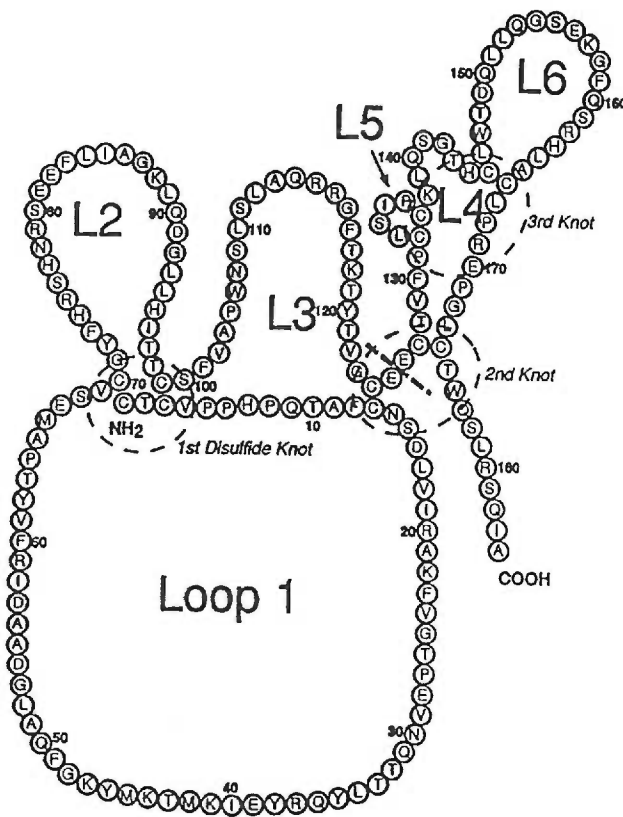
Inhibitory activity resides in the amino terminal domain of the TIMPs. That is to say that the amino-terminal domain of the TIMP interacts with the amino-terminal domain of the MMPs (Bodden et al. 1994, Murphy et al. 1991b, Nguyen et al. 1994, Willenbrock et al. 1993). Interestingly, while the carboxyl-terminal domain of the MMPs seems to enhance their interaction with the TIMPs (Baragi et al. 1994, Murphy et al. 1992a, Murphy et al. 1992d),

the presence of the carboxyl-domain of the TIMP-1 can have the opposite effect. It has been shown that the presence of the carboxyl-terminal domain of TIMP-1 adversely affects its binding to stromelysin and gelatinase B, increasing the K_i in both cases (Murphy et al. 1991b). TIMP-1 can bind latent gelatinase B and TIMP-2 can bind latent gelatinase A, but neither TIMP can bind latent stromelysin (Baragi et al. 1994, Kleiner et al. 1993, Willenbrock et al. 1993). It is only after the propeptide has been removed that TIMP can bind to stromelysin.

PRIMARY STRUCTURE OF STROMELYSIN

There are three basic species of stromelysin. These species are based on the primary structure of the enzyme at different stages of activation. The nomenclature for these species varies in the published literature. For clarification, the nomenclature that will be used in this dissertation and corresponding primary structures are presented in Figure 3.

Propeptide	Amino terminal domain	Carboxyl terminal domain

‡------------------------------prostromelysin--‡

‡------------------------------45 kDa species----------------------------‡

‡----------28 kDa species----------------‡
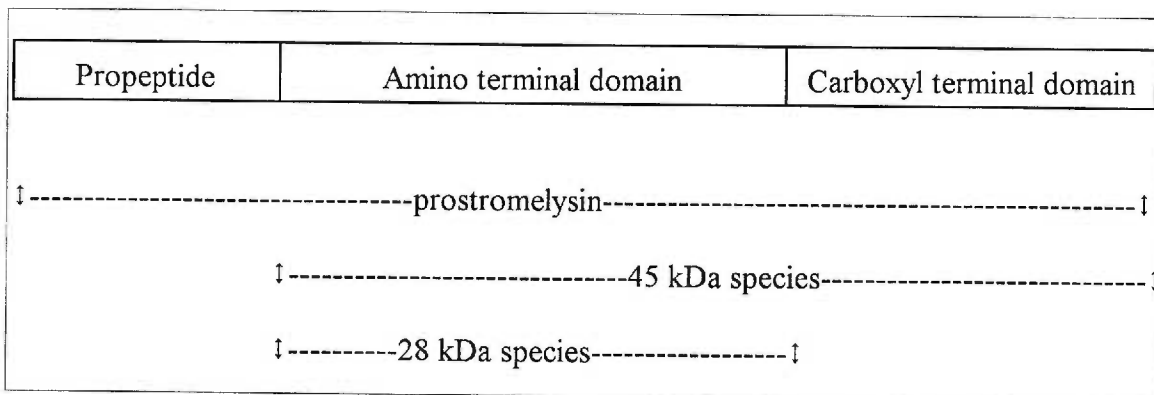
Figure 3
Diagrammatic representation of the three different species of stromelysin, and how they correspond to the propeptide, amino-terminal domain and carboxyl-terminal domain.

PROPEPTIDE

The propeptide maintains the latency of the secreted MMPs. Within the propeptide there is an autoinhibitory domain. In stromelysin the propeptide is 82 residues long, and the autoinhibitory domain spans residues 73-79. The autoinhibitory domain contains the free cysteine, indicated in Figure 1, which is ligated to the active site zinc atom in the latent zymogen. This is commonly referred to as the "cysteine switch". In order to generate an active form of the enzyme, the interaction of the propeptide with the active site zinc must be at least disrupted if not proteolytically removed.

Although the Cys/Zinc interaction is important, it is not this interaction alone which is responsible for maintaining latency (Chen et al. 1993). There is also a salt bridge between Arg^{74} and Asp^{79} which is believed to play an importnat role in maintaining latency (Galazka et al. 1996, Park et al. 1991).

Figure 4 is a sequence alignment of the region of the enzymes that surround the Cys^{75} equivalents of some of the MMPs. The peptide of high identity, PRCGVPD, is unchanged in all of the MMPs shown except for MMP2, 72 kD gelatinase, which has a single change from valine to asparagine. This peptide has been investigated for its inhibitory activity toward stromelysin, as well as the inhibitory activity of amino acid-substituted derivatives. These studies had shown a peptide inhibitor spanning stromelysin residues Ser^{64} to Gly^{88} exhibited an IC_{50} of $2.7\mu M$, peptide RCGVPD yielded an IC_{50} of $4.5\mu M$, and RCGVP inhibited with an IC_{50} of $10.5\mu M$. Also, substituting Tyr-(2,6-dichlorobenzyl) for Val in the parent hexamer yielded a more effective inhibitor, decreaseing the IC_{50} to $2\mu M$ (Fotouhi et al. 1994, Hanglow et al. 1993, Hanglow et al. 1994).

The crystal structure of prostromelysin revealed that the amino to carboxyl orientation of the propeptide in the active site groove is in the reverse orientation of all synthetic peptide inhibitors that have been crystallized with either stromelysin or collagenase. Presumably the peptide inhibitor orientation is the same as that of substrates. In either orientation, β-structure-like hydrogen bonds are formed. This data also confirmed that Cys^{75} is in direct contact with the active site zinc atom (Becker et al. 1995). Indicating a *cysteine switch* inhibition mechanism.

```
K V M K Q P R C G V P D V A Q - - - - - - - - - -*F *V *L T E G N P R W  FIB-CL
D M M K K P R C G V P D S G G - - - - - - - - - - F  M *L T P G N P K W  PMN-CL
E V M R K P R C G V P D V G H - - - - - - - - - -*F  R T F P G I P K W  SL-1
E V M R K P R C G V P D V G H - - - - - - - - - - F  S S F P G M P K W  SL-2
S S L R P P R C G V P D P S D G L S A R N R Q K R F  V L S G G - - R W  SL-3
E I M Q K P R C G V P D V A E - - - - - - - - - - Y  S L F P N S P K W  PUMP-1
E T M R K P R C G N P D V A N - - - - - - - - - -*Y  N F F P R K P K W  M, 72K GL
K *A*M R T P R C G V P D L G R - - - - - - - - - - F  Q T F E G D L K W  M, 92K GL
```

Figure 4
The sequence alignment of the autoinhibitory domains of MMP-1, MMP-8, MMP-3, MMP-10, MMP-11, MMP-7, MMP-2 and MMP-9 (from top to bottom). From: H. Birkedal-Hansen, et. al., "Matrix Metalloproteinases: A Review," *Critical Reviews in Oral Biology and Medicine* Vol. 4, No.2, page 212 (1993). *Autolytic cleavage sites.

ACTIVATION OF MMPs

The actual *in vivo* activation cascade for MMPs has not been completely verified. However, Figure 5 is a schematic representation of a proposed cascade based on *in vitro* activity, and analysis of activation in cell culture. This cascade shows plasmin as an activator of stromelysin. Either plasmin, or activated stromelysin can activate both MMP-1 and MMP-9 (Knauper et al. 1993, Murphy et al. 1987, Shapiro et al. 1995, Suzuki et al. 1990). Not shown in Figure 5 is that stromelysin can also activate MMP-7 (Imai et al. 1995). Activation

of MMP-2 is somewhat unique. It is not capable of activation by either plasmin or stromelysin (Murphy et al. 1992b). There has been evidence that it is instead activated at the cell surface by proteolytic cleavage by a membrane-type MMP (Cao et al. 1996, Sato and Seiki 1996, Sato et al. 1994).

The MMPs are often activated *in vitro* with the organomercurial, amino-phenylmercuric acetate. The amino-phenylmercuric acetate disrupts the cysteine switch, which allows a water molecule to ligate to the zinc (Figure 6). Once this occurs, activation by both intra- and intermolecular cleavage occurs (Engler et al. 1992, Grant et al. 1992, Nagase et al. 1992, Tschesche et al. 1992).
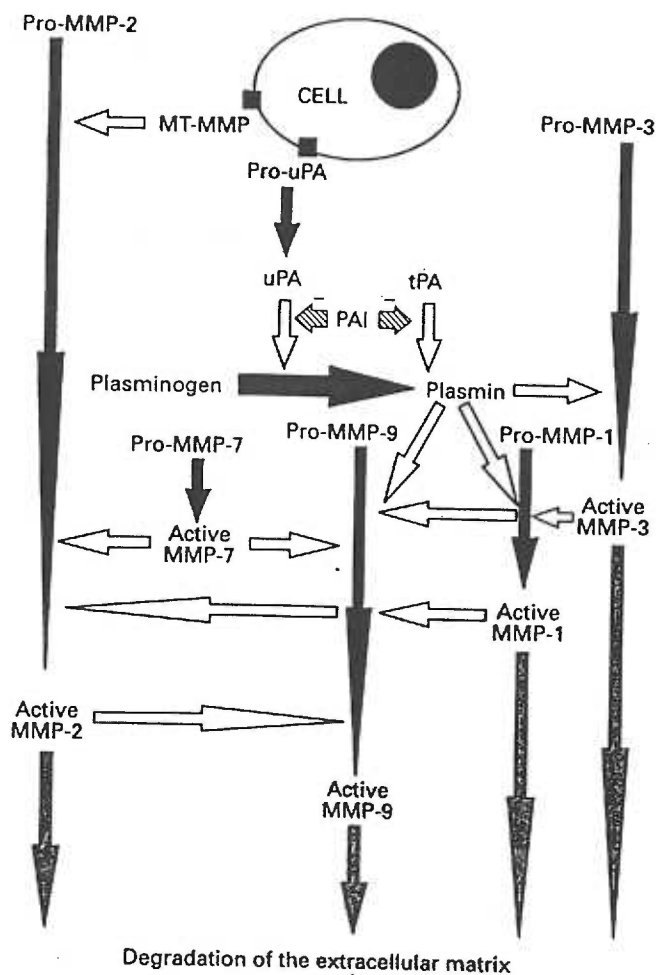
Figure 5
Proposed MMP activation cascade based on *in vitro* activation studies. From: S.L. Parsons, et. al., "Matrix Metalloproteinases," *British Journal of Surgery* Vol. 84, page 161 (1997).
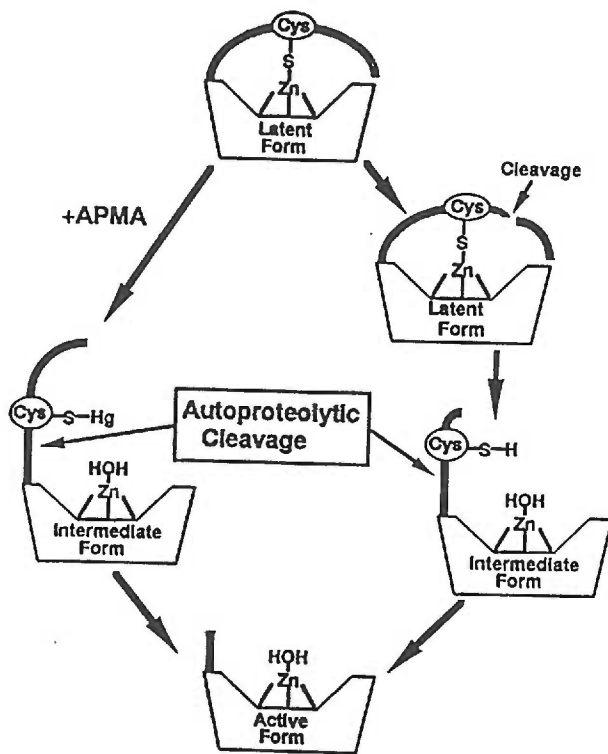
Figure 6
Diagram of the molecular activation of an MMP molecule. From: H. Sato and M. Seiki, "Membrane-type Matrix Metallo-proteinases (MT-MMPs) in Tumor Metastasis," *Journal of Biochemistry* Vol 119, page 210 (1996).

ACTIVATION OF STROMELYSIN

Although plasmin is capable of activating stromelysin, the endogenous mode of stromelysin activation is not known (Murphy et al. 1992b). There are, however, several *in vitro* techniques that yield active stromelysin.

Since the activation of stromelysin involves proteolytic cleavage, it results in different molecular weight bands of the active proteinase by zymogram analysis. The zymogram is an SDS-PAGE into which substrate has been co-polymerized. After the electrophoresis is complete, incubation of the gel allows proteinase bands to digest substrate and themselves resulting in clear bands against a blue background upon Coomassie Blue staining. Activation of stromelysin occurs as a result of chemical perturbation of the cysteine switch by SDS and results in a band at approximately 57 kD (pro-stromelysin) on zymograms. In this case, the

12

propeptide has not been removed by proteolytic cleavage, but its ability to inhibit activity has been compromised. Proteolytic removal of the pro-peptide results in a band of approximately 45 kD on zymograms. Additional proteolytic removal of the carboxyl terminal hemopexin repeats results in a zymogen of approximately 28 kD. Both the pro-form of the enzyme and the 45 kD form generally appear as a doublet representing a glycosylated and a non-glycosylated form of the enzyme. The 28 kD species appears as multiple bands in PAGE analysis, due to proteolysis of different peptide bonds near the hinge region.

Proteinases capable of activating stromelysin *in vitro* include trypsin, chymotrypsin, plasmin, cathepsins B and L, plasma kallikrein and neutrophil elastase (Murphy et al. 1992c, Nagase et al. 1990). Chymotrypsin, plasma kallikrein and neutrophil elastase cleave different peptide bonds within the propeptide of stromelysin (Nagase et al. 1990). The final cleavage occurs by stromelysin autolysis at the His^{82}-Phe^{83} peptide bond in a bimolecular reaction (Nagase et al. 1990). Trypsin, however, cleaves the Arg^{84}-Thr^{85} peptide bond which is carboxyl-terminal to the autolytic amino terminus (Phe^{83}), leaving the enzyme two residues short (Benbow et al. 1996).

Stromelysin can also be activated chemically with 4-amino-phenylmercuric acetate (APMA). It is believed that the APMA perturbs the cysteine switch as well as other critical interactions within the propeptide, allowing H_2O to ligate to the active site zinc atom followed by intramolecular autolysis (Okada et al. 1988). After the initial proteolytic event, bi-molecular reactions yield the 45 and 28 kD active forms of the enzyme (Freimark et al. 1994, Galazka et al. 1996, Nagase et al. 1990). A similar process takes place in zymography where

SDS is the agent of activation. This explains zymogen activity that occurs at an apparent molecular weight of 57 kD, representing pro-stromelysin.

It has also been reported that stromelysin is activated at acidic pH. In a set of studies in which prostromelysin was incubated with aggrecan beads at various proton concentrations, it was discovered that stromelysin is activated at low pH, with peak activation occurring at pH 5.5. By SDS-PAGE analysis it was revealed that the stromelysin that was active still retained the pro-peptide. It was concluded that the acidic environment caused a conformational change making the active site accessible to substrate (Gunja-Smith and Woessner 1993).

Another method of activation is by heat. Stromelysin will undergo bimolecular autolytic activation (Wetmore and Hardman 1996) when incubated in 25 mM Tris, 50 mM NaCl, 10 mM $CaCl_2$ and 0.05% NaN_3 at 55 °C. This method of activation results in the a doublet at approximately 45 kD and a multiplet species of approximately 28 kD. All are active, and have Phe[83] as the amino terminal residue (Koklitis et al. 1991).

Comparison of the x-ray crystallographic structures of stromelysin residues 1-255 (pro-form), and 83-255 (activated form) had shown a 17Å difference in the position of Phe[83] in the two different species (Becker et al. 1995). However, by residue 90 the conformations of the two species are in register. Their data revealed that once activated, the terminal amine nitrogen of Phe[83] formed a salt bridge with the side group carboxyl of Asp[237]. Figure 7 is a stereo image showing the backbone structure of residues 83-255, and the salt bridge between the Phe[83] and Asp[237] homologous MMP-8 residues.

14

The removal of Phe[83] due to trypsin activation would result in the loss of the salt bridge between Phe[83] and Asp[237] (Becker et al. 1995). It has been demonstrated that in MMP-1 and MMP-8 the residues homologous to the Phe[83] of stromelysin is necessary in order for the salt bridge to form (Reinemer et al. 1994), (Figure 7). If either of the activated enzymes is even one residue shorter at the amino terminus, the salt bridge does not form. This has a dramatic effect on the level of enzyme activity that is observed. The presence of the salt bridge results in a 4-12 fold higher activity (He et al. 1989, Knauper et al. 1993, Murphy et al. 1987, Suzuki et al. 1990). This may be another mode of regulating enzyme activity levels.
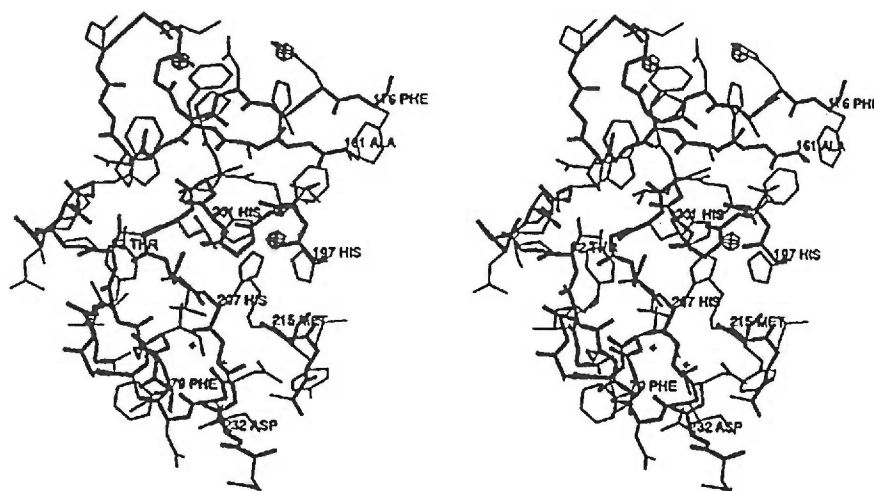
Figure 7
Stereo image of amino-terminal residues Phe[79]-Gly[242] of MMP-8 showing the salt bridge between the amine of Phe[79] and side chain carboxyl of Asp[232]. These two residues are homologous to stromelysin Phe[83] and Asp[237], respectively.
From: P. Reinemer et. al., "Structural Implications for the Role of the N terminus in the 'Superactivation' of Collagenases - A Crystallographic Study," *FEBS Letters* Vol 338, p. 229, (1994).

3° STRUCTURE OF CATALYTIC DOMAIN

To date, all of the structural studies of stromelysin have been restricted to the amino-terminal, catalytic, domain of the enzyme. The first tertiary structure studies used heteronuclear NMR to solve the tertiary structure of stromelysin residues 83-255. The data revealed that the overall structure of this truncated form of the enzyme was made up of 5 β-strands (all parallel but 1) four of which are in a β-sheet, and 3 α-helices (Gooley et al. 1994, Gooley et al. 1993, Van Doren et al. 1993).

The NMR data had also revealed that the active site zinc was coordinated by His[201] and His[205] from helix B, and His[211]. A second zinc had been suggested by atomic absorption data reported by Salowe et. al. in 1992. Their data had shown a Zn^{2+}/ stromelysin molar ratio of 1.82 and 1.75 for the prostromelysin (residues 1-255) and stromelysin (residues 83-255) respectively (Salowe et al. 1992). The NMR data confirmed the presence of a second zinc atom and identified His[151], His[166], and His[179] as three of the coordinating residues. The fourth coordinating residue of the second zinc atom could not be positively identified but three candidate residues were selected: Asp[153], Tyr[155], and Tyr[168] (Gooley et al. 1994, Gooley et al. 1993). Later, by x-ray diffraction the fourth coordinating residue of the second zinc atom was identified as Asp[153] (Becker et al. 1995). This second zinc atom in the MMPs is very tightly bound, and cannot be exchanged without denaturation (Bode et al. 1994, Salowe et al. 1992). The x-ray diffraction data also revealed the residues coordinating two calcium atoms: Asp[158], Gly[159], Gly[161], Val[163], Asp[181], and Gly[184] for the first Ca^{2+} atom, and Asp[141], Gly[173], Asn[175], Asp[177], and two water molecules for the second Ca^{2+} atom.
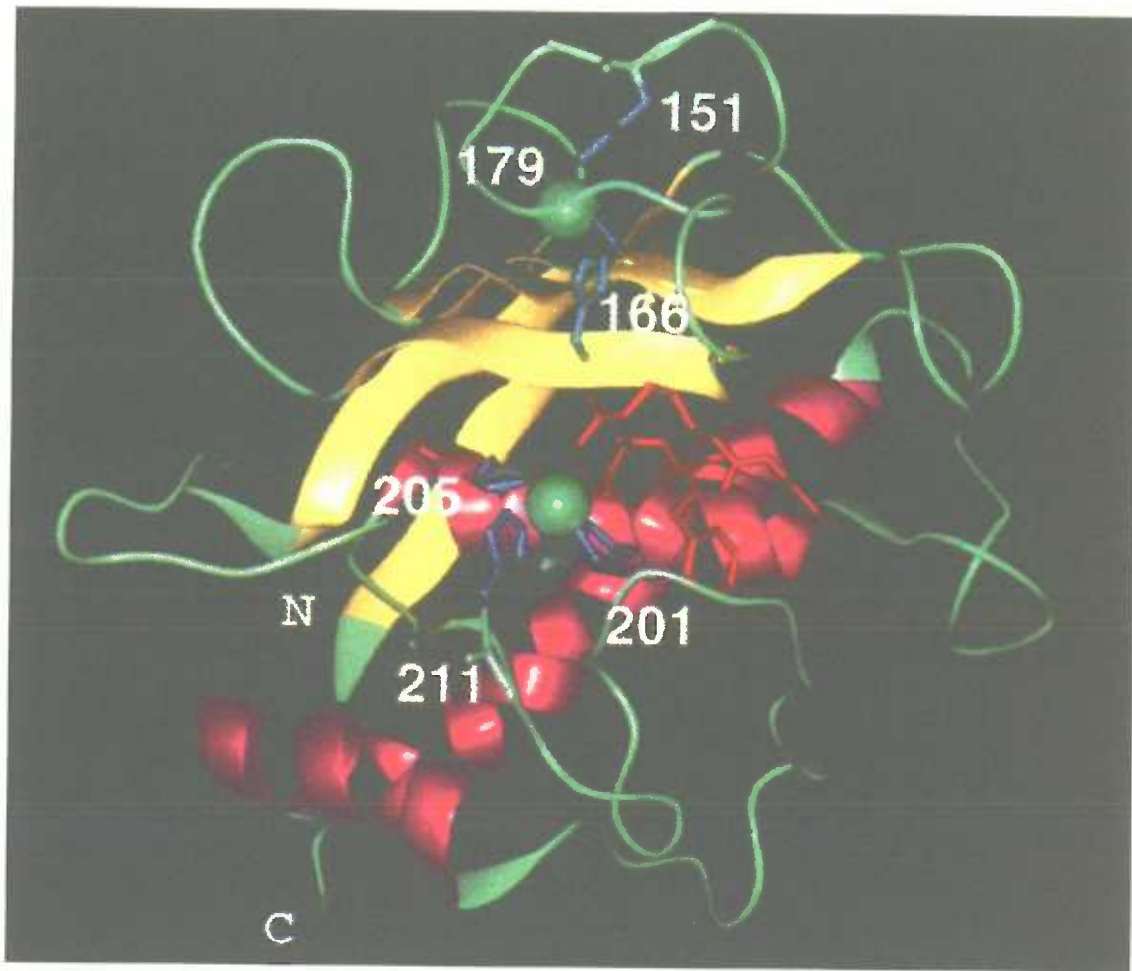
Figure 8

Ribbon diagram of the catalytic domain of stromelysin showing the 3 alpha helices in magenta and five beta strands in yellow. The two green spheres represent the zinc atoms with ligating histadine residues shown in blue with their residue numbers. The inhibitor peptide is shown in red.

From: Gooley, et al., "The NMR structure of the inhibited catalytic domain of human stromelysin-1," *Nature Structural Biology* Vol. 1, No. 2, p 114 (1994).

CARBOXY-TERMINUS

Figure 9 is the solution for a crystal structure of the carboxy-terminal domain of MMP-2 (Libson et al. 1995). The structure reveals a four-bladed β-propeller with a pseudo four-fold axis. The crystal structure of full length porcine MMP-1 shows a very similar structure for the carboxy-terminal domain (Li et al. 1995). While the MMPs have less sequence homology in the carboxy-terminal domains compared to their amino-terminal domain, their carboxy-terminal domain primary structures are pexin-like for all of the MMPs with the exception of MMP-7 which does not have a carboxy-terminal domain.
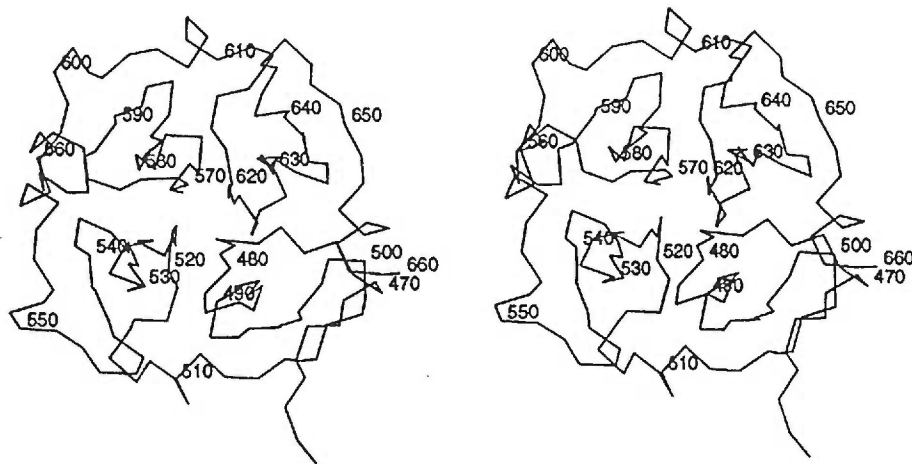
Figure 9
Stereo image of the haemopexin-like domain of MMP-2.
From: M. Libson, et. al., "Crystal structure of the Haemopexin-like C-terminal domain of gelatinase A," *Nature Structural Biology* Vol 2, No. 11, p. 938 (1995).

Not shown in Figure 9 is a calcium ion found in this structure. It has recently been shown that the calcium is important in the binding of this domain to fibronectin and heparin (Wallon and Overall 1997). Also, EDTA disrupts the interaction between this domain and TIMP-4 suggesting that the calcium may be important for that interaction as well (Bigg et al. 1997).

18

In stromelysin, a role in enzyme stabilization has been proposed for the carboxy-terminal domain. It has been reported by Willenbrock et. al., that the structural zinc that is present in their short-form of stromelysin (residues 1-216) is not present in the full-length enzyme as determined by inductively coupled plasma mass spectroscopy. They proposed that the carboxy-terminal domain of stromelysin has a role in stabilizing the amino-terminal domain, and that upon loss of the carboxy-terminal domain by proteolysis, a structural zinc binds the amino terminal domain to stabilize it (Willenbrock et al. 1995).

The presence of the carboxy-terminal domain also enhances the ability of activated stromelysin to bind to TIMP-1. The difference in K_i values of 45 kD species compared to a short-form stromelysin (Phe^{100}-Pro^{273}) is significant: 8.3×10^{-10} M for the 45 kD species, and 5.95×10^{-9} M for the activated short-form stromelysin, a greater than 7-fold difference (Baragi et al. 1994).

FOLDING AND STABILITY

The ability of stromelysin to recover from heat denaturation is rather remarkable. Hardman and Wetmore have shown that the secondary structure as evaluated by CD is recoverable after heating stromelysin, and that zinc was not required for re-folding. The activated form of the enzyme could be denatured, re-folded in the absence of zinc, and reactivated by the addition of zinc (Wetmore and Hardman 1996).

The thermal resilience of the enzymatic activity of stromelysin was demonstrated by showing that after heating the enzyme to 80°C for 15 minutes, the 45 kD species stromelysin loses only 35% of its activity and the 28 kD species loses only 5% (Okada et al. 1986). In

19

preparation for zymography stromelysin is boiled in the presence of SDS and subjected to electrophoresis with its activity still recoverable, as is evidenced by the clearing of substrate from the gel.

It is the characteristic of thermal stability that allows the use of heat for activation. It is thus far the only MMP that has been shown to be capable of autolysis under these conditions. It is possible even in zymography to shorten the 37°C incubation to 3 hours by increasing the incubation temperature to 55°C (see *Methods*).

PROTEIN SUBSTRATES

Stromelysin has the widest range of substrate specificities among the MMPs. Its protein substrates include: aggrecan (Fosang et al. 1991 56, Fosang et al. 1992); fibronectin, laminin, elastin (Murphy et al. 1991a); collagens type III, IV, V, IX, and X; and gelatins type I, III, IV, and V. Stromelysin is also capable of activating MMP-1, interstitial collagenase (Murphy et al. 1987); MMP-8, neutrophil collagenase (Knauper et al. 1993); and MMP-9, 92 kD gelatinase (Shapiro et al. 1995).

Although β-casein is not a natural substrate, it is degraded by stromelysin and many of the other MMPs. It is an inexpensive, readily available substrate that is frequently used to measure proteinase activity both in zymograms and tube assays.

STROMELYSIN KINETICS

The Effect of Calcium: Housely et.al. demonstrated that stromelysin thermal stability and stability in the presence of trypsin were both enhanced in the presence of 5.0 mM $CaCl_2$

compared to 0.1 mM CaCl$_2$ (Housley et al. 1993). Activity of stromelysin is also dramatically affected by the amount of calcium ion present with a minimum of 1.0 mM needed to achieve maximum activity (Housley et al. 1993, Okada et al. 1986). This is true even in the case of autolysis in the presence of amino-phenylmercuric acetate (Housley et al. 1993). The calcium concentration can be increased to at least 10 mM with no adverse effect on activity.

pH Effect: Two peaks of human stromelysin activity can occur as a function of pH, one at pH 5.5 and one at pH 7.5 (Harrison et al. 1992, Wilhelm et al. 1993). However, a single peak of activity at pH 7.5-7.8 for both the 45 kD and 28 kD species of human stromelysin has also been reported (Okada et al. 1986). Interestingly, in a study with the mouse homolog of stromelysin, a single peak of activity at approximately pH 7.5 was reported by Farmer and Yuan (Farmer and Yuan 1991). The reason for these differences is not known.

SYNTHETIC INHIBITORS

Three synthetic inhibitors were used in the studies presented in this dissertation: minocycline, a semi-synthetic tetracycline derivative; tryptophan hydroxamate and the peptide, RCGVP. Derivatives of all three had been previously shown to have inhibitory activity toward the MMPs (Fife and Sledge Jr. 1995, Fotouhi et al. 1994, Gijbels et al. 1994, Guerin et al. 1992, Hanglow et al. 1993, Schneider et al. 1992). Our purpose for re-evaluating these inhibitors was to supplement our data on the effects of MMPs on ocular outflow and will be presented in the second data-chapter of this dissertation.

METHODS

STROMELYSIN SEPARATION

Conditioning Media

HT1080 skin fibroblast cells (American Type Culture Collection, Rockville, MD) were cultured to 80% confluency in D-MEM (Gibco BRL, Gaithersburg, MD) containing 10% fetal bovine serum (Hyclone Laboratories, Inc; Logan, Utah) and at a CO_2 concentration of 5%. To stimulate stromelysin production, cells were incubated, serum-free, with 100 U/ml of interleukin-1α (R & D Systems, Minneapolis, MN). After 5 days of treatment, conditioned medium was harvested and 1μl of 100 mM PMSF (Sigma, St. Louis, MO) was added per 1 ml of media to inhibit serine proteinase activity. Calcium chloride was added to a final concentration of 5 mM to stabilize the metalloproteinases. Brij 35 was added to 0.05% (v/v), NaN_3 was added to 0.05% (w/v) and pH was adjusted to 7.9. Conditioned medium was then subjected to centrifugation to pellet cellular debris. The supernatant was then degassed on ice and subjected to Reactive Red column chromatography.

Reactive Red Column

The protocol for the Reactive Red column (Sigma) is based on that published by Koklitis et. al. (Koklitis et al. 1991). Prior to column chromatography, all solutions and the column were degassed. The 8 ml column was washed with 2 M KCl, degassed and pre-equilibrated with Reactive Red column buffer [25 mM Tris buffer (pH 7.9), 5 mM $CaCl_2$, 0.05% Brij 35, and 0.05% NaN_3].

The degassed crude culture medium was applied to the column. The column was washed with 100 ml of 300 mM NaCl in Reactive Red column buffer. Stromelysin was eluted

with 50 ml of 750 mM NaCl Reactive Red column buffer. Selected fractions were then treated with gelatin-agarose beads.

Gelatin-Agarose Beads

Gelatin-agarose beads (Sigma) were used to remove 72 kD gelatinase from the high salt eluate of the Reactive Red column. The beads were de-fined and pre-equilibrated with Reactive Red column buffer. The prepared gelatin-agarose beads (1 ml) were added to the fraction and allowed to bind overnight at 4 °C. The beads were then removed by filtration. The 25 ml filtrate was then dialyzed overnight at 4 °C against 2 liters of 25 mM Tris (pH 7.9), 10 mM $CaCl_2$, 0.05% Brij 35, and 0.05% NaN_3. The following day, the dialysis buffer was changed and dialyzed for an additional 5 hours.

Protein Quantitation

Concentration of protein was determined by absorption at 280 nm. Using the Beers-Lambert equation:

$$A_{280} = cl\epsilon$$

were A_{280} is the absorbance value at 280 nm, c is protein concentration, l is the pathlength of light passing through the sample, and ϵ is the extinction coefficient which is 69,614 $M^{-1}cm^{-1}$ for prostromelysin.

The BioRad micro assay procedure for measuring protein concentrations ≤ 25 $\mu g/ml$ was also used. A standard curve ranging from 0 to 25μg was generated using bovine serum albumin as the standard protein. BioRad reagent (200 μl) was added to each sample to a

24

final volume of 1 ml. After reacting for 20 minutes, the absorbance was measured at 594 nm. Concentration was determined from the standard curve.

SDS-PAGE

SDS-PAGE was conducted according to standard procedures (Laemlli 1970, Sambrook et al. 1989). Generally a 5% acrylamide stacking gel (pH 6.8) and 10 or 12% acrylamide resolving gel (pH 8.8) were cast. Protein bands were visualized with Coomassie Brilliant Blue R250 staining solution. Gels were de-stained and dried onto a cellophane membrane backing.

Western Immunoblot

The Western Blot protocol of Sambrook et al. was followed (Towbin et al. 1979, Burnette 1981, Sambrook et al. 1989). Briefly, samples were subjected to SDS-PAGE and transferred to solid support nitrocellulose membrane by electroblotting. Protein bands were stained with Ponceau S stain and the membrane was photocopied for a permanent record. The membrane was then de-stained in preparation for immunoblotting.

Non-specific antibody binding was reduced by blocking with 4% (w/v) non-fat dry milk prior to incubation with the primary antibody. All three primary antibodies used were generated by Preston Alexander in the Acott laboratory. All are polyclonal antibodies generated against MMP sequence-specific synthetic peptides. After incubation with the primary antibody solution, an appropriate alkaline phosphatase-conjugated secondary

antibody was used. The immunolocalized alkaline phosphatase was visualized with 5-bromo-4-chloro-3-indolyl phosphate and nitro blue tetrazolium.

Zymography

The zymography gel electrophoresis technique used in this dissertation is based on the protocol of Heussen (Heussen and Dowdle 1980); however, modifications which permit the use of BioRad mini-PROTEAN® II apparatus have been made by the author.

Briefly, a 50 mg/ml β-casein stock solution was prepared by dissolving β-casein in a 1.5 M Tris (pH 8.8) buffer containing 0.1% SDS. This stock was added at 10 μl per 1 ml of resolving gel to give a final β-casein concentration of 0.05%. A 10% final acrylamide concentration was used and TEMED and 10% ammonium persulfate solutions were added at 0.6 μl and 6.6 μl per 1ml of resolving gel, respectively. A standard Laemlli 5% acrylamide stacking gel was used (Laemlli 1970, Sambrook et al. 1989). Gels were cast using mini-PROTEAN® II apparatus with 0.75 mm spacers.

Samples were prepared by boiling for 5-10 minutes in SDS gel-loading buffer (Sambrook et al. 1989) in the absence of reducing agents. Samples underwent elecrophoresis at 175 V for approximately 40 minutes. After electrophoesis, SDS was removed from the gel by washing with a 2.5% Triton X-100 solution two times for 10 minutes each. Following the Triton washes, the gel was washed two times with water for 10 minutes each to reduce the Triton concentration.

The gel was then incubated in an enzyme reaction buffer: 50 mM Tris (pH 8.0), 150 mM NaCl, 10 mM $CaCl_2$ and 1 μM $ZnCl_2$. During the incubation, bands of proteinases

26

degrade the local β-casein, and both the product and the proteinase in the band diffuse out of the gel. Incubation traditionally takes place at 37 °C overnight. Due to the thermal stability of stromelysin, the incubation time may be shortened to 3 hours if conducted at 55 °C. After the incubation, the gel was rinsed with water then stained with Coomassie Blue, de-stained and dried as described under the SDS-PAGE protocol.

INHIBITION AND OUTFLOW FACILITY STUDIES

Zymogram of Minocycline Inihibition

The zymogram of minocycline inhibition was performed by subjecting equal amounts of prostromelysin in each lane of a single zymogram gel to electrophoresis. The gel was cut into strips corresponding to a single lane of the gel. The strips were placed into individual tubes containing various concentrations of minocycline for the zymogram incubation. Each strip was stained with Coomassie Blue stain, de-stained and dried as described in SDS-PAGE protocol.

FITC/β-casein conjugation

The preparation of FITC-labeled β-casein was performed according to the conjugation protocol of Twining (Twining 1984). β-casein (1 gm) (Sigma) was dissolved in 100 ml of 50 mM sodium carbonate buffer (pH 9.5) containing 150 mM NaCl. FITC isomer I (40 mg) (Sigma) was added and the solution was stirred for 1 hour at room temperature in the dark. The reaction was stopped by the addition of 0.6 gm Tris base, and the solution was dialyzed against 50 mM Tris (pH 8.5) overnight in the dark. The solution was further dialyzed against

50 mM Tris (pH 7.2) changing the buffer frequently. An aliquot was removed, precipitated with 10% trichloroacetic acid and subjected to centrifugation. The A_{494} of the supernatant was determined spectrophotometrically at pH 7.9. Dialysis was terminated when minimal absorbance of the free FITC was observed.

Using the Beer-Lambert equation shown above, the concentration of FITC of the preparation was determined using the extinction coefficient of 61,000 M-1cm-1. The protein concentration of the preparation was known, and from these two molar values, a molar ratio of FITC/β-casein was calculated.

Stromelysin heat activation

Unless otherwise stated, the active stromelysin used herein was activated by heating. The protein concentration was at least 100 ng/ml in 50 mM Tris (pH 7.5 at room temperature), 10 mM $CaCl_2$, 25 mM NaCl, 0.015% Brij 35 and 0.05% NaN_3. Standard incubation conditions were 55 °C for 2.5 hours.

FITC-β-casein assay

The protocol of Twining was followed (Twining 1984) with some modifications. Briefly, reactions were carried out in 25 mM Tris buffer containing 5 mM $CaCl_2$ and 10 μM $ZnCl_2$. The pH of the buffer was adjusted to 7.5 at the temperature at which reactions would take place. Reactions were performed in 1 ml volumes. Substrate was added to buffer and allowed to reach reaction temperature before stromelysin was added. The addition of stromelysin initiated the reaction, and at specific time intervals a 200 μl aliquot was removed

28

and added to 200 μl of a 10% trichloroacetic acid solution. The sample was precipitated overnight at 4 °C, protected from light. The precipitate was pelleted by centrifugation, supernatant was removed and neutralized with 750 mM boric acid (pH 10.0) at a 1:2 ratio of supernatant to boric acid.

The A_{494} and A_{550} of the neutralized supernatant were recorded. The wavelength of maximum fluorescein absorption at neutral pH is 494nm. The A_{550} was recorded as background absorption and the difference between these two was absorption attributed to fluorescein.

To determine product concentration, the absorption value was then converted to a molar substrate concentration using an extinction coefficient of 61,000 $M^{-1}cm^{-1}$ for fluoroscein, and the ratio of 1.96 moles of FTC per mole of β-casein (method for determination is described in *FITC/β-casein conjugation* protocol). An initial velocity was determined by performing linear regression on the multiple time points of a single sample.

Human Anterior Segment Perfused Organ Culture Model

Human donor eyes were obtained within 48 hours postmortem from the Portland Lion's Eye Bank. Anterior segments, containing the undisturbed trabecular meshwork, sandwiched between the intact cornea and a 15-mm rim of sclera, were cultured for seven days in stationary organ culture prior to perfusion (Acott et al. 1988). Eyes from patients with potentially confounding diseases were not used. Anterior segments were then mounted in a standard perfusion culture apparatus (Clark et al. 1995, Erickson-Lamy 1992, Erickson-Lamy et al. 1988, Johnson et al. 1990, Johnson and Knepper 1994, Johnson and Tschumper

1987, Johnson and Tschumper 1989, Tschumper et al. 1990) and perfused with culture medium (without amphotericin B, at a constant perfusion head of 10 cm (approximately 7.35 mm Hg) for 3-5 days allowing outflow to stabilize. Explants that did not stabilize between 1.5 and 8 μl/min at 7.35 mm Hg perfusion pressure after 7 days were not used.

Culture conditions were: 37°C, 100% humidity, 5% CO_2 and 95% air. Outflow rates were determined gravimetrically to ±10 μl approximately every 12 hours. Normalized outflow facility (%C_0) is the flow rate in units of μl/(min·mm Hg) normalized to 100% of the pre-treatment flow rate (Erickson-Lamy 1992, Kaufman 1988). Outflow has been shown to be through the trabecular meshwork (Erickson-Lamy 1992, Johnson and Tschumper 1987, Johnson and Tschumper 1989). Flow rates and trabecular cellularity are maintained for at least three weeks (Johnson 1996, Johnson et al. 1990, Johnson and Knepper 1994, Johnson and Tschumper 1987, Johnson and Tschumper 1989, Tschumper et al. 1990).

Inhibitors were dissolved in water or at 10,000 x final treatment concentrations in absolute ethanol for both flow and kinetic studies; vehicle controls were run in parallel. Except as specifically noted, all treatments were continuous exposures to the agent in the perfusion medium, beginning at treatment time = 0, and perfusion head was maintained at 7.35 mm Hg.

PEPTIDE SUBSTRATE KINETICS

TIMP-1 titration of active enzyme concentration

The concentration of activated stromelysin (Biogenesis, Poole, England) was determined by titration with human TIMP-1 (donated by the Sakai Laboratory, Shiners Childrens Hospital; Portland, OR). The concentration of TIMP-1 had been determined by amino acid analysis. The enzyme titration was conducted according to the protocol described in Methods in Enzymology (Nagase 1995), with the following modifications: pre-incubation of inhibitor and enzyme was for 2 hours and the substrate used was NFF3 at 4 μM.

Briefly, TIMP-1 is a competitive, slow, tight-binding (irreversible) inhibitor of stromelysin that binds at a 1:1 molar ratio with enzyme. TIMP-1 can therefore be used to titrate stromelysin active sites. Various known concentrations of the inhibitor were incubated with a fixed amount of the enzyme preparation to allow the inhibitor to bind. After incubating for two hours, substrate was added and the activity was recorded. The activity was then plotted as a function of TIMP-1 concentration, giving a negative slope with the x-intercept indicating the minimum TIMP-1 concentration required to inhibit all stromelysin activity. Since the TIMP-1 binds at a 1:1 ratio with stromelysin, this value also corresponds to the molar concentration of active stromelysin.

Trypsin activated stromelysin

A 4 μl aliquot of a 0.5 mg/ml solution of TPCK trypsin (Pierce, Rockford, IL) was added to 5 μg of stromelysin in 4.5 ml of Tris buffer (pH 7.5). The solution was incubated

31

at 37 °C for 45 minutes at which time 2 μg of trypsin inhibitor (Sigma, St. Louis, MO) were added.

NFF3 peptide substrate kinetics

Human stromelysin-1 was purchased from Biogenesis. NFF3 (Peptides International) was reconstituted in water to approximately 1 mM final concentration. Concentration was determined by absorbance at 410 nm using $\epsilon = 7,500$ cm^{-1}M^{-1}. Fluorescence was monitored using a Perkin Elmer LS50B Luminescence Spectrometer equipped with a thermostatted four-cell holder. Temperature was maintained with a Lauda RM6 water bath. Initial velocities were determined using least squares fitting performed by the FL Data Manager software. Initial velocity data was plotted and analyzed using Grafit software (Erithacus Software Limited; Staines, UK).

For reactions at pH 7.5 and 8.0, Tris buffer was used at 50 mM concentration containing 10 mM CaCl$_2$, 50 mM NaCl, and 0.015 % Brij 35. For reactions at pH 6.0, the Tris buffer was adjusted to pH 7.0 with HCl then adjusted to 6.0 with the addition of 200 mM Tris-maleate containing CaCl$_2$, NaCl and Brij. To control for any thermal effect, the pH of all buffers was adjusted at the temperature at which the buffer would be used.

Reactions were conducted in one ml volumes. A cuvette containing buffer and substrate was placed in the thermostatted cell holder and allowed to thermally equilibrate before the reaction was initiated with the addition of stromelysin. The excitiation wavelength was 328 nm and the emission wavelength of 393 nm was monitored. Initial slopes of fluorescence units per second were determined by least squares fitting, and y-axis intercepts

were used as baseline emissions values (F_i). The reaction was allowed to continue to completion, or was forced to completion with trypsin to obtain a final fluorescence value (F_f). Conversion from fluorescence units to product concentration units was accomplished making the assumption that all of the substrate had undergone hydrolysis at the time of completion and using the expression: (F_f - F_i)/(substrate concentration). This method allowed continuous monitoring of reactions containing high substrate concentrations.

SEPARATION OF STROMELYSIN

FROM MMP-2 IN CONDITIONED CULTURE MEDIA

▸Experimental Purpose

▸Experimental Design

▸Results

▸Discussion

▸Conclusions

34

EXPERIMENTAL PURPOSE

One of the main objectives of this thesis project was to examine the kinetic mechanism of stromelysin. It was not until after these projects were initiated that purified stromelysin became commercially available. Thus, for our early kinetic and inhibition studies stromelysin was extracted from cell culture media.

Based on studies performed in the Acott laboratory, the best source of stromelysin was IL-1α treated skin fibroblast cell culture medium. Treatment with IL-1α stimulates stromelysin production without significantly increasing MMP-2 production. MMP-2 is, however, constitutively expressed by skin fibroblasts. Due to substrate cross-reactivity, a protocol for separating the two MMPs was therefore developed.

Separation of the MMPs from one another is difficult due to their high homology. However, a protocol was established based on published purification protocols (Bayne et al. 1992, Koklitis et al. 1991, Okada et al. 1986) and the resultant stromelysin preparation contained very little contaminating MMP-2.

This section covers the procedure used to extract stromelysin from conditioned media, and to separate it from contaminating MMPs, especially MMP-2. Conditions for heat activation were also evaluated and will be discussed.

EXPERIMENTAL DESIGN

HT1080 skin fibroblast cells were treated with IL-1α to increase production of stromelysin. The conditioned media was harvested and subjected to column chromatography. Fractions from the columns were assessed by SDS-PAGE, Western immunoblot and zymography. Conditions for heat activation were evaluated and are presented in the final portion of this chapter.

Two columns were used in the separation protocol. The Reactive Red column was used to separate the MMPs from other proteins in the media. MMP-2 was then separated from stromelysin with gelatin agarose beads. The unbound filtrate was subjected to Western immunoblot using a polyclonal antibody made against a stromelysin hinge region peptide to provided positive identification of stromelysin. Western immunoblots to detect MMP-1 and MMP-2 were also performed on the final preparation. These data indicated that MMP-2 had been thoroughly separated from stromelysin with these two columns.

Activation of stromelysin was accomplished by incubating an aliquot of the final stromelysin preparation at 55 °C. The length of incubation time yielding optimal activation and the effect of zinc were evaluated by zymography. Stability of activated stromelysin was assessed by SDS-PAGE analysis.

RESULTS

Reactive Red Column

This column was used to separate the MMPs from contaminating proteins present in the culture media and generally follows the protocol of Koklitis et. al. (Koklitis et al. 1991). Under our conditions, the column will bind stromelysin as well as MMP-2.

After the media has been passed over the column, contaminating proteins and phenol red dye were eluted with Tris buffer containing 300 mM NaCl (Figure 10, lanes 3-6). Stromelysin and MMP-2 were then eluted with buffer containing 750 mM NaCl (Figure 10, lanes 7-9).

The SDS-PAGE of the Reactive Red column fractions shows a doublet at approximately 57 kD as the most abundant protein bands in the crude media sample. These protein bands are not detectable in the column flow through, indicating that those proteins bound to the column. A small amount is eluted in the last three 300 mM salt fractions. The majority of the doublet was eluted in the first 750 mM salt fraction. Also present in this fraction is a small amount of higher molecular weight proteins. These higher molecular weight proteins are less apparent in the second and third high salt fractions.

37
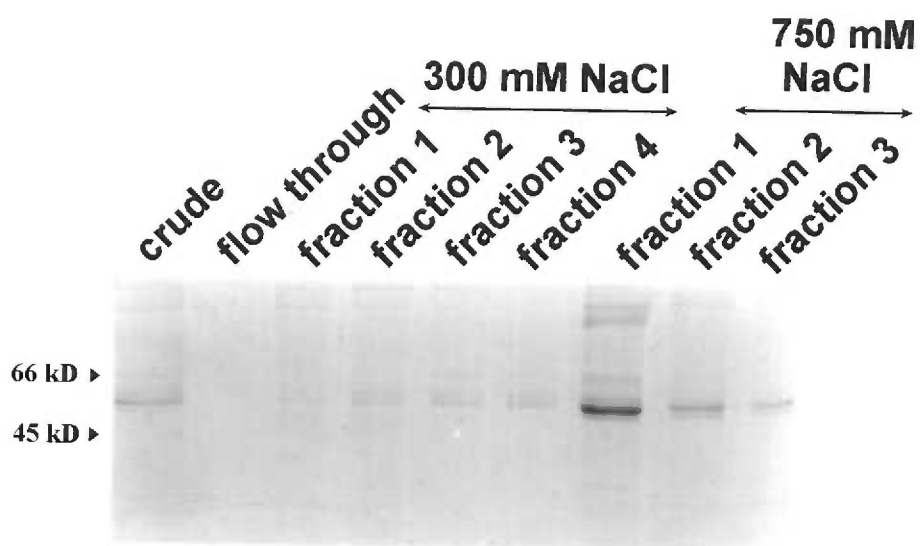
Figure 10

Fractions from the Reactive Red column were subjected to SDS-PAGE and Coomassie Blue staining.

Gelatin Agarose beads

To remove contaminating MMP-2, 1 ml of gelatin-agarose beads was added to fraction 1 of the 750mM salt eluate from the Reactive Red column. Binding took place overnight at 4°C. Those conditions allowed the MMP-2 to bind with little binding of stromelysin. The beads were then filtered out of solution leaving the majority of the stromelysin in the filtrate. Samples were evaluated by SDS polyacrylamide gel electrophoresis followed by staining with Coomassie Brilliant Blue, Figure 11.

Each lane in this gel contains the same volume of the various preparations. The first lane contains crude medium, and the second contains the unbound filtrate from the gelatin-agarose beads. It is clear that the concentration of stromelysin relative to total protein is greatly enhanced after the Reactive Red and gelatin-agarose steps. The third column shows the protein that bound to the beads, indicating binding of MMP-2 and some stromelysin.

Western Immunoblot Identification of Stromelysin

The supernatant from the gelatin-agarose beads was subsequently dialyzed against Tris buffer (pH7.9) and aliquots stored at -80 °C. Positive identification of the major band was achieved by Western immunoblot (Figure 12) using a polyclonal antibody that recognizes a stromelysin hinge region peptide. To further ensure the identity of the band, a small portion was activated by heat for 1 hour at 55°C. The resultant bands from heat activation of stromelysin appear as a 47 kD/45 kD doublet and 28 kD broad band.

39
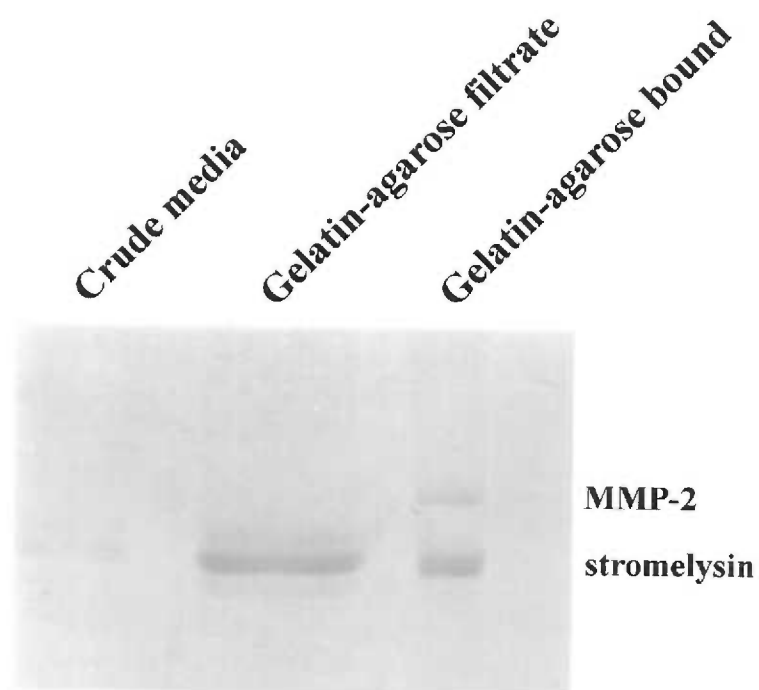
Figure 11

SDS-PAGE of gelatin-agarose
unbound and bound proteins
stained with Coomassie Blue.

1   **2**   **3**

66 kD➤

45 kD➤

31 kD➤

Prostromelysin Doublet

45 kD Species Doublet

28 kD Species
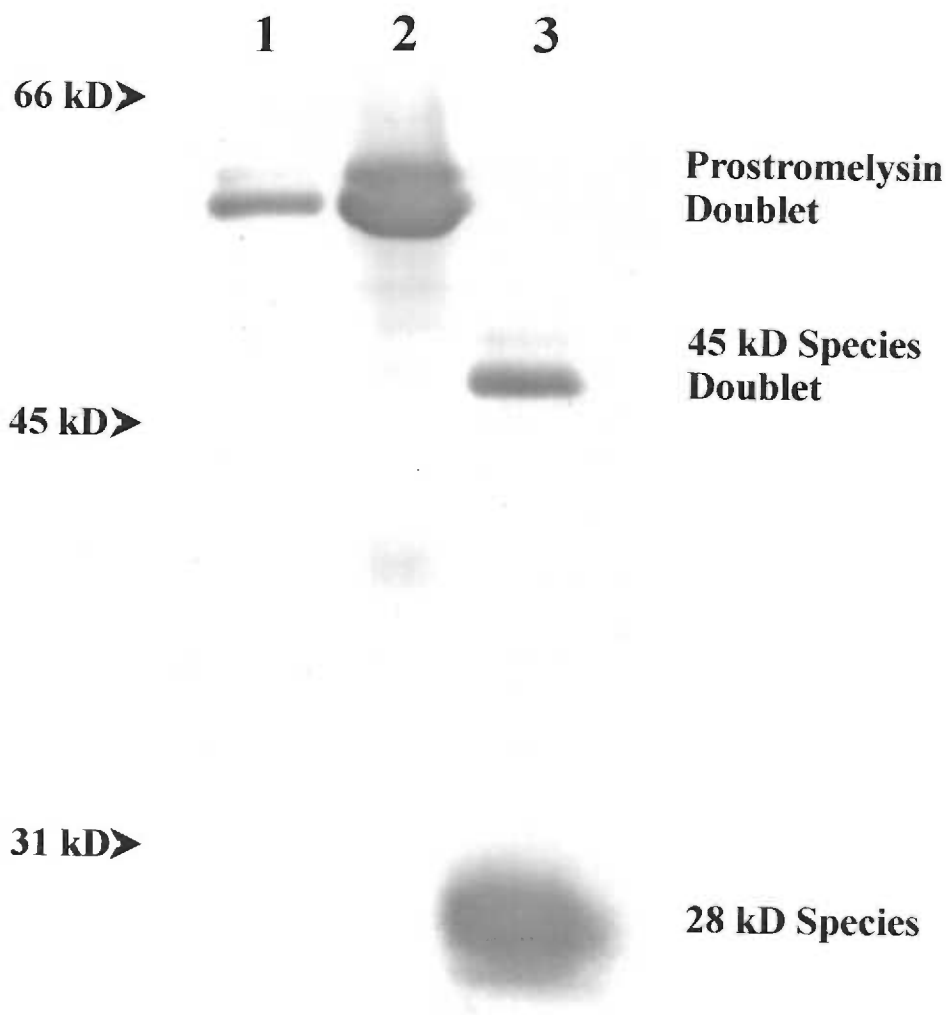
Figure 12
Western immunoblot of stromelysin
lane 1: crude media
lane 2: post-gelatin-agarose beads
lane 3: heat activated, post-gelatin-agaroase beads

Western Immunoblot of MMP-1 and MMP-2

While contaminating MMPs were not present in significant amounts according to the Coomassie stained gel, Figure 11, we used a more sensitive assay to detect other MMPs in the preparation. Western immunoblotting is a more sensitive technique for detecting and identifying MMP-1 and MMP-2. Figure 13a shows a Western immunoblot using a primary antibody against MMP-1. In Figure 13b the primary antibody was against MMP-2.

Figure 13a shows strong MMP-1 bands in the stromelysin preparation. After heat incubation, MMP-1 appears to be activated. Figure 13b shows only cross reactivity of the MMP-2 antibody with MMP-1, but no detectable MMP-2 protein.
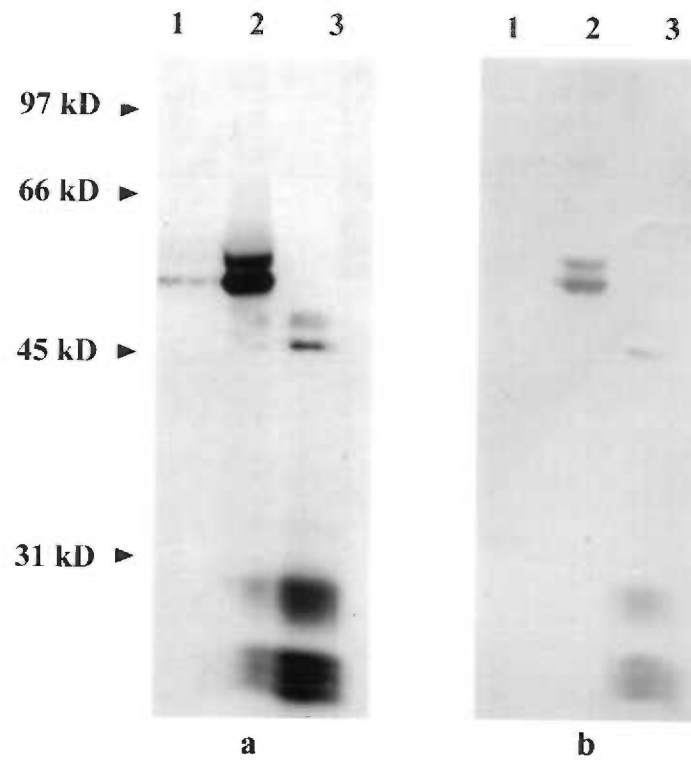
Figure 13
Western Immunoblot of (a) MMP-1 and (b) MMP-2
Lane 1: crude media
Lane 2: post-gelatin-agarose beads
Lane 3: heat-activated, post-gelatin-agarose beads

Optimizing length of time for heat activation, Figure 14

The technique of activating stromelysin by incubating it at high temperature in neutral buffer had been reported (Koklitis et al. 1991). Based on this report, we optimized the incubation conditions for our preparation. Stromelysin was incubated at 55°C for the time periods indicated and evaluated by β-casein zymography, Figure 14.

The 1 hour incubation time does not seem to be long enough for 100% activation. While 2 and 3 hours both result in almost 100% activation (both 45 and 28 kD species).

Heat activation ± ZnCl$_2$, Figure 15

The effect of zinc on heat activation has not been reported. Since zinc is required for activity and possibly for stability of stromelysin, we examined the effect of zinc on heat activation. Zinc was not added to the dialysis buffer at the end of the chromatography steps; therefore, the only zinc available to stromelysin was in trace amounts. Figure 15 is a β-casein zymogram showing the effect of heat activation with and without the addition of 10 μM ZnCl$_2$. The band intensities suggest no effect upon the addition of ZnCl$_2$.

Stability of heat activated stromelysin, Figure 16

Aliquots of stromelysin were activated by heating at 55°C in Tris buffer (pH 7.5) for either one hour or 30 minutes. Samples activated for 30 minutes were then left at room temperature for up to 3 days. Stability was estimated by evaluation using SDS-PAGE. These data suggest that activation is incomplete after 30 minutes at 55°C followed by incubation at room temperature over night. More activated enzyme was obtained by a one-hour incubation at 55°C. These results suggest that the activation is strongly temperature dependent.

44
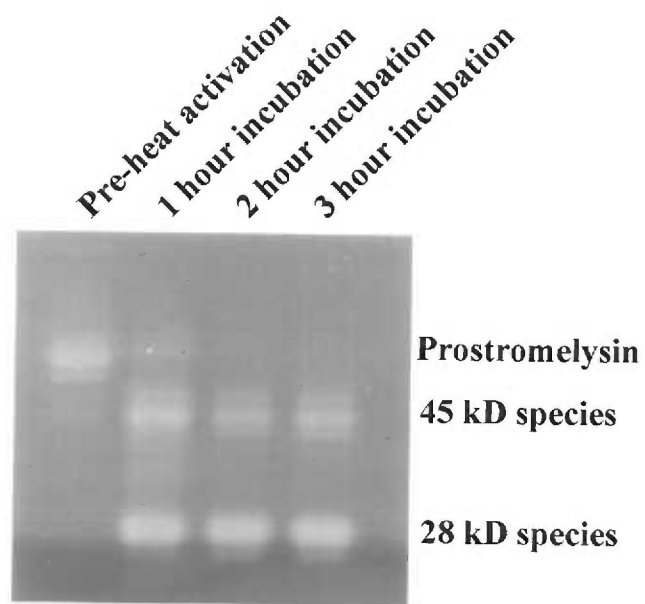
Figure 14
Zymogram of heat activated
stromelysin incubated at
55 C for times indicated.
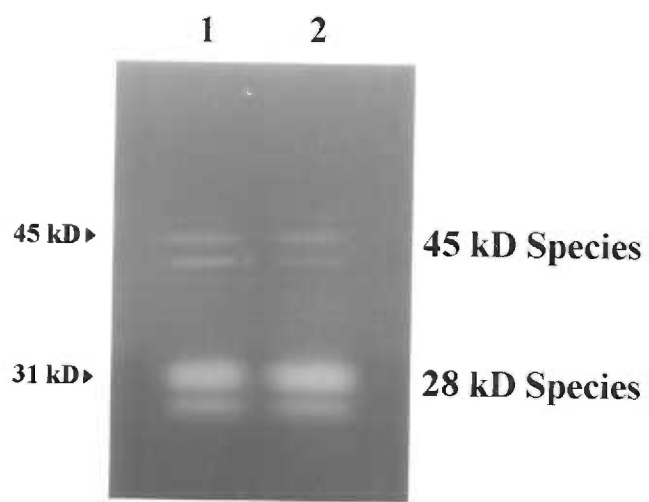
Figure 15
Zymogram of stromelysin
incubated in Tris buffer
at 55 C for 2 hours:
lane 1: without zinc
lane 2: with zinc

1   **2**

Prostromelysin

45 kD ▸   45 kD species

31 kD ▸   28 kD species
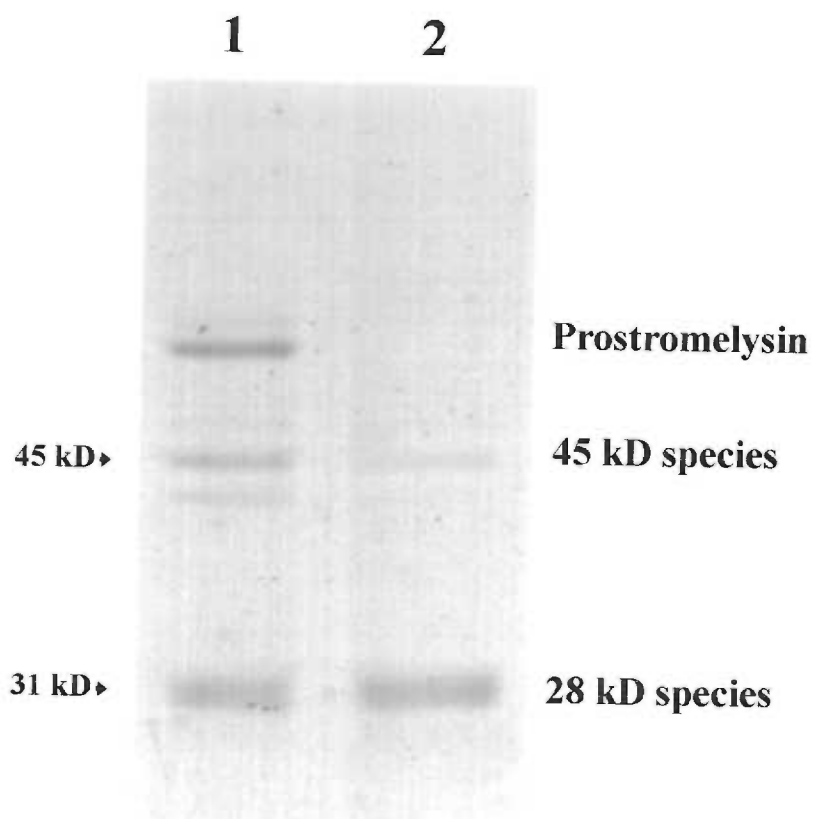
Figure 16
Coomassie Blue-stained SDS-PAGE
of heat activated stromelysin. Sample
in lane 1 was incubated at 55 C for
30 minutes, then at room temperature
overnight. Sample in lane 2 was
incubated at 55 C for 1 hour.

DISCUSSION

Separation of Stromelysin from MMP-2

Separation of stromelysin and MMP-2 was necessary to conduct kinetic experiments, since they both hydrolyze FITC-conjugated β-casein. Contaminating MMP-2 should not be activated by the heat activation method.

MMP-2 is constitutively expressed in culture media of many cell types, including HT1080 cells. To enhance the level of stromelysin production, the HT1080 cells were treated with IL-1α. While IL-1α causes a significant increase in the level of stromelysin produced, MMP-2 is still present in the media.

Reactive Red column (Figure 10) and gelatin agarose-beads (Figure 11) removed MMP-2 and allowed the kinetic analysis of stromelysin activity against FITC-labeled β-casein. MMP-2 could not be detected by western immunoblot or in β-casein zymograms. The minor contribution of MMP-2 proteolysis of β-casein that might occur would be evidenced in subsequent β-casein zymograms (Figures 14 and 15) and would appear at a band of molecular weight greater than pro-stromelysin. Any evidence of MMP-2 activity in the gels would be an overestimate of its activity in the kinetic assay since the MMP-2 is still in the proform. In the zymogram, activation is achieved due to the presence of SDS. In the kinetic assay however, MMP-2 would still be latent.

The Western immunoblot of MMP-2 shows no visible band at 72 kD, Figure 13b, although there was a fair amount of cross-reactivity with MMP-1 protein. An MMP-2 band is also not detectable in the β-casein zymograms of the final preparation. These data suggest

48

that, at this level of detection, all of the MMP-2 has been removed from the stromelysin preparation.

A weak band is detectable below the proform of stromelysin in both the Coomassie Blue staining of the SDS-PAGE, Figure 11, and in the β-casein zymogram of the final preparation, Figure 15. The Western Immunoblot of MMP-1 indicates that it is present in the final preparation, Figure 13a. It also appears to be activated during the 55°C incubation. This is likely due to heat-activated stromelysin activating the MMP-1. The MMP-1 is less of a concern than the MMP-2 would be because its specific activity toward casein is generally lower than that of stromelysin. The lower specific activity combined with its relatively low quantity present in the preparation made it less of a concern as well.

Heat Activation of Stromelysin

While activation of stromelysin can be accomplished by several methods, activation of stromelysin by heat is optimal for kinetic experiments for several reasons. First, it does not require the addition of compounds not already present in the buffer. Second, it does not require the addition of another proteinase. Third, the resultant zymogen begins at Phe[83] which is the putative endogenous amino terminus, whereas trypsin activation generates a Thr[85] amino terminus. Fourth, MMP-2 will not be activated during the process. Any other technique would yield activated MMP-2.

Activation by heat is accomplished by incubation in Tris buffer at 55 °C. Figure 14 (zymogram time line) shows that there is a significant difference in the extent of activation

between 1 and 2 hour incubation times, but that the extent of activation between 2 and 3 hours is equivalent. This suggests that a 2 hour incubation time is sufficient.

Since zinc is required for activity of stromelysin, 10 μM zinc was added to the activation buffer to test if it were necessary for activation. This did not appear to be the case (Figure 15). However, only a single incubation time was tested, and longer or shorter incubation times might have shown a difference.

Heat-activated stromelysin is vary stable against autolysis. Figure 16, lane 1, is a Coomassie Blue stained SDS-PAGE of stromelysin that had been incubated for 30 minutes at 55 °C, then left at room temperature overnight. This lane shows a significant amount of protein still present in the sample even though active stromelysin is present in the preparation. In fact, an activated sample that has been held at room temperature for up to three days showed no loss of enzyme or activity as determined by SDS-PAGE and zymography.

CONCLUSIONS

The objective of the experiments presented in this chapter was to generate a preparation of stromelysin containing minimal levels of contaminating MMP-2 and MMP-1. The media of IL-1α-stimulated skin fibroblast cells contains stromelysin, MMP-2 and MMP-1. Separation of stromelysin from MMP-2 and MMP-1 was achieved using a Reactive Red column and gelatin-agarose beads. Separation of stromelysin from contaminating MMPs was sufficient to allow us to proceed with kinetic experiments, based on the results from the western immunoblots and zymograms showing only traces of MMP-2. The small amount of MMP-2 remaining in the preparation would not be activated by the heat activation method.

While there are measurable amounts of MMP-1 present, it is anticipated that its contribution to kinetic reactions would be minor due to its relatively low specific activity toward β-casein.

Activation of stromelysin for use in kinetic experiments was achieved by heating to 55 °C for 2.5 hours in Tris buffer. Activation under these conditions yields both the 45/47 kD pair, and the 28 kD forms of stromelysin. The active stromelysin is very stable with little or no loss of activity at room temperature for up to 3 days.

This preparation of stromelysin was subsequently used for kinetic analysis of stromelysin using β-casein substrate. The stromelysin in those studies was standardly activated by incubation at 55°C for 2.5 hours in Tris buffer.

AQUEOUS HUMOR OUTFLOW STUDIES

- ▸Epidemiology of Glaucoma

- ▸Ocular Anatomy

- ▸Clinical Diagnosis & Treatment

- ▸Etiology of Glaucoma

- ▸Experimental Purpose

- ▸Results

- ▸Conclusions

BACKGROUND

Epidemiology of Glaucoma

Primary open angle glaucoma is a blinding disease affecting approximately 2.5 million people in the United States (Quigley 1993, Quigley 1996, Quigley and Vitale 1997), and 66.8 million worldwide (Quigley 1996). Glaucoma is thus the second leading cause of blindness in the United States, second only to age-related macular degeneration. The disease is particularly devastating, in part because the onset of blindness occurs late in life (Dielemans et al. 1994, Leske et al. 1994, Quigley and Vitale 1997), a time when adjusting to loss of vision is particularly difficult. Here we will discuss the clinical diagnosis of glaucoma and our hypothesis of its etiology.

Ocular Anatomy

The portion of the eye anterior to the vitreous humor is anatomically divided into two chambers: the posterior chamber which is behind the iris, and the anterior chamber in front of the iris and lens, Figure 17. Both chambers are filled with a fluid called the aqueous humor, which provides nutrients to the avascular lens, cornea and trabecular meshwork. The aqueous humor is produced by the ciliary body at a rate of about 2.75 ± 0.63 μl/min (Brubaker 1991, Larsson et al. 1995) and exits the anterior chamber through the trabecular meshwork to Schlemm's canal (Newell 1982, Stevens and Lowe 1997), Figure 18. The trabecular meshwork is a ring of semi-permeable tissue at the anterior base of the iris and is shown in Figure 19.

53

Figure 17
Anatomical structure of the eye.
(From: Daniel Vaughan, et.al., General Ophthalmology,
Chapter 1, First Ed., Lange Medical Publications (1968).

54
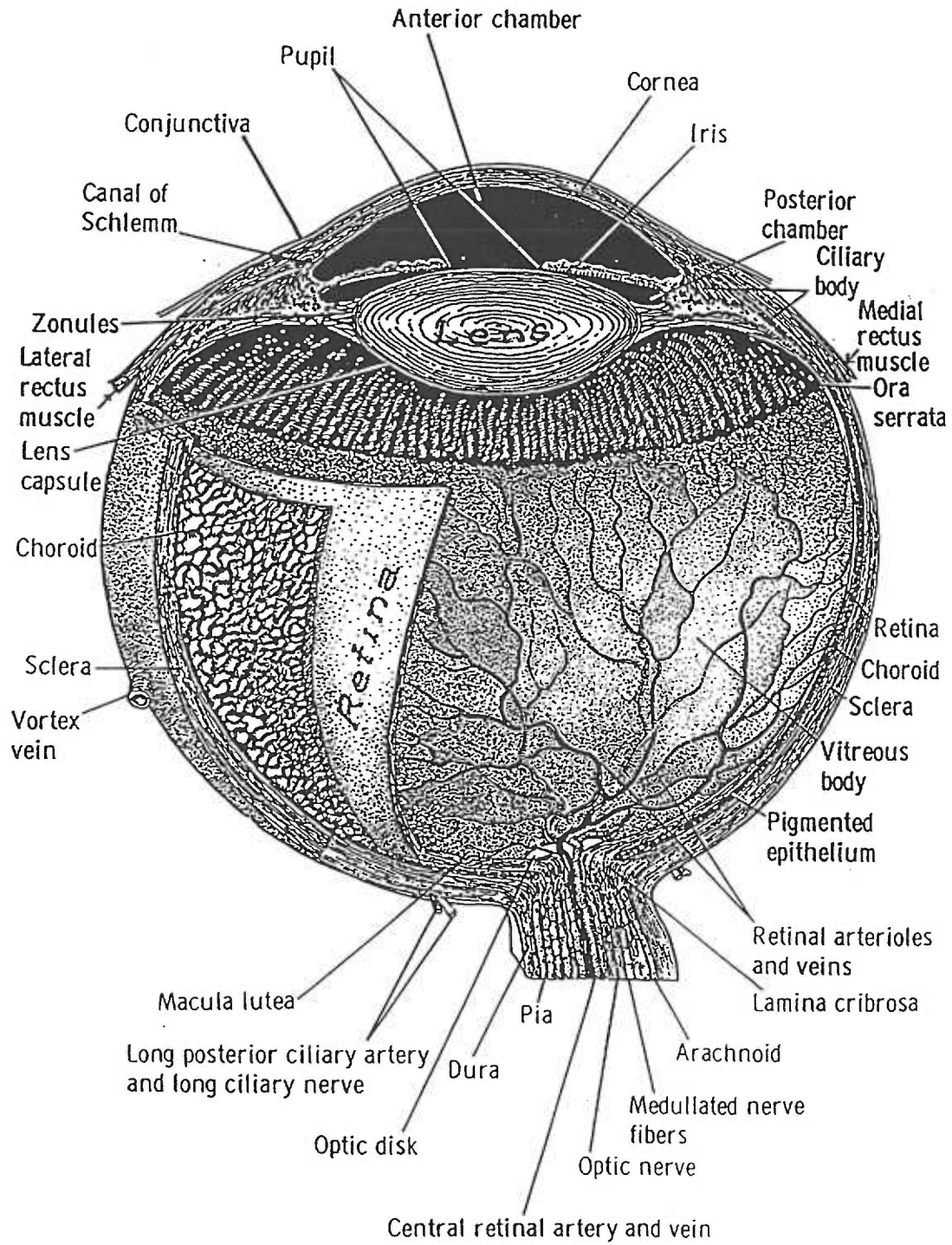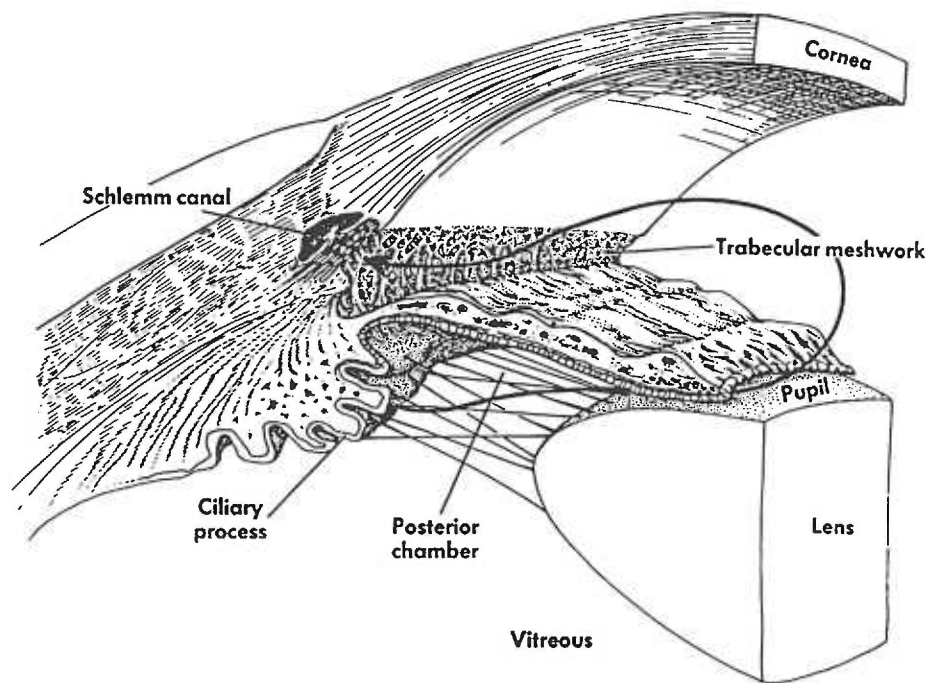
Figure 18
Drawing of the aqueous humor outflow pathway.
From: Frank W. Newell, "Ophthalmology: Principles and Concepts," Fifth edition, The C.V. Mosby Company, St. Louis, p.75, (1982).
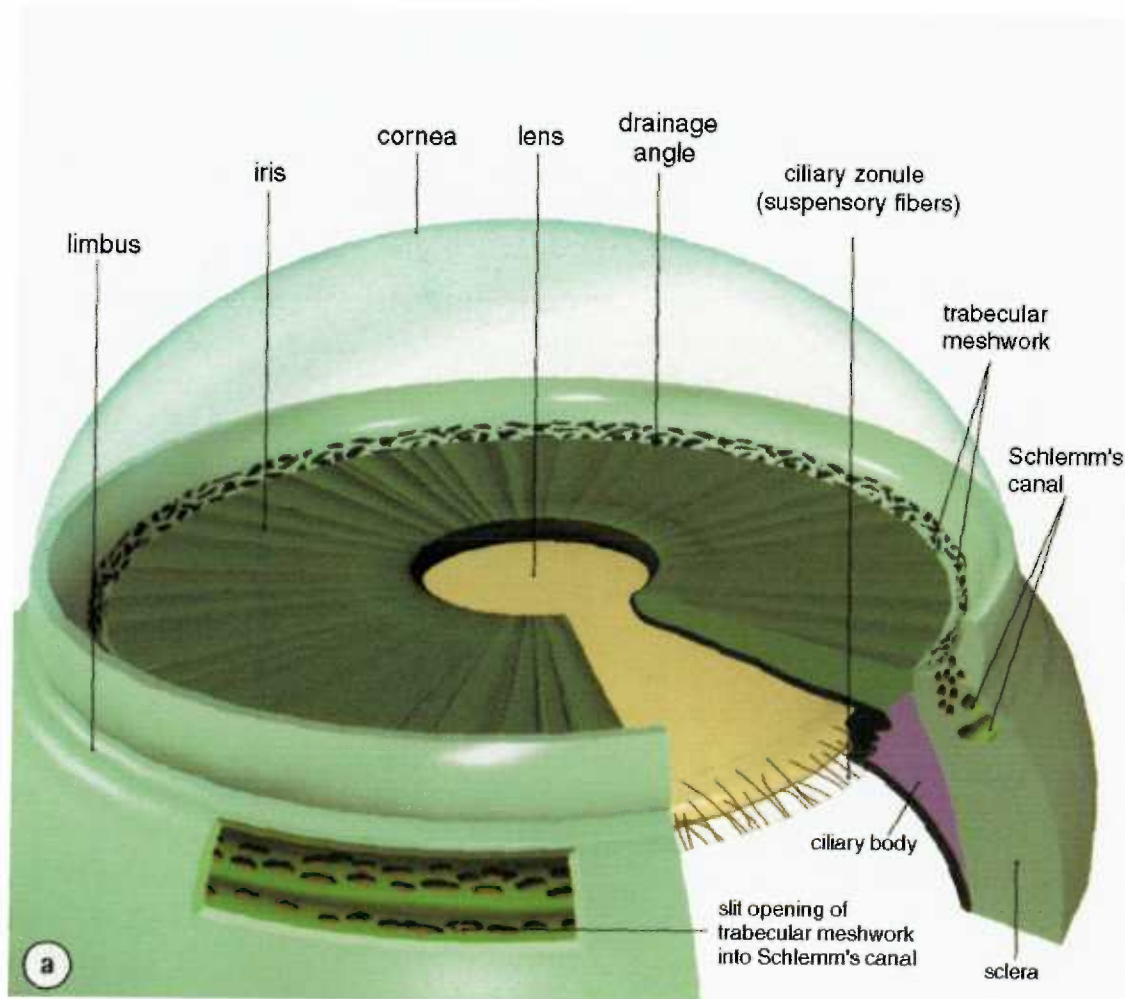
Figure 19

Artistic representation of the anterior portion of the eye
showing the ring of trabecular meshwork at the base of the iris.

From: A. Stevens and J. Lowe, "Human Histology" Second
edition, Mosby, London, p. 393 (1997).

Clinical Diagnosis & Treatment

Clinical diagnosis of glaucoma is based primarily on presentation of optic nerve cupping, visual field loss, and increased intraocular pressure. It is generally accepted that increased intraocular pressure is the primary risk factor for glaucomatous visual field loss (Quigley 1993). Sustained elevation of intraocular pressure damages the optic nerve, although the mechanism by which this occurs is unclear.

The increase in intraocular pressure is due to a decrease in aqueous humor outflow and not increased aqueous humor production (Brubaker 1991). Although the aqueous humor is the nutrient source for the anterior chamber tissues, most of the current drug therapies reduce aqueous humor production rather than increase aqueous humor outflow (Brubaker 1991, Kaufman and Mittag 1994). This is in part due to a lack of understanding of the biochemical aspects of the outflow mechanism.

Etiology of Glaucoma

In primary open-angle glaucoma, the trabecular meshwork has not collapsed, appears normal, and is not blocked by the iris. The mechanism of obstruction is unknown; however, different hypotheses have been proposed (Acott and Wirtz 1996, Allingham et al. 1996, Knepper et al. 1996, Parshley et al. 1996, Umihira et al. 1994). Our working hypothesis is that the decrease in outflow is due to a decrease in the turnover of extracellular matrix, normally maintained by the MMPs in the trabecular meshwork. Trabecular extracellular matrix turnover is relatively rapid. The half-life of trabecular glycosaminoglycans is approximately 1.5 days, while in the adjacent tissues of cornea and sclera it is 7-14 days

57

(Acott et al. 1988). In support of our hypothesis, a sustained upregulation of the MMPs specifically in the trabecular region occurs in response to laser trabeculoplasty, a common treatment for glaucoma (Parshley et al. 1996, Parshley et al. 1995).

Experimental Purpose

Data from an ocular anterior chamber explant organ culture system (Figure 20) to test our hypothesis is presented in this chapter. In this culture system, culture medium fills the anterior chamber and flows through the trabecular meshwork. Preliminary experiments using media containing blue dye had shown that the media flows through the trabecular meshwork into Schlemm's canal (data not shown). The ciliary body has been removed so that there is no aqueous humor production. In this system either flow or pressure can be monitored to assess changes in outflow facility (Erikson-Lamy and Rohen 1991, Johnson and Tschumper 1987).

In order to test our hypothesis that the MMPs and TIMPs are crucial to the maintenance of ocular outflow, we manipulated the MMP and TIMP content of the culture media flowing through the trabecular meshwork in the organ culture system. This was accomplished by either the addition of MMPs or TIMPs, or the addition of modulators of their activity or their production. The effectiveness of the various synthetic metalloproteinase inhibitors was examined concurrently using the FITC conjugated β-casein substrate.

The outflow measurement studies were conducted by John Bradley in the Acott lab. Once the eye explant was mounted in the flow apparatus and its flow had stabilized, the MMPs, TIMPs, and various modulators were tested for their effects on outflow.

58

Perfused Anterior Segment Explant Organ Culture

Perfusion Reservoir

Perfusion Head

Explant in Flow Cell

Facility (C)

C = flow / pressure
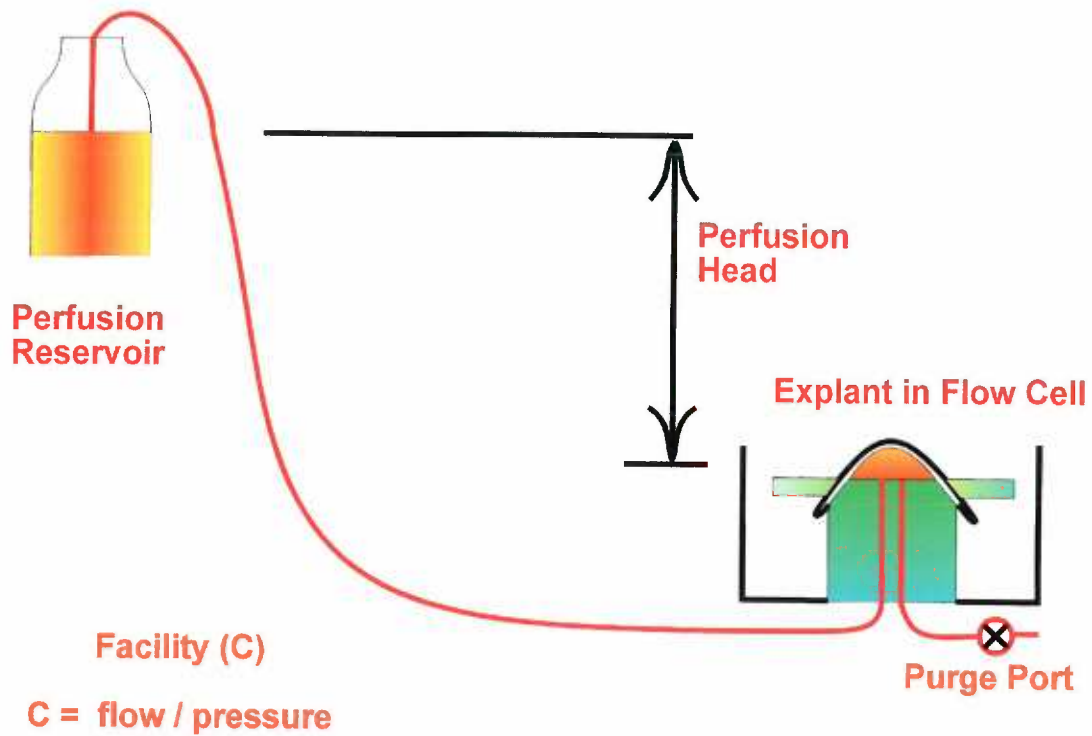
Purge Port

Figure 20

Diagram of flow apparatus showing the media reservoir flowing to the anterior segment, mounted in the flow cell. Also shown is the purge port used to purge the system of test agent in studies where agent was removed at a given time point during the experiment.

RESULTS

MMP Flow Data

The media used in the flow system was serum-free. In all of the plots of flow data, the abscissa represents time in units of hours where 0 hour time is the time of treatment, i.e. the time the agent tested was added to the system. Agents were either injected into the perfusion chamber or added to the reservoir media. The ordinate is the flow rate plotted as a percent of the control outflow facility. The control outflow facility is designated 100% and is determined for each eye after a 3-5 day equilibration period.

The open circles in Figure 21 show that the control protein, bovine serum albumin does not cause a change in outflow facility. However, the addition of a mixture of MMP-2, -3 and -9 (Figure 21, filled circles) shows a resultant increase in outflow facility to approximately 160 %C_0.
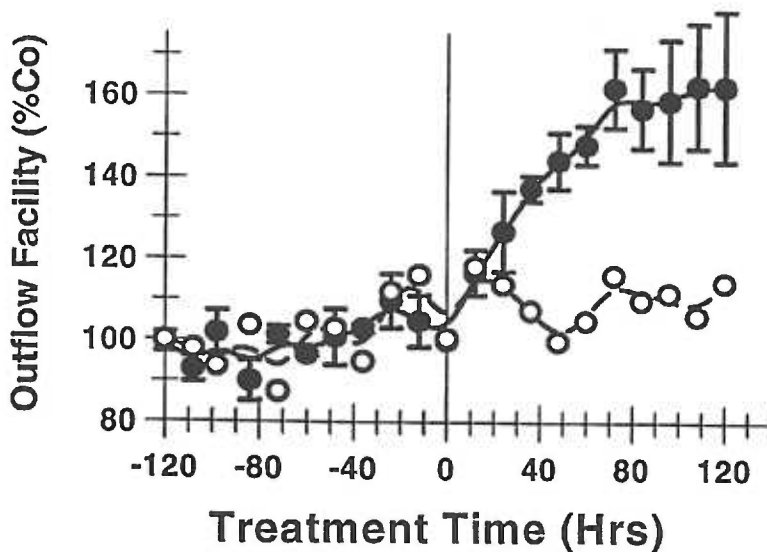
Figure 21 (*Bradley*)
Percent outflow facility as a function of time. Open circles represent bovine serum albumin treated eyes, n=1. Solid circles represent MMP mix treated eyes, n=2. Error bars represent standard error of the mean.

60

Synthetic Inhibitors

RCGVP peptide - This peptide sequence taken from MMP propeptides is a known inhibitor

of MMPs and specifically targets MMP activity. Figure 22 shows the effect on outflow facility

when this peptide is added at 0 hours and removed at 48 hours. At 48 hours the outflow

facility is below 10% C_0. Removal of the peptide (indicated by the arrow) results in rapid

recovery, reaching almost 100% C_0 by 130 hours.
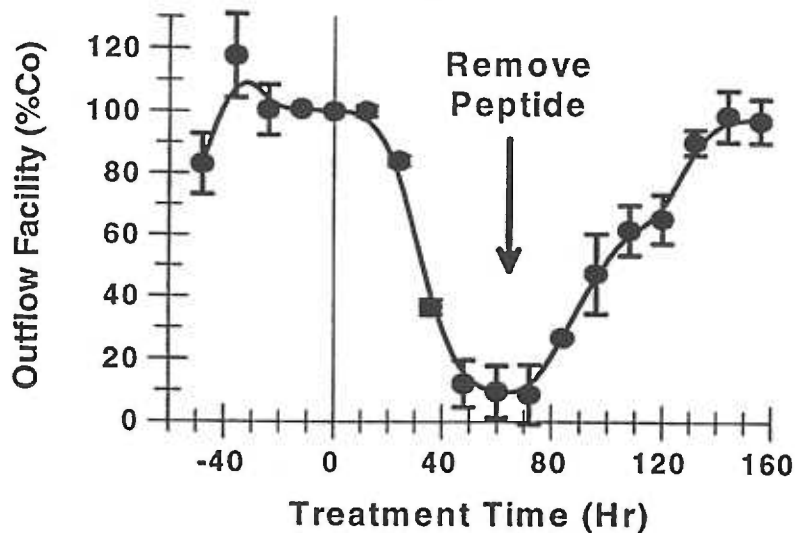
Figure 22 (*Bradley*)- RCGVP peptide
Percent outflow facility as a function of time as it is affected
by the addition of 200μM RCGVP peptide, and its removal,
indicated by the arrow, n=3. Error bars represent standard
error of the mean.

The kinetic activity of the peptide inhibitor was also examined *in vitro* by IC_{50} plots. These are semi-log plots of the initial velocity as a function of the log of inhibitor concentration. The IC_{50} is a function of the K_i and enzyme concentration as well as the inhibitor concentration, and is the concentration of inhibitor required to inhibit 50% of the enzyme activity. Figure 23 is an IC_{50} plot of stromelysin activity on 4 μM FITC-conjugated β-casein as a function of the log of RCGVP peptide concentration. The plot indicates that complete inhibition of stromelysin activity is possible with this peptide. The IC_{50} determined from this plot is 173 μM.
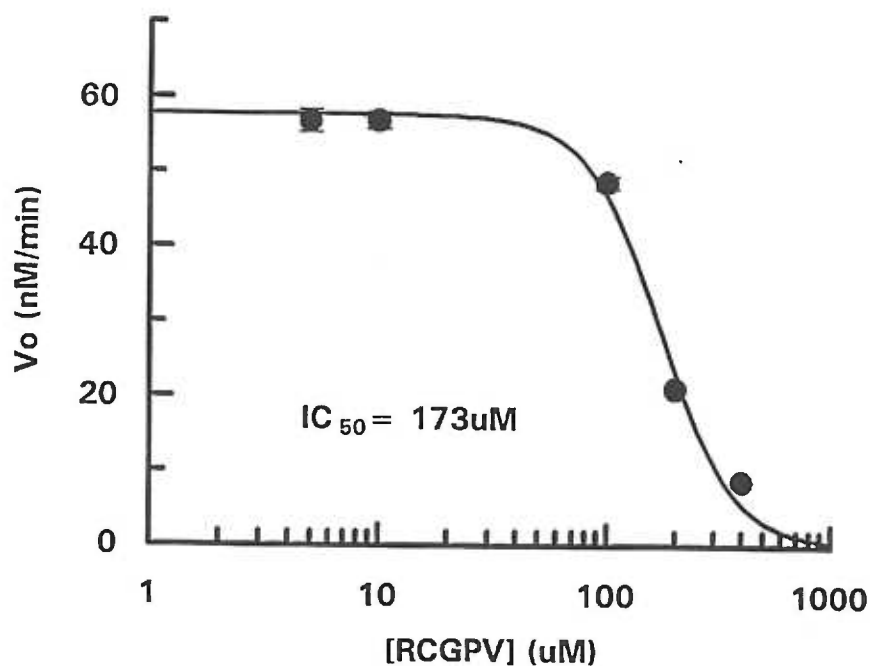
Figure 23
IC_{50} curve of RCGVP inhibition of stromelysin, n=2.
Error bars indicate standard deviation.

Tryptophan Hydroxamate - Another agent tested was tryptophan hydroxamate (Figure 24). This inhibitor is presumed to bind in the active site of stromelysin by coordinating the hydroxamate to the active site zinc atom. Other hydroxamic acid inhibitors have been shown by crystallography to bind to MMPs in this manner (Gooley et al. 1994, Gooley et al. 1993, Van Doren et al. 1993).

Figure 25 shows that tryptophan hydroxamate causes a steady decrease in outflow facility, while the addition of IL-1α (indicated with an arrow) causes an increase in outflow facility in the presence of the inhibitor .
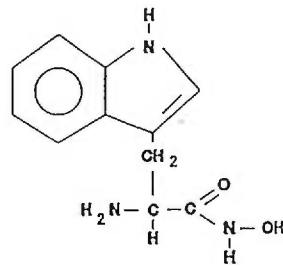
Figure 24
Molecular structure of tryptophan hydroxamate.
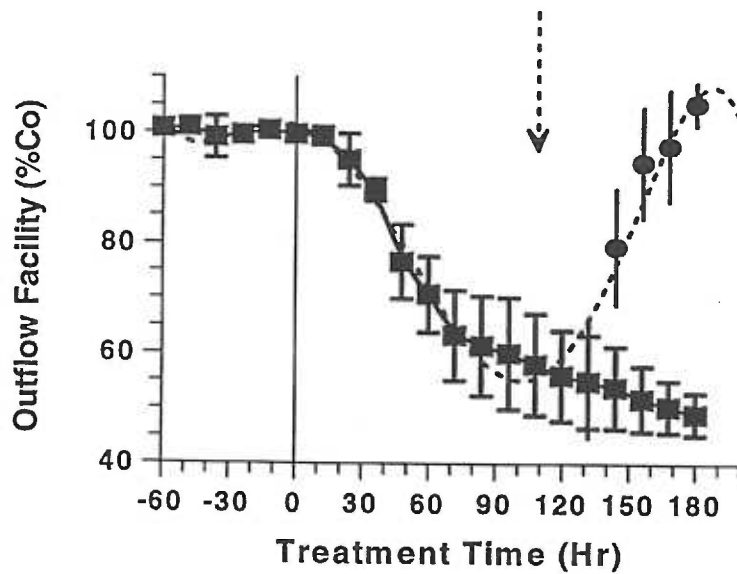
Figure 25 (*Bradley*)
The effect of tryptophan hydroxamate (50 μM) on outflow facility, squares, n=3. Arrow indicates addition of IL-1α (50U/ml), circles, n=4. All error bars represent standard error of the mean.

Data was collected for both an IC_{50} plot and a double reciprocal plot of tryptophan hydroxamate inhibition of caseinolytic activity of stromelysin.

Figure 26
IC$_{50}$ plot of tryptophan hydroxamate inhibition of stromelysin. [s] is 4μM. Error bars indicate standard deviation, n=3-5.

IC$_{50}$ = 187uM
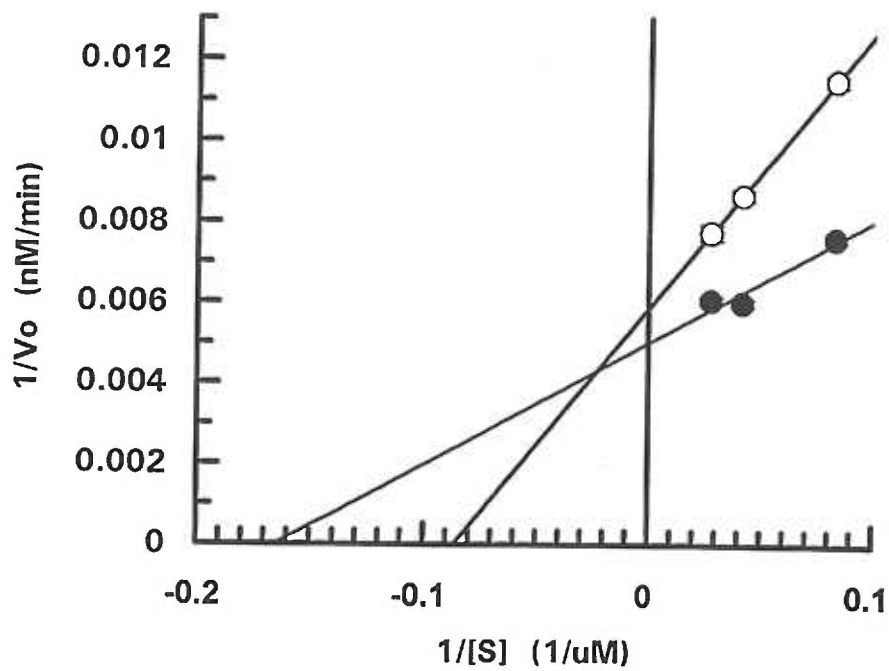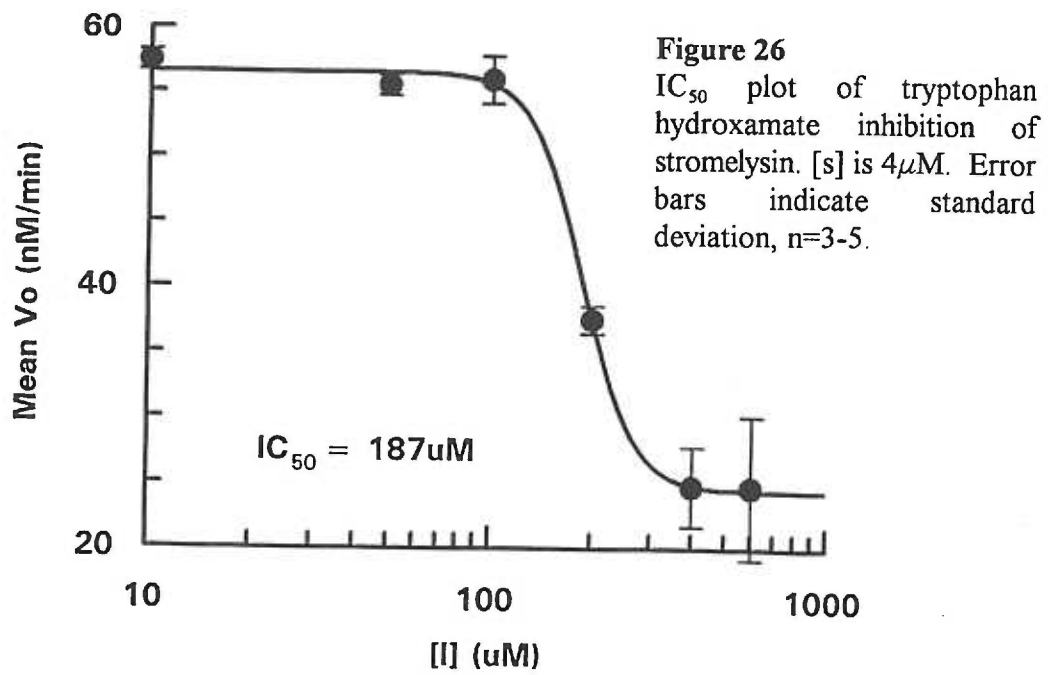
Figure 27
Double reciprocal plots of tryptophan hydroxamate inhibition of stromelysin. Initial velocities in the presence (open circles) and absence (filled circles) of tryptophan hydroxamate. Inhibitor concentration is 100μM, n = 3. Error bars indicate standard deviation on both plots.

64

Unlike the peptide inhibitor, the IC_{50} of tryptophan hydroxamate indicates that complete inhibition does not occur. Only 50% inhibition occurred with the highest concentration of tryptophan hydroxamate. Thus the IC_{50} value determined in this case represents the concentration of tryptophan hydroxamate required to inhibit 50% of the enzyme capable of enzyme/inhibitor interaction. Changes in the intercept and the slope of the double reciprocal plots shown in Figure 27 indicate mixed inhibition.

Minocycline - Minocycline is a tetracycline derivative that inhibits MMPs. Its molecular structure is shown below, Figure 28. Minocycline was tested on the flow system (Figure 29), data for IC_{50} (Figure 31) and double reciprocal (Figure 32) plots were collected, and evaluation by zymography was performed (Figure 30).
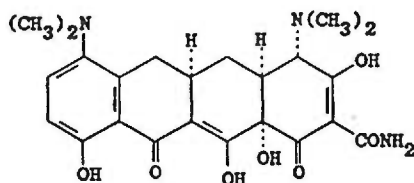
Figure 28
Molecular structure of minocycline

The addition of minocycline to the flow system causes an immediate decrease in flow reaching less than 40% C_0 within 48 hours, and about 30% C_0 at about 6 days. Spectroscopic analysis of the media exiting the eye indicated that the minocycline was retained in the tissue and was gradually released over several days (*Bradley*).

65
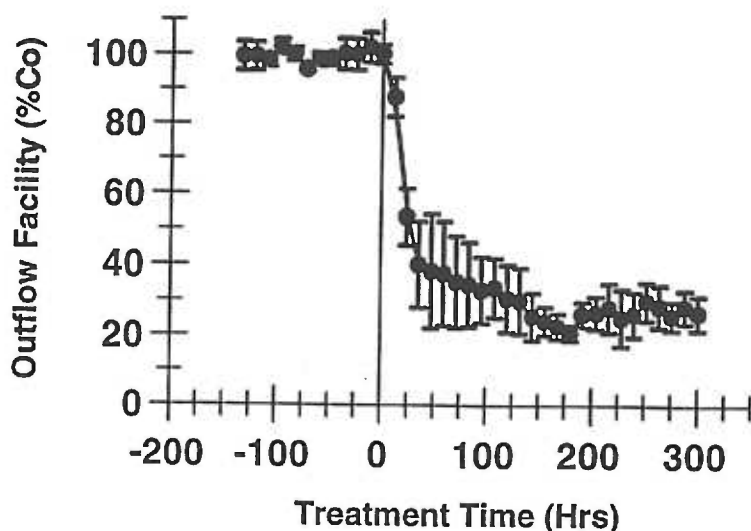
Figure 29 (*Bradley*)
Effect of minocycline (100μM) on outflow facility. Error bars represent standard error of the mean, n=4.

Minocycline inhibition of stromelysin was analyzed by zymography. The data show that addition of increasing amounts of minocycline to the zymogram incubation buffer results in decreasing stromelysin activity. Inhibition of the glycosylated and non-glycosylated forms of stromelysin appears to be equal.

The IC_{50} plot (Figure 31) shows complete inhibition of stromelysin activity with minocycline. Double reciprocal plots shown in Figure 32 show no change in V_{max} and a large change in K_m, characteristic of competitive inhibition.

Figure 30
Negative (top row), and positive (bottom row) images of the strips of the minocycline zymogram showing stromelysin activity and inhibition by minocycline. The images of the strips were adjusted to approximately equal background levels. The micromolar concentration of minocycline present in the incubation buffer is indicated above each negative/positive pair.

66

Minocycline (uM)

0   10   25   50   75   100   150   175   200

Glycocylated
Non-Glycocylated

Glycocylated
Non-Glycocylated
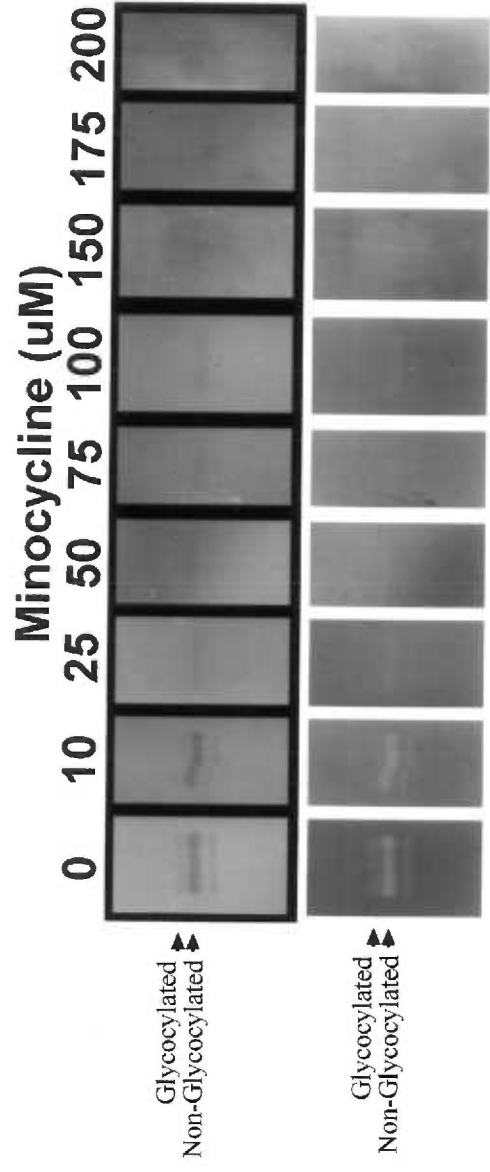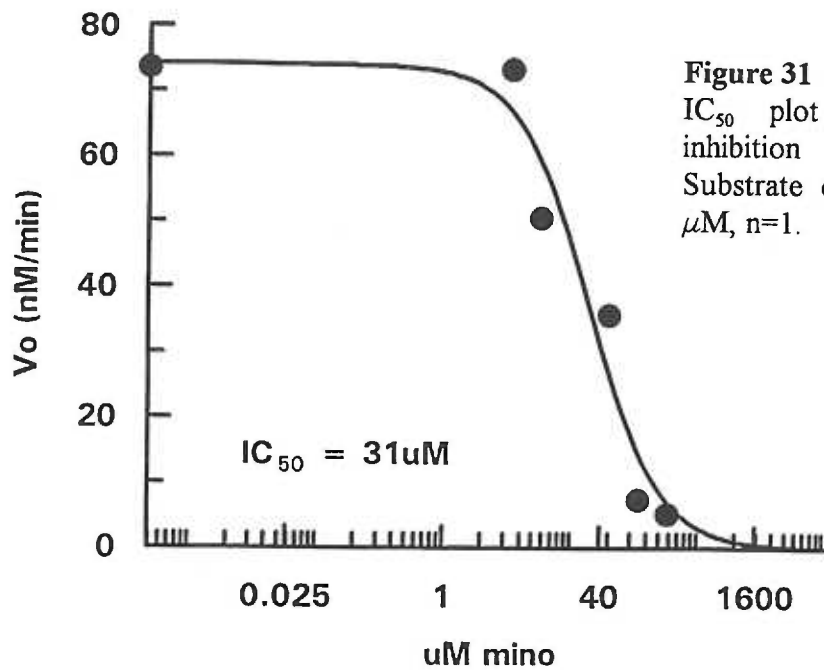
Figure 31
IC$_{50}$ plot of minocycline inhibition of stromelysin. Substrate concentration is 4 μM, n=1.

$$IC_{50} = 31uM$$
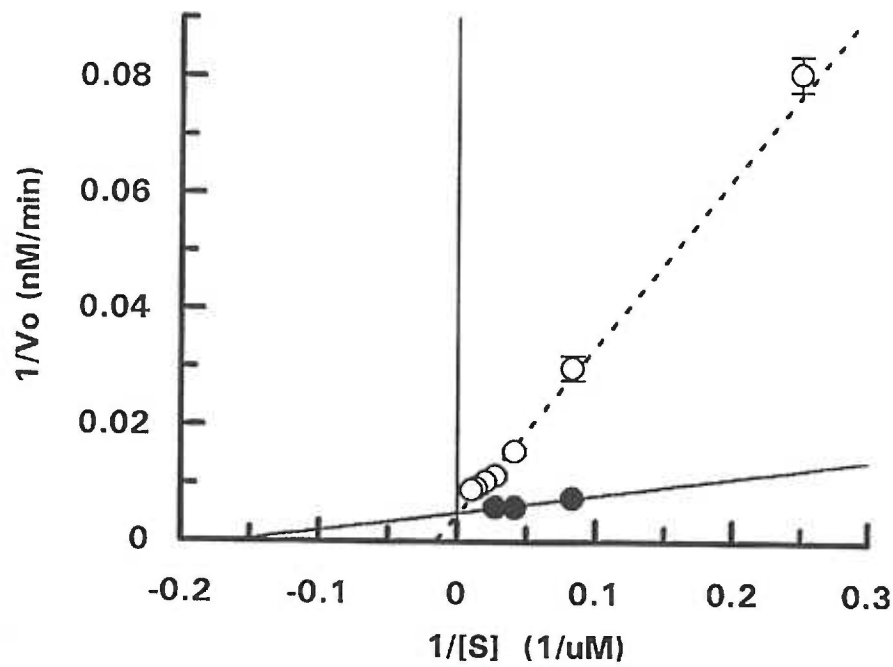
Figure 32
Double reciprocal plots of minocycline inhibition of stromelysin. Minocycline concentration is 100 μM. Error bars represent standard deviation of the data, n=3.

The IC_{50} values that were determined for these inhibitors with stromelysin, MMP-2 and MMP-9 are presented in Table 2. Also in this table are the concentrations of these inhibitors used in the outflow system that caused a decrease in outflow facility.

Table 2 Table of inhibition of metalloproteinases and of outflow.

Inhibitor	Stromelysin IC_{50} (μM)	MMP-2[*] IC_{50} (μM)	MMP-9[*] IC_{50} (μM)	Concentrations used for inhibition of outflow (μM)
Minocycline	31	113.1	101.5	100
Tryptophan hydroxamate	187	57.5	95.5	50
Pro-peptide	173	103.7	115.5	200

[*] measured by J.Vranka

IL-1α and TIMP-2

IL-1α has been previously shown to upregulate stromelysin in cultured trabecular meshwork cells (Samples et al. 1993). Figure 33a shows that the addition of IL-1α to the outflow system results in an increase in outflow facility. Conversely, the addition of TIMP-2 to the flow system results in an initial increase in outflow facility to approximately 120% C_0 followed by a decrease to approximately 50% C_0 (Figure 33b, filled circles). Also plotted in Figure 33b (open circles) is data from the simultaneous addition of TIMP-2 and IL-1α. The concurrent addition results in a gradual decrease in outflow facility, suggesting that TIMP-2 is capable of blocking the IL-1α effect.

69
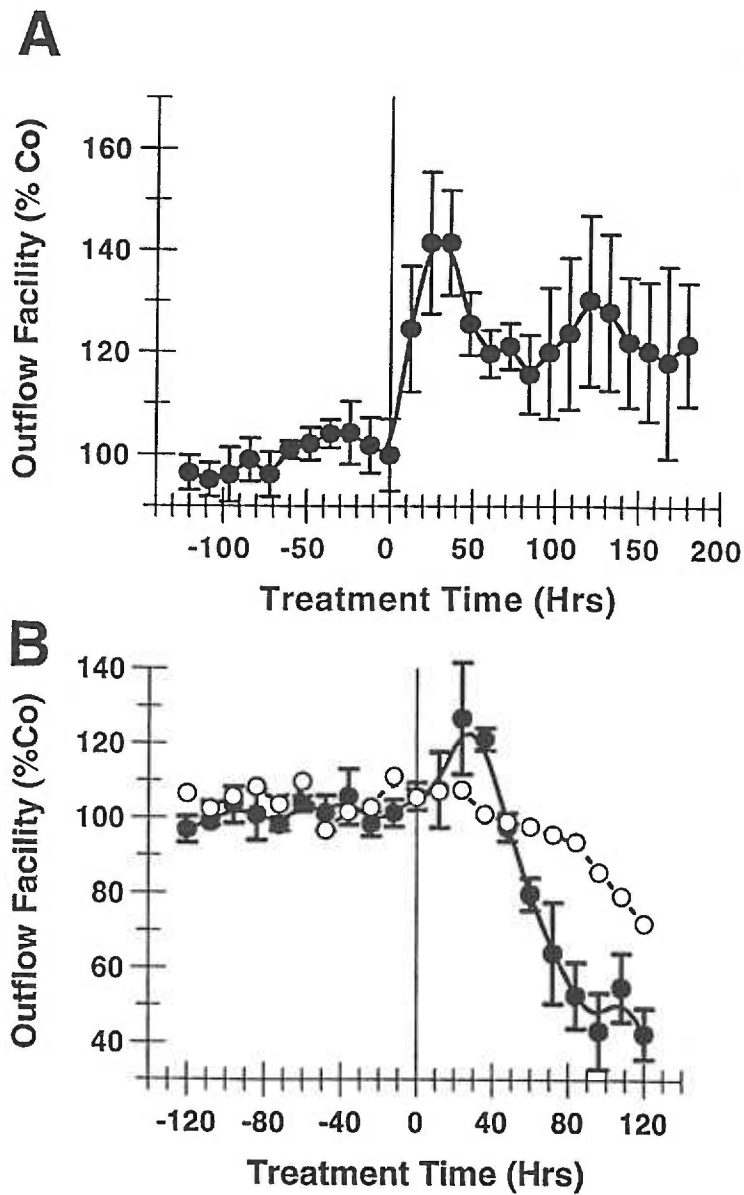
Figure 33
(A) Effect of IL-1α on outflow facility, error bars represent standard error of the mean, n=4. (B) Effect of TIMP-2 on outflow facility, filled circles, error bars represent standard error of the mean, n=3. Effect of simultaneous addition of IL-α and TIMP-2 on outflow facility, open circles, n=1.

70

DISCUSSION

The objective of these experiments was to test the hypothesis that disruption of the balance between the MMPs and TIMPs in the trabecular meshwork causes changes in the outflow facility similar to those seen in primary open angle glaucoma. There is currently no animal model to test this hypothesis. Therefore, we used a primary organ culture system in which a human anterior hemisphere with iris, lens and ciliary body removed was mounted in a flow apparatus (Figure 20). This apparatus allowed us to measure the flow and changes in the flow of media through the trabecular meshwork. Different agents were added to the system and their effects on outflow facility were monitored.

We found that the addition of bovine serum albumin had no substantial effect on outflow facility. This result suggests that any effects that are seen with MMPs or TIMPs are due to functional properties of those molecules, and not merely a generic effect due to the addition of protein.

An increase in the outflow facility was observed when activated MMPs were added to the system. This suggests that MMPs are capable of increasing outflow, but does not address the question of whether they are normally active in trabecular meshwork. A set of experiments targeting the enogenous MMPs present in the trabecular meshwork suggested that the MMPs are present and active.

In these experiments, MMP inhibitors tryptophan hydroxamate (Figure 25), peptide RCGVP (Figure 22), minocycline (Figure 29), or TIMP-2 (Figure 33) were added to the media. All are inhibitors of MMPs, and all had the same effect on outflow. The addition of any of the inhibitors resulted in a decrease in outflow. This suggested that the MMPs are

71

active in the trabecular meshwork, and that this activity is involved in maintaining outflow facility.

It has been shown that IL-1α causes a marked increase in the amount of MMP secreted by trabecular meshwork cells (Samples et al. 1993). The addition of IL-1α to the flow system results in an increase in outflow facility, Figure 33a. We interpret the increase to approximately 140 %C_0 as the result of increased MMP production in the trabecular meshwork. The increased outflow facility then levels off at approximately 125 %C_0.

While the IL-1α data supports the hypothesis, it does not implicate the MMPs and TIMPs specifically, since IL-1α can have other effects. To test more specifically for an MMP effect, TIMP-2 was added concurrently to attempt to block the IL-1α effect. First, the filled circles in Figure 33b show that the addition of TIMP-2 alone caused a significant decrease in outflow facility. The open circles in Figure 33b show that the presence of TIMP-2 suppresses the increase in outflow facility seen when only IL-1α is added (Figure 33a), and then causes a continuous decrease in outflow facility to well below 100 %C_0. This suggests that the IL-1α effect is MMP-based.

All of the inhibitors used in the flow system had been tested for their activity against stromelysin, as well as MMP-2 and MMP-9 (Vranka 1997). The TIMP-2 and RCGVP peptide data is perhaps the most compelling since they are, of all of the agents tested, the most specific for MMP activity. The bovine serum albumin control experiment had shown that addition of even a large protein has no effect on outflow, making it difficult to argue that the TIMP-2 or the small peptide, RCGVP, is acting non-specifically.

Although it is not shown here, it should be noted that all of the effects were reversible with the exception of the decrease in outflow facility due to minocycline. The reversibility of all effects suggests that the tissue is able to recover from treatment. The irreversibility of minocycline is likely due to retention of minocycline by the tissue which has been observed spectroscopically in the media exiting the eye.

Also not presented here is histology data generated by John Bradley in which the cells of the trabecular meshwork were stained to detect both living and dead cells. These data show that the cells in the trabecular meshwork are alive after being in the flow cell for several days.

The kinetic studies supplementing the outflow experiments showed that inhibition of the MMPs occurred at the molecular level. The IC_{50} data for the inhibition of stromelysin suggests that minocycline inhibits 50% of the stromelysin at approximately 1/6 the concentration that would be required of tryptophan hydroxamate or the peptide RCGVP (Table 2).

The double reciprocal plots indicate that the minocycline inhibition affects the K_m without affecting k_{cat} (Figure 32). These effects are characteristic of competitive inhibition. Double reciprocal plots of tryptophan hydroxamate inhibition show effects of K_m and k_{cat} which is characteristic of mixed inhibition (Figure 27).

CONCLUSIONS

While it is fairly well established that the primary outflow pathway is through the trabecular meshwork, the process by which that pathway is blocked is not clear. Here we have shown that the addition of MMPs to the system medium causes an increase in outflow through the trabecular meshwork. Conversely, there is a resultant decrease in ocular outflow facility upon the addition of MMP inhibitors, tryptophan hydroxamate, minocycline and auto-inhibitory domain peptide, to our culture system. The addition of TIMP-2 to the system also results in a significant decrease in outflow facility. While outflow facility increases with the addition of IL-1α, a known inducer of MMPs in trabecular meshwork cells, this increase could be blocked by the concurrent addition of TIMP-2, suggesting that the IL-1α effect is MMP-based. Taken together, these experiments support the hypothesis that the MMPs are involved in maintenance of outflow facility in an open angle.

KINETIC AND THERMODYNAMIC STUDIES

WITH PEPTIDE SUBSTRATE, NFF3

- ▸Stromelysin kinetics

- ▸Experimental design

- ▸Results and Discussion

- ▸Conclusions

STROMELYSIN KINETICS

We observed non-linear Arrhenius plots of stromelysin activity with protein substrate. Subsequently, we performed studies with a peptide substrate with similar results. This lead us to believe that the non-linearity was not due to the protein substrate, but that it was more likely due to some characteristics of stromelysin.

Scheme 1 is a proposed kinetic mechanism for stromelysin based on observations of trypsin-activated stromelysin activity on substance P analog, RPKPNNFFGL(Nle)-NH$_2$ (Harrison et al. 1992). Four different protonation states of the enzyme are represented by E, EH, EH$_2$ and EH$_3$. The substrate and product are represented by S and P, respectively. In Harrison's study, k_{cat}/K_m was determined at a substrate concentration of 28 μM where 0.4 mM $< K_m <$ 1.2 mM (dependent on pH) and by applying equation 5. The plot of k_{cat}/K_m as a function of pH ranging from pH 5.0 to 10.0 resulted in a peak at approximately pH 6.0 with a shoulder of about 50% relative activity level at pH 8.0. The initial velocity as a function of pH data was fit to Equation 1 to yield 3 pK$_a$ values: 5.4, 6.1 and 9.5.

$$
\begin{array}{lll}
\text{Scheme 1} & \text{EH}_3 & \\
& K_{a3}\updownarrow \qquad (k_c/K_m)_2 & \\
& \quad \text{EH}_2 + \text{S} \quad \rightleftharpoons \quad \text{EH}_2 + \text{P} \\
& K_{a2}\updownarrow \qquad (k_c/K_m)_1 & \\
& \quad \text{EH} + \text{S} \quad \rightleftharpoons \quad \text{EH} + \text{P} \\
& K_{a1}\updownarrow & \\
& \quad \text{E} &
\end{array}
$$
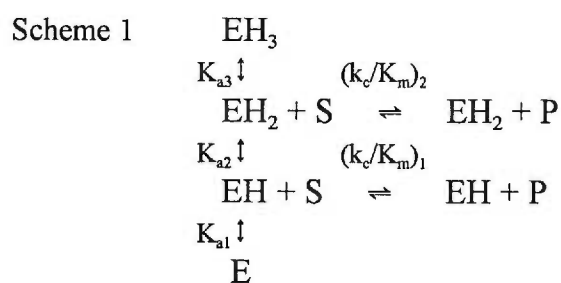
$$(k_{cat}/K_m)_{obs} = \frac{(k_{cat}/K_m)_2}{\dfrac{[H^+]}{K_{a3}} + 1 + \dfrac{K_{a2}}{[H^+]} + \dfrac{K_{a1}K_{a2}}{[H^+]^2}} + \frac{(k_{cat}/K_m)_1}{\dfrac{[H^+]^2}{K_{a3}K_{a2}} + \dfrac{[H^+]}{K_{a2}} + 1 + \dfrac{K_{a1}}{[H^+]}} \qquad \text{(Eq. 1)}$$

Equation 1 is the mathematical representation of Scheme 1. While this is the form in which the equation can be utilized, its significance is not very obvious. However, rewriting the acid dissociation constants of Equation 1 in terms of their molecular concentration components, i.e. $K_a = [E][H]/[EH]$, yields Equation 2:

$$(k_{cat}/K_m)_{obs} = \frac{(k_{cat}/K_m)_2}{\dfrac{[EH_3]}{[EH_2]} + 1 + \dfrac{[EH]}{[EH_2]} + \dfrac{[E]}{[EH_2]}} + \frac{(k_{cat}/K_m)_1}{\dfrac{[EH_3]}{[EH]} + \dfrac{[EH_2]}{[EH]} + 1 + \dfrac{[E]}{[EH]}} \qquad \text{(Eq. 2)}$$

The right-hand side of Equation 2 simplifies to Equation 3:

$$(k_{cat}/K_m)_{obs} = \frac{[EH_2]}{[E]_T}(k_{cat}/K_m)_2 + \frac{[EH]}{[E]_T}(k_{cat}/K_m)_1 \qquad \text{(Eq. 3)}$$

where $[E]_T$ is total enzyme concentration ($[E] + [EH] + [EH_2] + [EH_3]$).

Thus, the denominators on the right side of Equations 1 and 2 determine the concentration of each of the two active enzyme forms, $[EH_2]$ and $[EH]$ as a fraction of total enzyme concentration. These equations suggest that the k_{cat}/K_m observed is the sum of two k_{cat}/K_m values and that the contribution of each is dependent on the proton concentration and the relevant acid dissociation constants as they pertain to $[EH]$ and $[EH_2]$.

The pK$_a$ values may be due to protons of either substrate residues, or residues of the enzyme or one of each. The possibility of any substrate effect was eliminated by Harrison et al. when the use of three other substance P variants resulted in no significant change in the pK$_a$ values. This lead them to the conclusion that the three pK$_a$ values could be attributed to residues of the enzyme, although the pK$_a$ values were not attributed to specific residues.

At the time of the studies of Harrison et al. (Harrison et al. 1992) no peptide substrate with high solubility and high specific activity for stromelysin was available . A high substrate concentration in this context is determined by the K$_m$. High solubility allows the study of kinetic activity at substrate concentrations well over the K$_m$. This is important because if the substrate solubility is so poor that experiments can only be done in the [S] << K$_m$ range, then only the ratio of k$_{cat}$/K$_m$ can be determined. This determination is made indirectly from the observed initial velocities and applying Equation 5.

First, Michaelis-Menten kinetics is assumed:

$$E+S \rightleftharpoons ES \rightarrow E+P$$

$$v_o = \frac{[E][S]k_{cat}}{K_m + [S]} \quad \text{(Eq. 4)}$$

and if [S]<<K$_m$, then

$$v_o = \frac{[E][S]k_{cat}}{K_m} \quad \text{(Eq. 5)}$$

Since [E] and [S] are known, and v_o is determined experimentally, the ratio of k_{cat}/K_m can be calculated.

Since poor substrate solubility prevents the determination of the individual kinetic constants, a more detailed understanding of these constants is impossible. Thus the effects that different conditions have on the enzyme activity can not be attributed to an effect of one or the other or both constants.

In 1994 Nagase et.al. published a paper describing a peptide substrate, NFF3. They had reported solubility up to 250 μM with k_{cat}/K_m values of 218,000 $M^{-1}s^{-1}$ for stromelysin, 10,100 $M^{-1}s^{-1}$ for MMP-9, and undetectable activity for MMP-1 and MMP-2 (all at 37 °C, pH 7.5) (Nagase et al. 1994). NFF3 is a peptide conjugated to a fluorophore, methoxycoumarin (Mca), and a fluorescence quencher, DNP (Figure 34b). The Mca fluroescence is quenched by resonance energy transfer to DNP. A schematic representation of the resonance energy transfer is shown in Figure 34a. Proteolysis of the NFF3 Glu-Nva bond by stromelysin releases the Mca from the DNP, thereby liberating the fluorophore from the quenching agent and resulting in an increase in detectable fluorescence. Due to the nature of this substrate, the reaction can be fluorometrically monitored continuously, and k_{cat} can be determined independently of K_m because of its high solubility. The purpose of this section was to determine the thermodynamic parameters of the observed k_{cat} and to test whether or not the thermodynamic behavior is in agreement with Scheme 1.

A
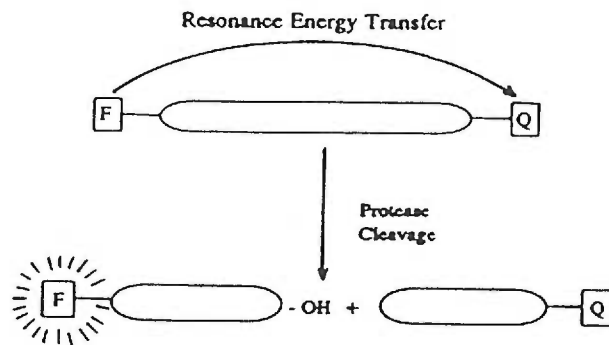
B
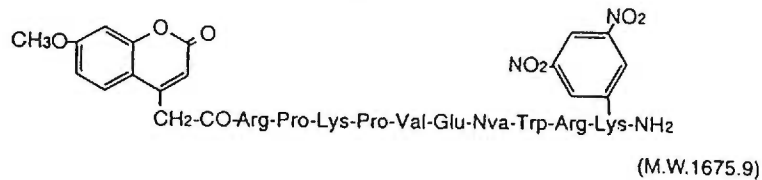
Figure 34

(A) Schematic representation of resonance energy transfer used in the fluorescence quench-release assay of NFF3. (B) Molecular structure of NFF3 showing the fluorophore group, Mca, and the quenching molecule DNP.

80

EXPERIMENTAL DESIGN

The temperature dependence of an enzyme reaction provides thermodynamic information about steps of a kinetic mechanism. The experiments in this section were performed using the peptide substrate NFF3 and heat-activated stromelysin (Biogenesis, Inc.) unless otherwise stated. Initial velocities, v_o, were determined at several concentrations of NFF3 and were measured in fluorescence units per second, then converted to molar concentration per second as described in *Methods*.

The high solubility of NFF3 permitted the determination of observed k_{cat} values. We had hypothesized that if the mechanistic scheme of stromelysin resembled that of Scheme 1 with two parallel pathways to product that are separated from one another by proton ionization, then the thermodynamic plots of the observed k_{cat} should show characteristic features of Scheme 1.

The Arrhenius plot is a plot of the natural log of k_{cat} versus the reciprocal of temperature. In the case of a simple mechanism, such as the Michaelis-Menten mechanism, an Arrhenius plot of the data will generally yield an almost linear plot. If the mechanism is more complex, then the plot may deviate from linearity. This may occur if each of the potentially rate determining steps in the complex mechanism have different temperature dependencies. Later we will discuss other possible causes of non-linear Arrhenius plots.

In a parallel mechanism resembling Scheme 1, we had hypothesized that at proton concentrations near K_{a2}, the Arrhenius plots would show the characteristic non-linearity of a complex mechanism, and that shifting the proton concentration away from K_{a2} would decrease the degree of non-linearity.

81
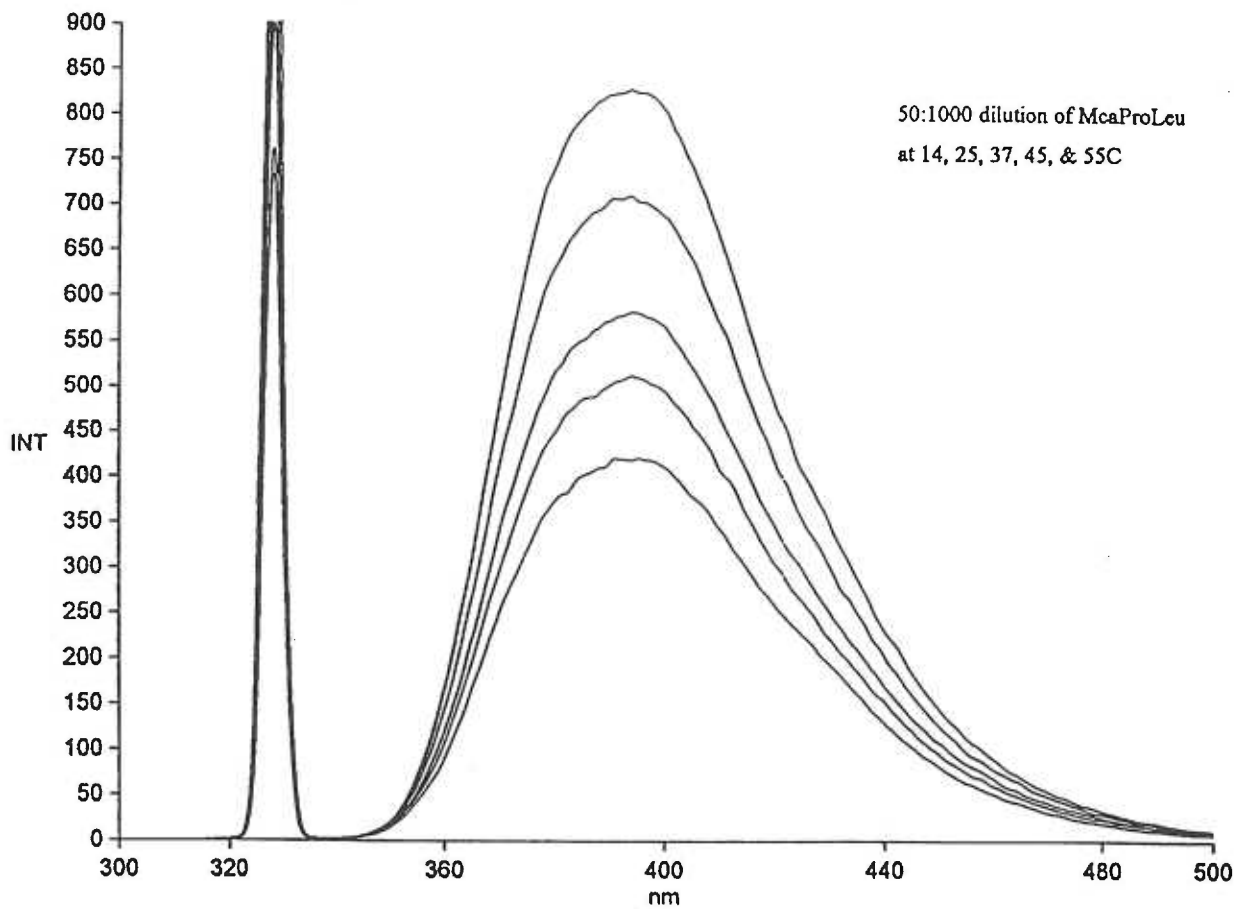
Figure 35
Fluorescence emissions spectra of a single sample of McaProLeu peptide at five different temperatures (14, 25, 37, 45 and 55 °C) showing fluorescence decreases as temperature increases. Spectra are from 300nm to 500nm with intensity (INT) measured in fluorescence units. Excitation wavelength of 328nm was used.
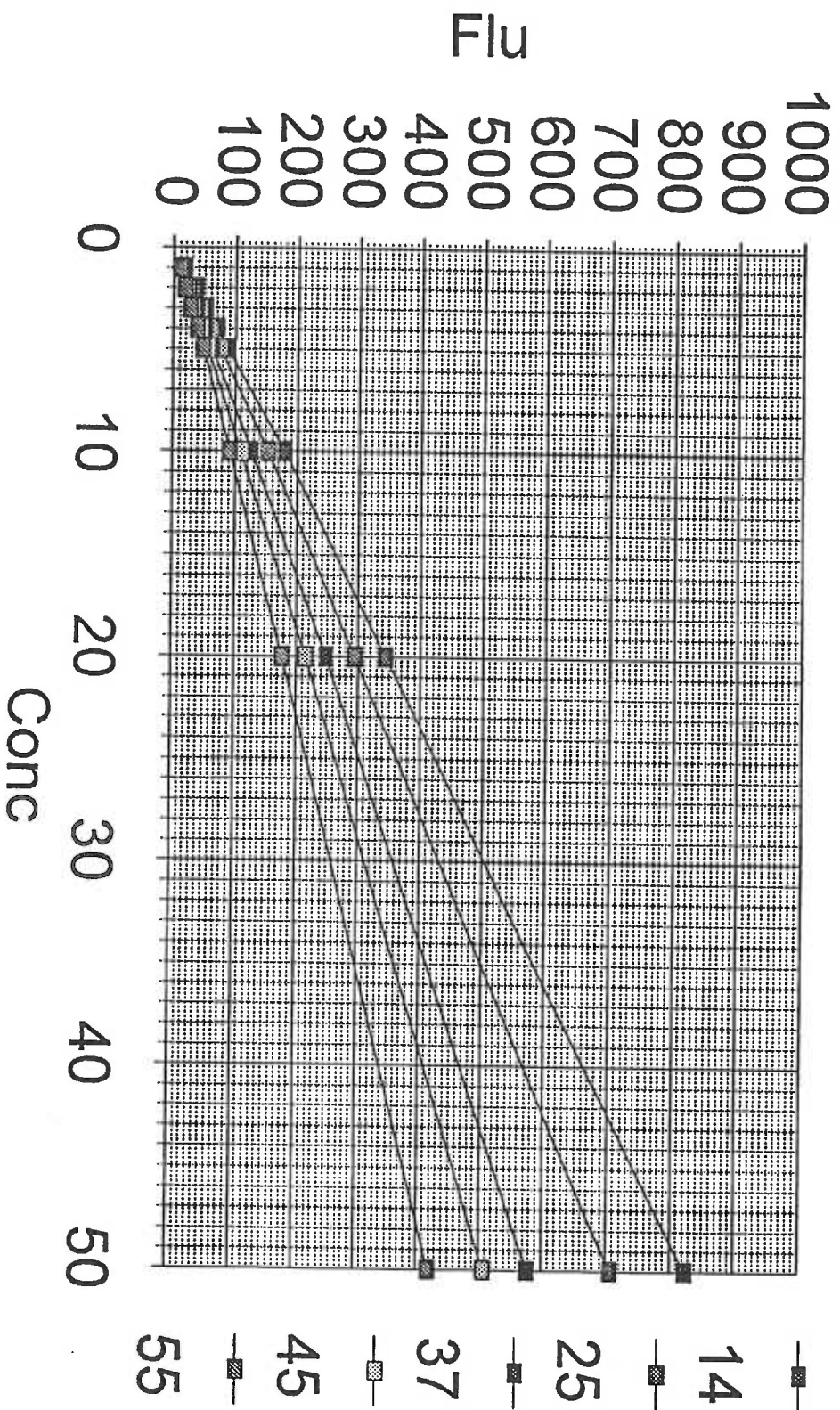
Figure 36 Plot of fluorescence intensity at 393 nm as a function of relative concentration of McaProLeu peptide at five different temperatures (14, 25, 37, 45 and 55 °C). At each peptide concentration a single sample was prepared and its fluorescence measured at each temperature.

In addition to the effects of temperature, another common characteristic of fluorescent molecules is self-quenching. Self-quenching, or filter effect, occurs at increasing concentrations of the fluorophore (Lakowicz 1983). The effect on progress curve fluorescence is shown in Figure 37. Due to self-quenching, the progress curve for 50 μM NFF3 appears below that of 20 μM at the same enzyme concentration. If the self-quenching is not accounted for, these slopes would imply that the activity on 20 μM substrate is better than that on 50 μM substrate. Substrate inhibition could cause such an effect; however, the reactions followed to completion result in a lower final fluorescence for the 50 μM NFF3. This was true whether complete conversion to product was performed by stromelysin or trypsin, suggesting that the decreased fluorescence was not due to substrate inhibition.
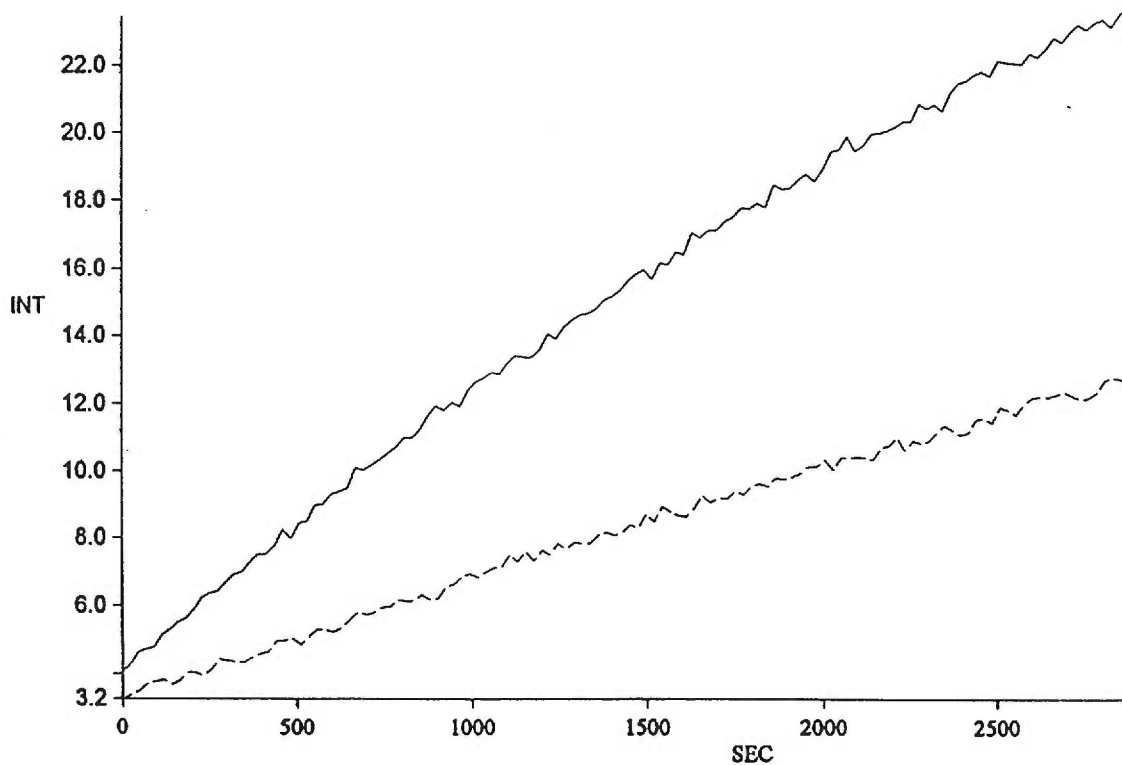
Figure 37
Progress curves demonstrating the self-quench effect of NFF3. Both curves are at the same enzyme concentration and at 20 μM (—) and 50 μM (- -) NFF3 concentrations.

The extent of NFF3 degradation in the absence of enzyme was also examined and is represented by the dotted line in Figure 38. This experiment demonstrated that the extent of degradation in the absence of enzyme was negligible.
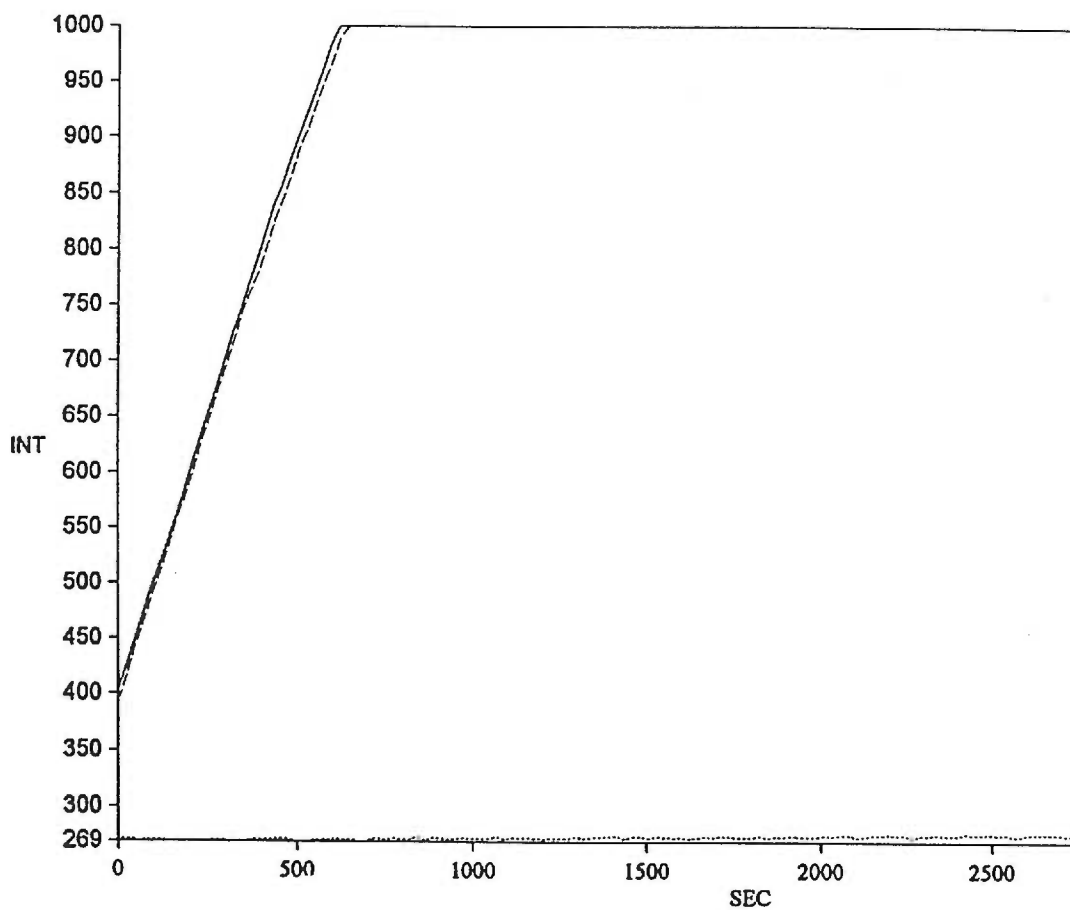
Figure 38
Progress curves of NFF3 peptide substrate in the presence (—) and (- -), and absence (···) of stromelysin.

Figure 39 shows representative progress curves, fluorescence as a function of time, for stromelysin activity with NFF3. The initial slopes of the progress curves were used to determine initial velocity. Generally these slopes corresponded to the curve from 0-600 seconds or less. The conversion from fluorescent units to molar concentration units is described in *Methods*.
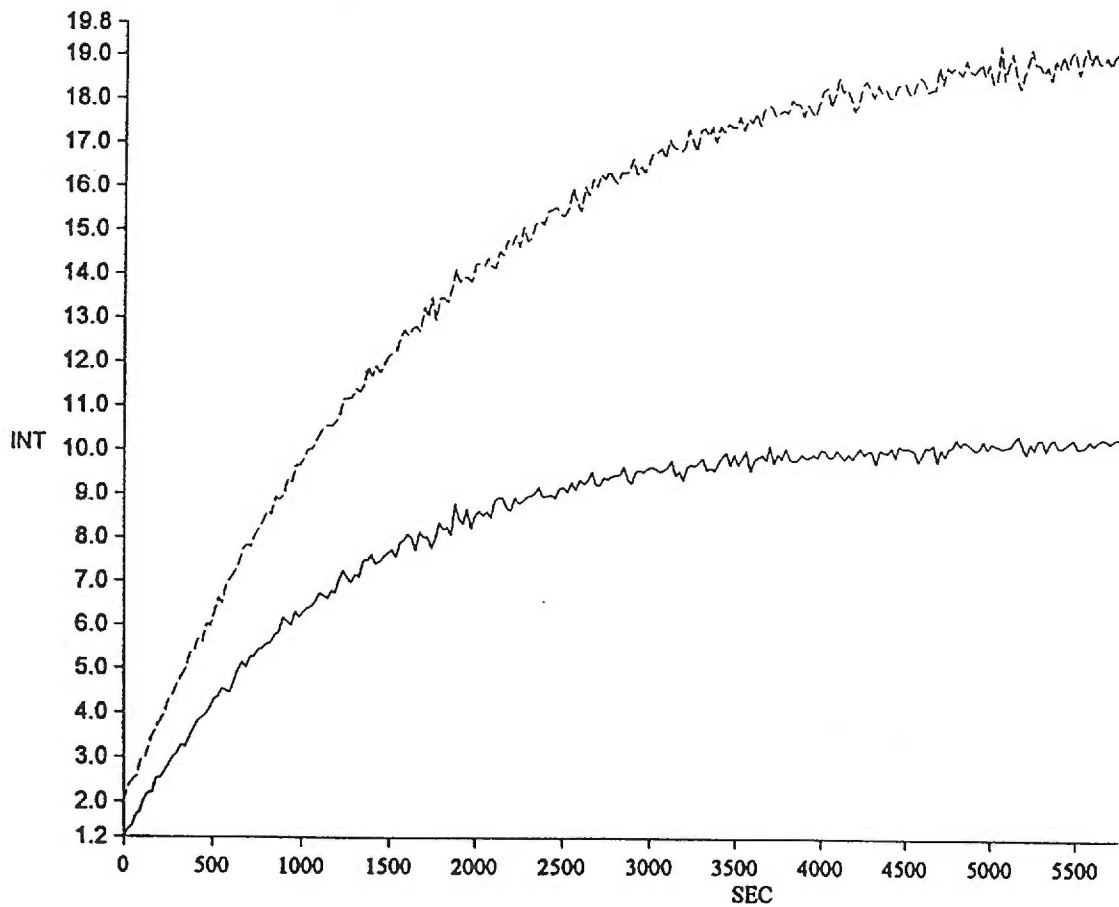
Figure 39

Representative progress curve of stromelysin activity on NFF3 plotted in fluorescence units as a function of time. Initial velocity is determined from the initial slope and fluorescence units are converted to molar concentration.

When NFF3 was developed by Nagase et al., they reported the k_{cat} and K_m values for stromelysin activity on NFF3 at pH 6.0 and pH 7.5 at 37 °C. Interestingly while the k_{cat}/K_m from these studies was found to be greater at pH 6.0 than pH 7.5 (302,000 and 218,000 $M^{-1}s^{-1}$ respectively), the increase was an effect of K_m. In fact, the k_{cat} at pH 6.0 was less than half that at pH 7.5 (2.20 and 5.40 s^{-1}, respectively). These values were obtained from double reciprocal plots of activity using a substrate range of 2.5 - 75 μM NFF3 (Nagase et al. 1994) with sodium acetate (pH 6.0) and Tris (pH 7.5) buffers.

Our kinetic studies were conducted using NFF3 with a Tris (pH 7.5 and 8.0) buffer and a mixture of Tris and Tris-maleate (pH 6.0). These buffers were chosen in order to minimize buffer differences at different proton concentrations. It has previously been shown that a mixture of Tris and Tris-maleate yields similar activity to that of MES buffer at the same pH (Wilhelm et al. 1993). By using the Tris/Tris-maleate buffer at pH 6.0 instead of MES or sodium acetate, we minimized the difference in buffer conditions between reactions conducted at pH 6.0 and those conducted at pH 7.5 and 8.0 with Tris buffer.

The k_{cat} and K_m values can be calculated from plots of $[s]/v_o$ as a function of $[s]$ (Hanes plots). The slope of the Hanes plot gives the reciprocal V_{max} value, and the x-intercept gives the negative K_m value. Figure 40 shows the resultant Hanes plots at pH 7.5 at 20, 25, 32, 37, 40 and 45 °C. The initial velocities at each substrate concentration are plotted as averaged values with error bars while linear fits were performed using individual velocity values to give equal weight to each point. The k_{cat} and K_m values obtained from these plots by least squares fitting of the data are presented in Table 3. These values were used in the subsequent thermodynamic analyses. Note that the k_{cat} increases with increasing temperature,

but that the K_m behavior appears much less predictable. However, a van't Hoff plot of $1/K_m$ (Figure 41), shows that there is a pattern of behavior indicating an optimum temperature for K_m of approximately 32 °C. This pattern is also apparent in the "K_m" column of Table 3.

The k_{cat} values presented in Table 3 were used to generate Arrhenius and Eyring plots. These plots correlate the reaction rates at different temperatures to yield thermodynamic parameters.
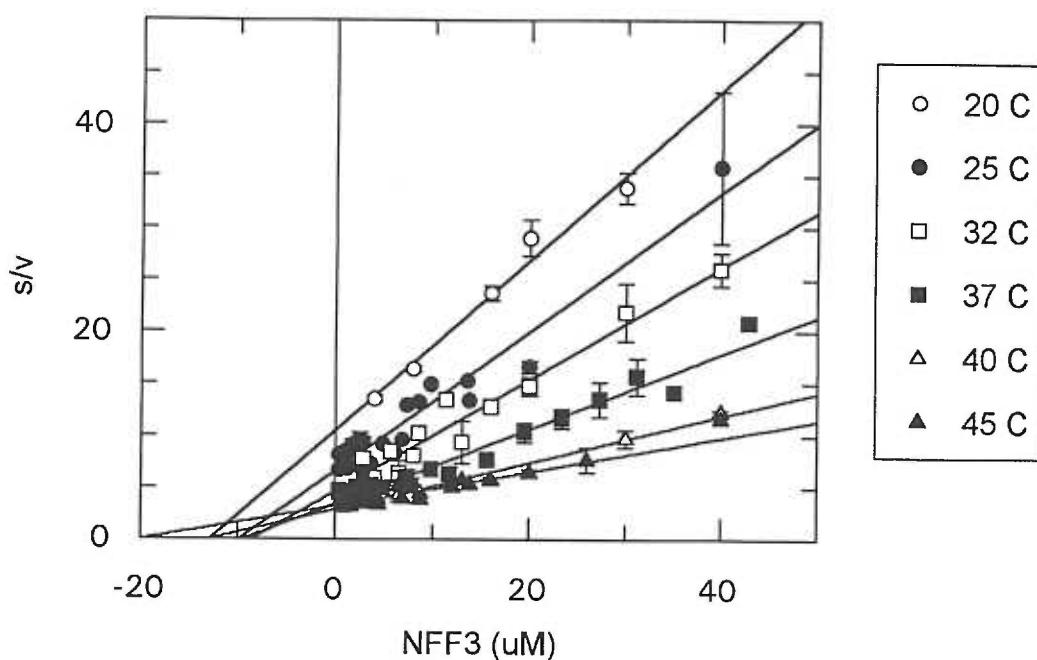
Figure 40
Hanes plots of stromelysin activity on
NFF3 at 20, 25, 32, 37, 40 and 45 °C
in Tris pH 7.5 buffer. Error bars
represent standard error of the mean,
n=1-9.

89

Hanes Plot Constants		
	pH 7.5	
°C	k_c	K_m
20	1.223	12.88
25	1.496	9.90
32	1.918	8.59
37	2.774	9.5
40	4.45	12.87
45	6.112	19.78

Table 3
The kinetic constants determined from the Hanes plots in Figure 40 are presented. The k_c values have units of s^{-1}, and K_m values have units of μM.

Figure 41
Van't Hoff plot of K_m values observed at pH 7.5.

90
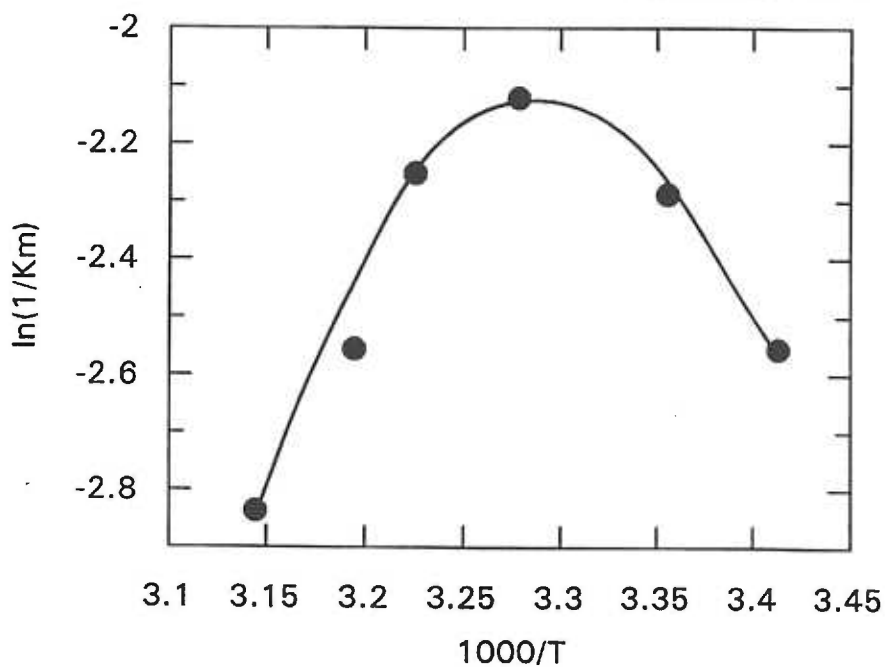
Arrhenius plot

Arrhenius was interested in the influence of temperature on kinetic observations. The Arrhenius plot is based on the Arrhenius rate equation (Equation 6),

$$k_c = Ae^{-E_a/RT} \quad \text{(Eq. 6)}$$

Where k_c is k_{cat}, A is the Arrhenius frequency factor, E_a is what Arrhenius called the *activation energy*, R is the gas constant and T is the Kelvin temperature. The transition state theory relates the frequency factor, A, to the transition state entropy according to Equation 7:

$$A = \frac{k_b T}{h} e^{\Delta S^{\ddagger}/R} \quad \text{(Eq. 7)}$$

where k_b is the Boltzmann constant, h is Planck's constant and $\Delta S^{\ddagger}$ is the transition state entropy. The transition state theory dictates that the transition state enthalpy is equal to:

$$\Delta H^{\ddagger} = E_a - RT \quad \text{(Eq. 8)}$$

Applying this relationship and substituting the right side of Equation 7 for A in Equation 6 gives:

$$k_c = \frac{k_b T}{h} e^{\Delta S^{\ddagger}/R} e^{-\Delta H^{\ddagger}/RT} \quad \text{(Eq. 9)}$$

Expressed as a natural log function, Equation 9 gives the equation:

$$\ln(k_c) = -\Delta H^\ddagger/RT + \Delta S^\ddagger/R + \ln(k_b T/h) \quad \text{(Eq. 10)}$$

Equation 10 correlates to the Arrhenius plot where y is the $\ln(k_c)$ and x is $1/T$.

One can see that the determination of the transition state enthalpy and entropy is not easily extracted from Equation 10. They would be most directly determined from an Arrhenius plot by using the natural log form of Equation 6 shown below:

$$\ln(k_c) = -E_a/RT + \ln A \quad \text{(Eq. 11)}$$

which can be related to the linear equation $y = mx + b$, where y is the $\ln(k_c)$; $-E_a/R$ is the slope, m; $1/T$ is x; and $\ln A$ is the intercept. Hence from the Arrhenius plot, E_a and A can be determined and subsequently $\Delta H^\ddagger$ can be determined using Equation 8 and $\Delta S^\ddagger$ can be determined using Equation 12:

$$\Delta S^\ddagger = R\ln(ANh/RT) - R \quad \text{(Eq. 12)}$$

where N is Avagadro's number.

An alternative to the Arrhenius plot is an Eyring plot of k_{cat}. The advantage of the Eyring plot is that the transition state thermodynamic parameters are determined directly from the plot without the need for additional equations. The equation used for the Eyring plot is developed below.

Eyring Plot

The reaction rate constant, k_{cat}, is related to the transition state equilibrium constant by the equation:

$$k_c = (k_b T/h) K^{\ddagger} \quad \text{(Eq. 13)}$$

where $K^{\ddagger}$ is the transition state equilibrium constant. The $\ln K^{\ddagger}$ is related to the the transition state Gibb's free energy, $\Delta G^{\ddagger}$, as:

$$\Delta G^{\ddagger} = -RT \ln K^{\ddagger} \quad \text{(Eq. 14)}$$

where R is the gas constant.

Expressing the inverse natural log function of Equation 14, and solving for $K^{\ddagger}$ gives:

$$K^{\ddagger} = e^{-\Delta G^{\ddagger}/RT} \quad \text{(Eq. 15)}$$

Substituting the right side of Equation 15 for $K^{\ddagger}$ in Equation 13 gives the relationship between the transition state Gibb's free energy and the reaction rate constant, k_{cat}.

$$k_c = \frac{k_b T}{h} e^{-\Delta G^{\ddagger}/RT} \quad \text{(Eq. 16)}$$

Isolating the inverse natural log function gives:

$$\frac{k_c h}{k_b T} = e^{-\Delta G^{\ddagger}/RT} \quad \text{(Eq. 17)}$$

93

Separating the $\Delta G^{\ddagger}$ in Equation 17 into the enthalpy and entropy components gives:

$$\frac{k_c h}{k_b T} = e^{-\Delta H^{\ddagger}/RT} e^{\Delta S^{\ddagger}/R} \quad \text{(Eq. 18)}$$

Expressing Equation 18 as a natural log function gives the Eyring equation for the relationship of k_{cat} to the transition state thermodynamic parameters:

$$\ln\frac{k_c h}{k_b T} = \frac{-\Delta H^{\ddagger}}{RT} + \frac{\Delta S^{\ddagger}}{R} \quad \text{(Eq. 19)}$$

Equation 19 can be related to the equation of a line, $y = mx + b$, where the ln function represents y, $-\Delta H^{\ddagger}/R$ is m, $1/T$ is x and $\Delta S^{\ddagger}/R$ is b. Therefore, from a plot of $\ln(k_c h/k_b T)$ as a function of $1/T$, the $\Delta H^{\ddagger}$ and $\Delta S^{\ddagger}$ can be determined and $\Delta G^{\ddagger}$ can be determined at any given temperature. By incorporating the Planck and Boltzmann constants into the natural log function, the transition state enthalpy and entropy values are attained more directly as compared with the Arrhenius plot and equation which yield the activation energy and the Arrhenius frequency factor. Therefore, although Arrhenius plots were generated, the thermodynamic parameters were determined from the Eyring plots. One can see, however, that Equation 11, (the final form of the Arrhenius equation) using transition state theory, would yield Equation 19. Therefore, values determined from either plot should be the same.

Figure 42 shows the Arrhenius (a) and Eyring (b) plots using k_{cat} values from Table 3 at pH 7.5. Both figures show non-linearity. Linear regression was performed on the three lower temperatures of each plot yielding values of 6.65 kcal/mol for the activation energy in

(a), and 6.046 kcal/mol for the enthalpy in (b). Linear regression was also performed on the

three higher temperatures of each plot yielding values of 18.88 kcal/mol for the activation

energy in (a) and 18.063 kcal/mol for the enthalpy in (b).
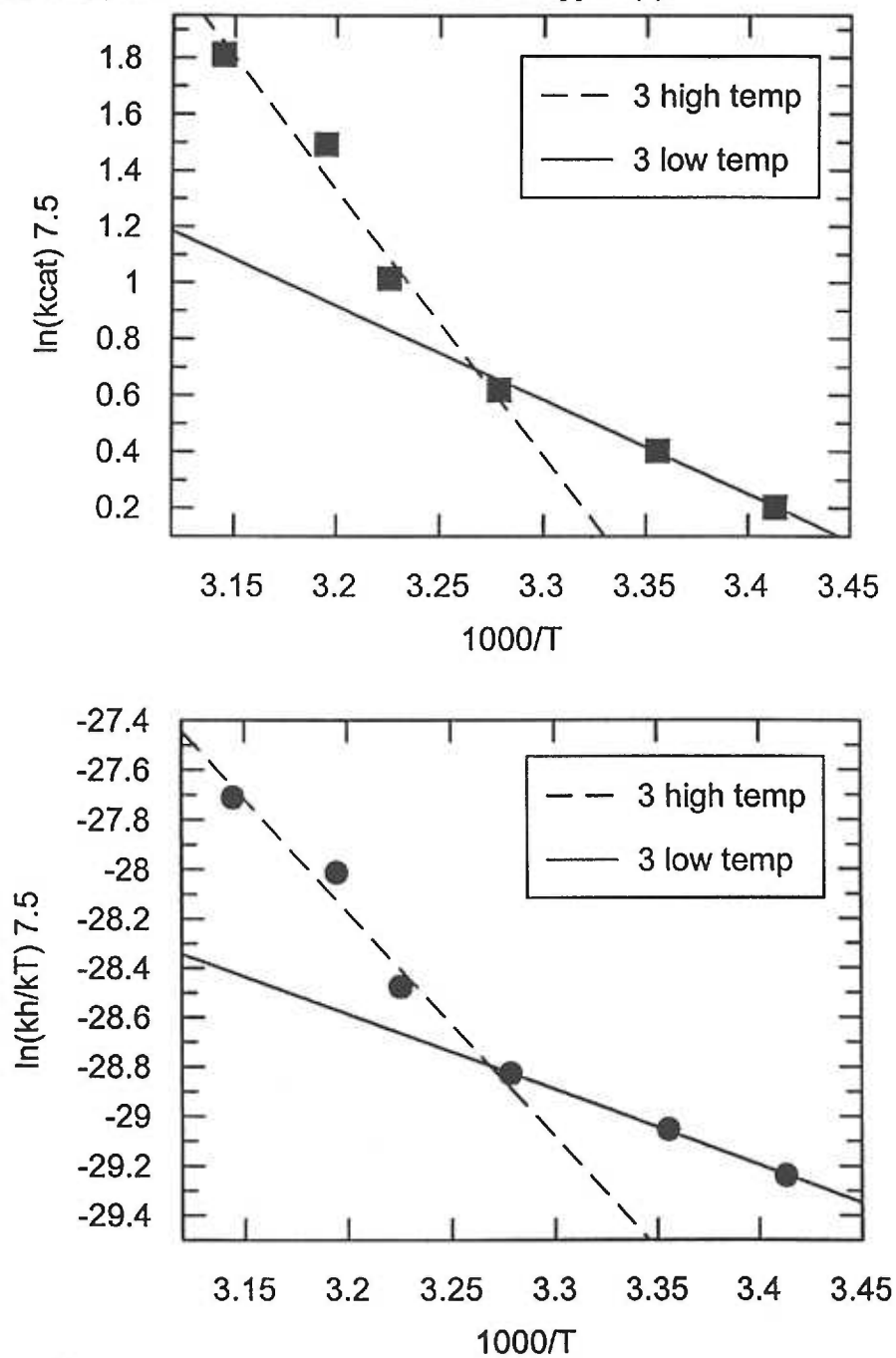
Figure 42

a) Arrhenius plot of k_{cat} data listed in Table 3. b) Eyring plot of the same data.

Stromelysin denaturation can be eliminated as the cause of the curvature since the activity is increasing more rapidly at higher temperatures rather than decreasing. There are, however, at least two possible explanations for the non-linearity of these plots. In the Arrhenius and Eyring treatments shown above, $(\partial \Delta H^{\ddagger}/\partial T)_p$ is set equal to zero, i.e. the transition state enthalpy is treated as though it is independent of temperature. However, if this is not equal to zero, the Arrhenius and Eyring plots would be non-linear. While temperature dependence of $\Delta H^{\ddagger}$ may exist, thermodynamics only defines this dependence in terms of the heat capacity which itself can have a temperature dependence (Blandamer et al. 1982).

In order to determine if the non-linearity of the Arrhenius and Eyring plots is due to a temperature dependent change in the heat capacity, $\Delta C_p^{\ddagger}$, of a simple Michaelis-Menten-like mechanism, $\Delta G^{\ddagger}$ is set equal to a second order polynomial equation (Blandamer et al. 1982, Izquierdo and Stein 1990):

$$\Delta G^{\ddagger} = a + bT + cT^2 \quad \text{(Eq. 20)}$$

and plotted as a function of temperature. Figure 43 shows the $\Delta G^{\ddagger}$ of k_{cat} as a function of temperature. Fitting this data to Equation 20 yielded the values of a, b and c, which are -112,256, 829 and -1.32, respectively.

The values of $\Delta C_p^{\ddagger}$, $\Delta H^{\ddagger}$ and $\Delta S^{\ddagger}$ are then calculated according to Equations 21, 22 and 23 (Blandamer et al. 1982).

$$\Delta C_p^{\ddagger} = -2cT \quad \text{(Eq. 21)}$$

$$\Delta H^{\ddagger} = (a-cT^2) - T\Delta C_p^{\ddagger} \quad \text{(Eq. 22)}$$

$$\Delta S^{\ddagger} = (-b-2cT) - \Delta C_p^{\ddagger}(\ln T) \quad \text{(Eq. 23)}$$

96
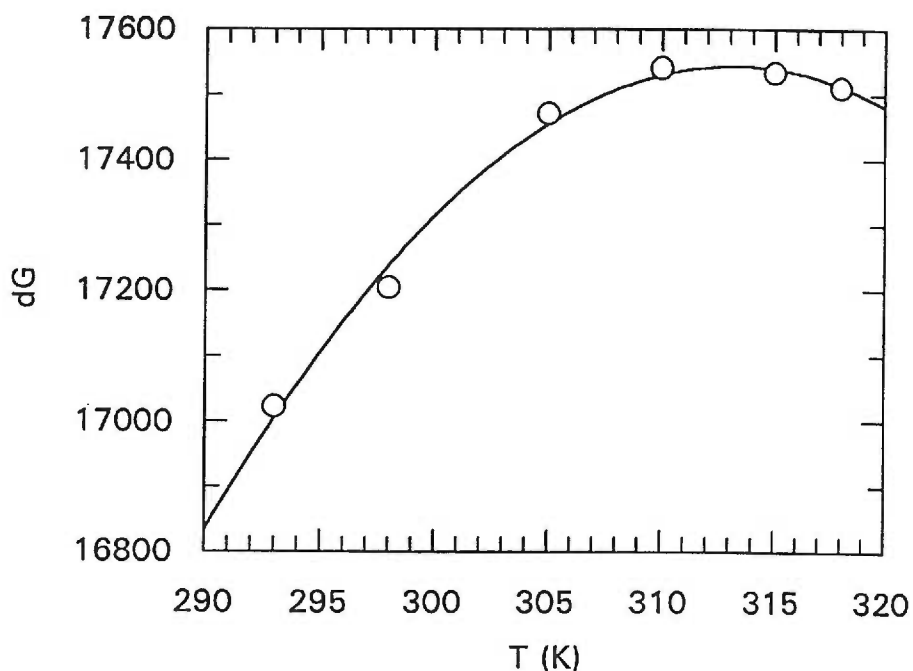
Figure 43

Plot of $\Delta G^{\ddagger}_{pH7.5}$ as a function of Kelvin temperature. $\Delta G^{\ddagger}_{pH7.5}$ was calculated from the k_{cat} values listed in Table 3 using Equation 18 and the relationship $\Delta G^{\ddagger} = \Delta H^{\ddagger} - T\Delta S^{\ddagger}$.

The thermodynamic parameters were calculated at 310 K giving values of 821 cal/mole·K for $\Delta C_p^{\ddagger}$, -239,577 cal/mole for $\Delta H^{\ddagger}$ and -4,712 cal/mole·K for $\Delta S^{\ddagger}$.

These values of $\Delta H^{\ddagger}$ and $\Delta S^{\ddagger}$ suggest large conformational changes much like those seen in protein folding or unfolding (Mathews and van Holde 1990). Much smaller values are anticipated for typical enzyme-substrate transition state parameters.

97

Another reason that the Arrhenius and Eyring plots may be non-linear is if the reaction mechanism deviates from simple Michaelis-Menten kinetics ($E + S \rightleftharpoons ES \rightarrow E + P$). If the mechanism contains two or more rate constants, each with a different temperature dependence, then Arrhenius and Eyring plots of k_{cat} could be non-linear. This possibility is interesting in light of Scheme 1 which has been proposed for stromelysin. If the mechanistic scheme of stromelysin resembles that of Scheme 1, it may explain the non-linearity seen in the pH 7.5 Arrhenius and Eyring plots. We would hypothesize that if the reaction mechanism resembles that of Scheme 1, then manipulation of the pH of the reaction may allow for selectively favoring one of the parallel reactions over the other, and in so doing, decreasing the non-linearity of the Arrhenius and Eyring plots relative to the pH 7.5 plots.

Since NFF3 has allowed the determination of an observed k_{cat} independently of K_m, the analysis requires an extension of Scheme 1 that separates each of the two k_{cat} components from their respective K_m. Without deviating from the proposed mechanism of Scheme 1, we can extend the catalytic reactions to give Scheme 2:

Scheme 2 EH_3

$$K_{a3}\updownarrow \qquad K_{m2} \qquad k_{c2}$$
$$EH_2 + S \rightleftharpoons EH_2S \rightarrow EH_2 + P$$
$$K_{a2}\updownarrow \qquad K_{m1} \qquad k_{c1}$$
$$EH + S \rightleftharpoons EHS \rightarrow EH + P$$
$$K_{a1}\updownarrow$$
$$E$$
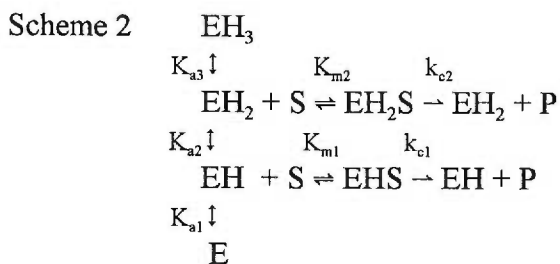
We arrive at Scheme 2 by extending the two horizontal reactions of Scheme 1 from $(k_{cat}/K_m)_1$ and $(k_{cat}/K_m)_2$ to their simple Michaelis-Menten forms. In Scheme 2, the two active forms of the enzyme, EH and EH_2, are separated from one another by the acid dissociation constant, K_{a2}, as they are in Scheme 1. The active enzyme forms are separated from the inactive forms by K_{a1} and K_{a3} as they are in Scheme 1. To help minimize the complexity of the mechanism, we have made the assumption that it is only the substrate-free forms of the enzymes that undergo the protonation or deprotonation reactions. We have assumed that there is no protonation or deprotonation of EHS or EH_2S, respectively.

Examining Scheme 2, we see that there are two active forms of stromelysin, EH and EH_2, and two inactive forms, E and EH_3. In this model, each differs from the other primarily in their protonation states. The two active forms are proposed to have distinct k_{cat} and K_m values. The pH of the environment and the pK_a values determine the proportional contribution of each enzyme form. According to Scheme 2, it would be anticipated that at some proton concentrations that straddle the two parallel reactions, both reaction rates would contribute significantly to the observed rate. It is under these conditions that non-linear Arrhenius and Eyring plots would be predicted based on the rate constants having different transition state enthalpies and entropies. According to Scheme 2, it would also be anticipated that as the pH is shifted to favor one or the other of the two active enzyme forms, the contribution of the second k_{cat} is decreased and the non-linearity would be less pronounced.

If, at pH 7.5, both of the two parallel reactions contribute significantly to the observed rate, and the reaction rates have different temperature dependencies, then non-linear Arrhenius and Eyring plots would be expected. According to Scheme 2, it may also be

99

possible that as the pH of the reaction is shifted away from 7.5, the degree of non-linearity would decrease. To test this hypothesis, data was collected to generate Arrhenius and Eyring plots of the k_{cat} values determined at pH 6.0 and 8.0.

Figure 44 shows the Hanes plots at 25, 32, 37, 40 and 45 °C at pH 6.0, and Table 4 lists the kinetic constants. The k_{cat} values were then used to generate Arrhenius (Figure 45a) and Eyring (Figure 45b) plots, which gave values of 8.96 kcal/mol and 8.32 kcal/mol for the activation energy and transition state enthalpy, respectively.

As predicted by Scheme 2 and the Arrhenius assumption of $(\partial \Delta H^{\ddagger}/\partial T)_{p}=0$, the non-linearity of the pH 6.0 Arrhenius and Eyring plots is less than that of pH 7.5. This is in agreement with a pH-based shift toward k_{cat2} of Scheme 2 with a decrease in the number of stromelysin molecules progressing via k_{cat1}. The result can be interpreted as an observed reaction rate where the major contributing component is k_{cat2} with a minor contribution from k_{cat1}. The reaction now approaches a simple Michaelis-Menten-like mechanism that has a single k_{cat}. Consequently, the Arrhenius and Eyring plots become more linear.

Figure 46 shows the Hanes plots from 25, 32, 37, 40 and 45 °C at pH 8.0. And in Table 5 the kinetic constants obtained from these plots are listed. These values were used to generate the Arrhenius (Figure 47a) and Eyring (Figure 47b) plots for pH 8.0. The activation energy and transition state enthalpy determined from these graphs were 20.9 kcal/mol and 20.3 kcal/mol, respectively. Shifting to the slightly more alkaline pH 8.0, results in an Eyring plot (Figure 47b) with an R value of -0.995 compared to an R value of -0.966 for pH 6.0, suggesting greater linearity. This is consistent with k_{cat1} of Scheme 2 being the predominant rate constant contributing to the observed k_{cat} at this pH at all temperatures plotted.

100

Figure 44
Hanes plots of stromelysin activity on NFF3 at 25, 32, 37, 40 and 45 °C in Tris/Tris-maleate buffer at pH 6.0. Error bars represent standard error of the mean, n=2-3.
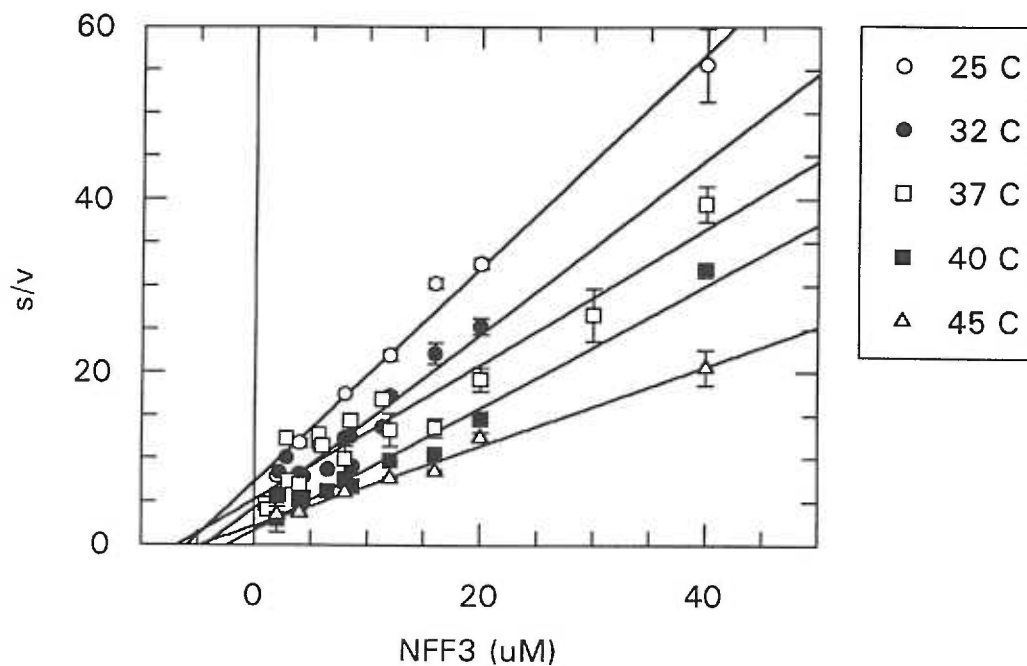
Hanes Plot Constants		
	pH 6.0	
°C	k_c	K_m
25	0.807	5.91
32	0.995	4.30
37	1.277	6.71
40	1.410	2.39
45	2.168	4.83

Table 4
The kinetic constants determined from the Hanes plots in Figure 44 are presented. The k_c values have units of s^{-1}, and K_m values have units of μM.
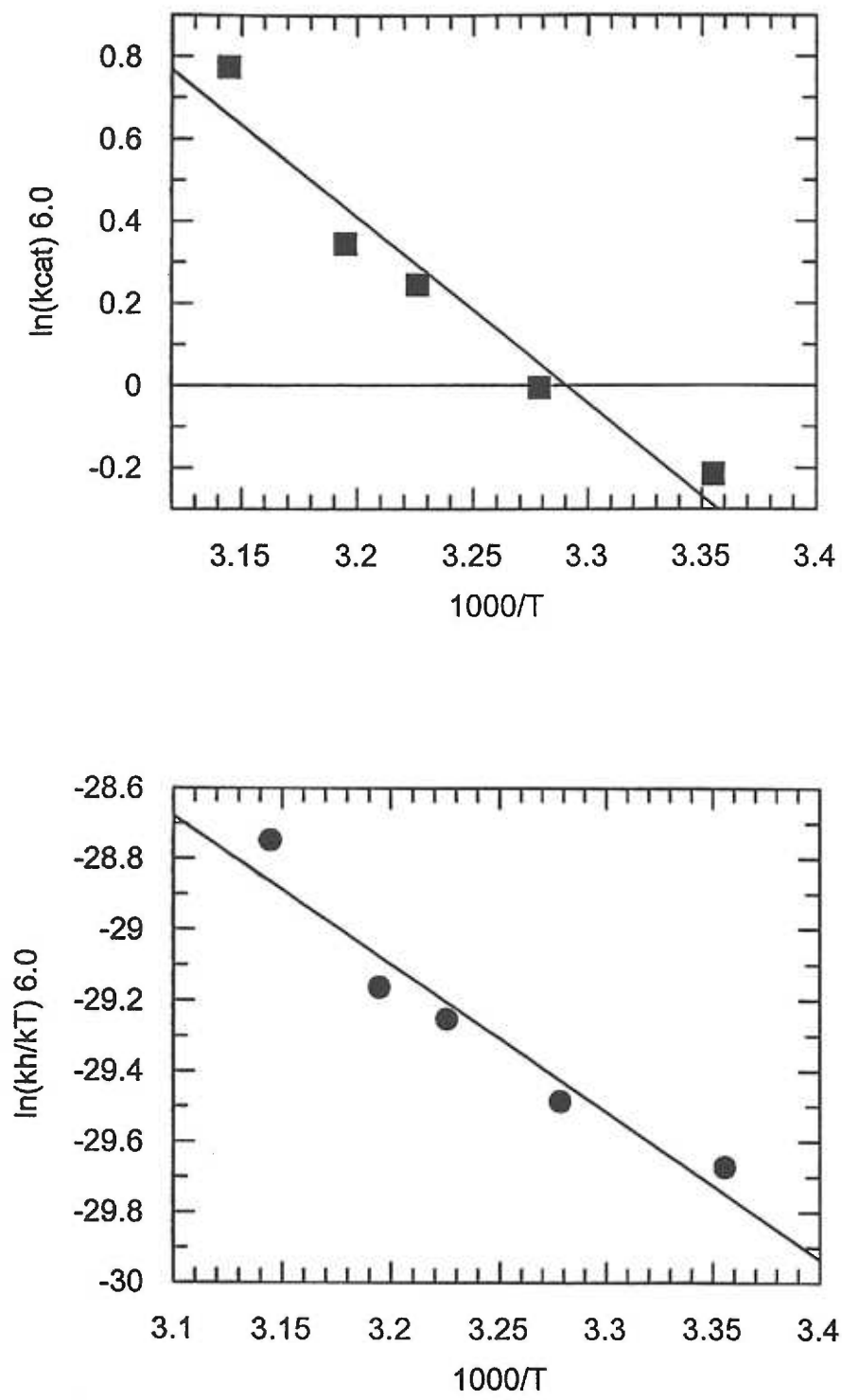
Figure 45
Arrhenius (a) and Eyring (b) plots of the k_{cat} values at pH 6.0 presented in Table 4.

Figure 46

Hanes plot of stromelysin activity on NFF3 at 25, 32, 37, 40 and 45 °C, all in Tris buffer pH 8.0. Error bars represent standard error of the mean, n=2-3.
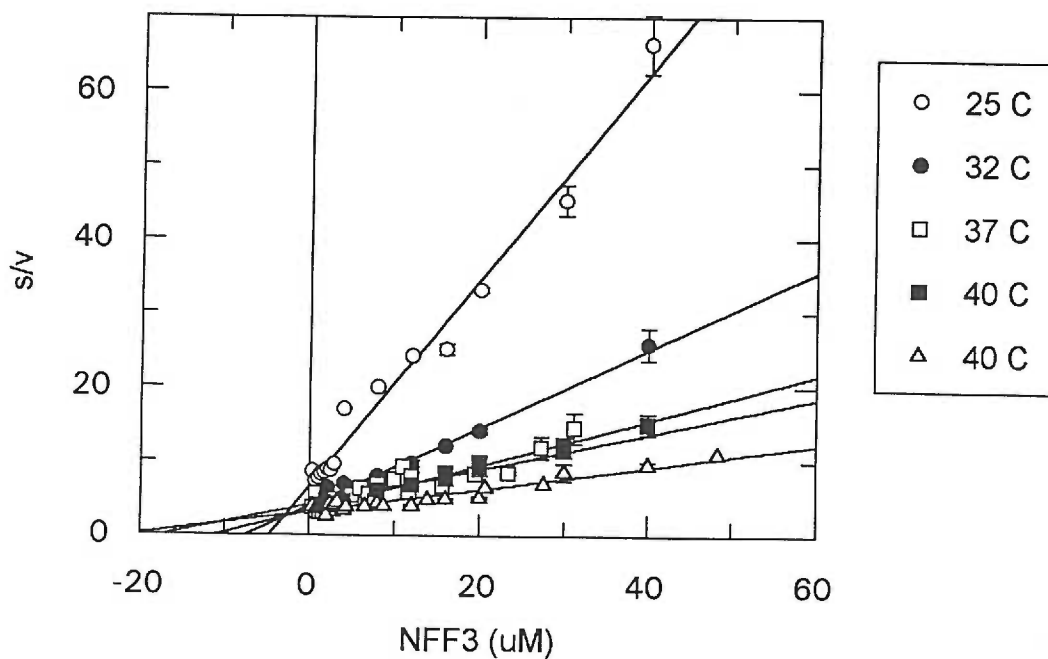
Hanes Plot Constants		
	pH 8.0	
°C	k_c	K_m
25	.7157	4.75
32	1.896	7.54
37	3.287	10.97
40	4.188	17.32
45	6.623	21.23

Table 5

The kinetic constants determined from the Hanes plots in Figure 46 are presented. The k_c values have units of s^{-1}, and K_m values have units of μM.
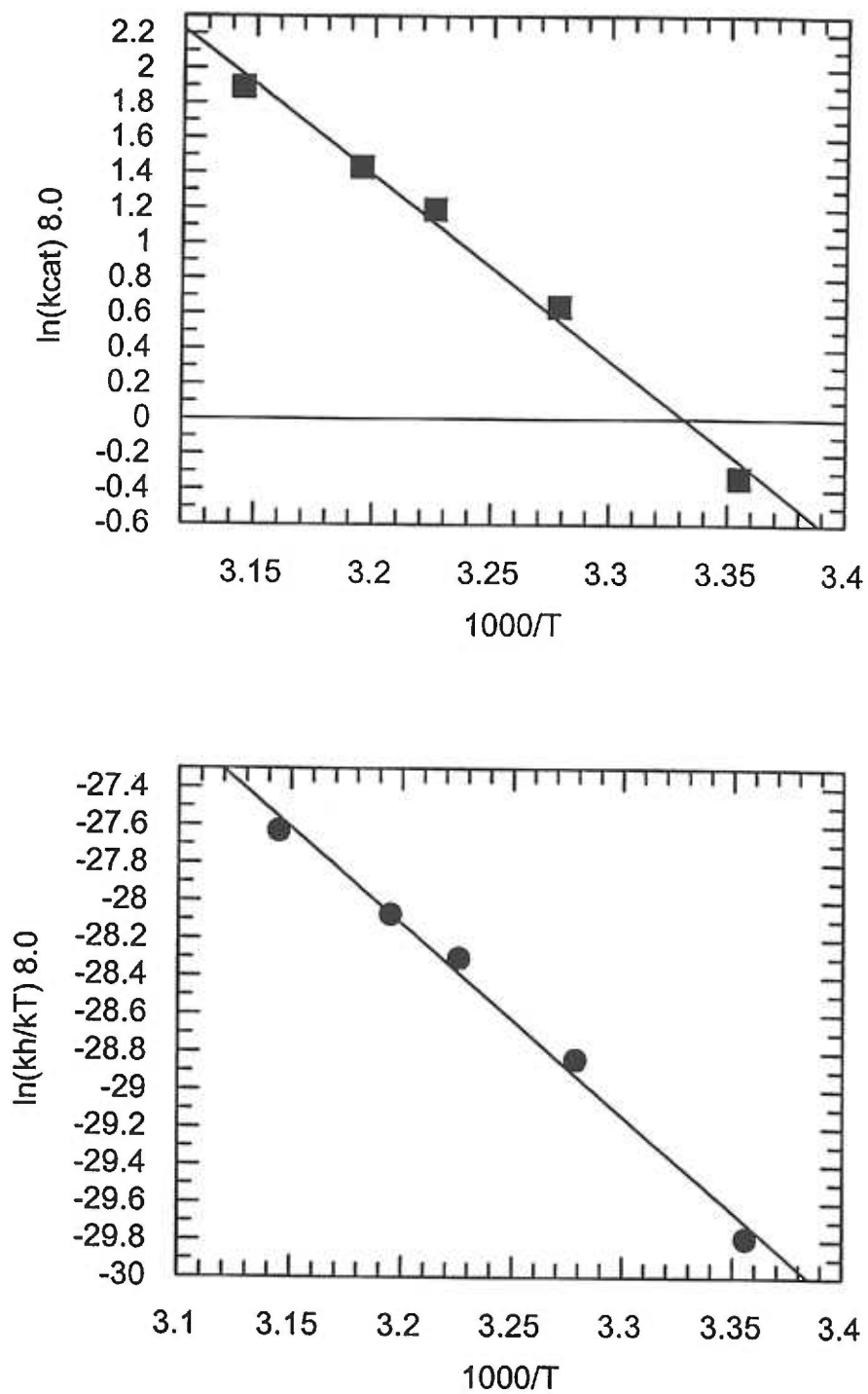
Figure 47
Arrhenius (a) and Eyring (b) plots of the k_{cat} values at pH 8.0 presented in Table 5.

We had hypothesized that if the mechanistic scheme of stromelysin resembled that of Scheme 2, with two parallel pathways to product that are separated from one another by proton ionization, then the thermodynamic plots of the observed k_{cat} should show characteristic features of Scheme 2. The hypothesis was that at proton concentrations near K_{a2}, the Arrhenius plots would show the characteristic non-linearity of a complex mechanism, and that shifting the proton concentration away from K_{a2} would decrease the degree of non-linearity. We tested this hypothesis, by examining the temperature dependence of k_{cat} at pH 7.5, pH 6.0 and pH 8.0. The data yielded a clearly non-linear plot at pH 7.5 with a significant decrease in the non-linearity when the proton concentration was shifted away from pH 7.5 to pH 6.0 or 8.0.

According to Scheme 2 and the data, the dependence of the natural log function of the individual rate constants, k_{cat1} and k_{cat2}, on reciprocal temperature approaches linearity. Since the pH 6.0 and 8.0 Arrhenius and Eyring plots approach linearity, the non-linearity at pH 7.5 is likely due to proportional contributions of each of the k_{cat} components of Scheme 2, whose distribution is dependent on the pH of the reaction and the pK_a values. Changes in any of these values will result in changes in the concentrations of EH and EH_2 and consequently to EHS and EH_2S thereby changing the fractional contribution of k_{cat1} and k_{cat2} and subsequently the thermodynamic parameters as well. Their fractional contributions can be calculated based on an equation corresponding to Scheme 2 shown below.

$$k_{cat_{obs}} = \frac{K_{m_2}K_{a_2}k_{cat_1} + K_{m_1}[H]K_{cat_2}}{K_{m_2}K_{a_2} + K_{m_1}[H]} \quad \text{(Eq. 24)}$$

105

This equation can be recast in terms of the different enzyme forms in a few simple steps to give an equation that may more clearly illustrate what the equation represents. First, the k_{c_1} and k_{c_2} components are separated:

$$k_{cat_{obs}} = \frac{k_{c_1} K_{m_2} K_{a_2}}{K_{m_2} K_{a_2} + K_{m_1}[H]} + \frac{k_{c_2}[H]K_{m_1}}{K_{m_2} K_{a_2} + K_{m_1}[H]} \qquad \text{(Eq. 25)}$$

The dissociation constants are then re-written in terms of their molecular components:

$$k_{cat_{obs}} = \frac{\dfrac{[EH_2][S]}{[EH_2S]} \cdot \dfrac{[EH][H]}{[EH_2]} \cdot k_{cat_1}}{\dfrac{[EH_2][S]}{[EH_2S]} \cdot \dfrac{[EH][H]}{[EH_2]} + \dfrac{[EH][S]}{[EHS]} \cdot [H]} + \frac{\dfrac{[EH][S]}{[EHS]} \cdot [H] \cdot k_{cat_2}}{\dfrac{[EH_2][S]}{[EH_2S]} \cdot \dfrac{[EH][H]}{[EH_2]} + \dfrac{[EH][S]}{[EHS]} \cdot [H]} \qquad \text{(Eq. 26)}$$

Canceling all possible variables gives the minimum equation, Equation 27:

$$k_{cat_{obs}} = \frac{\dfrac{k_{cat_1}}{[EH_2S]}}{\dfrac{1}{[EH_2S]} + \dfrac{1}{[EHS]}} + \frac{\dfrac{k_{cat_2}}{[EHS]}}{\dfrac{1}{[EH_2S]} + \dfrac{1}{[EHS]}} \qquad \text{(Eq. 27)}$$

which in its final form gives Equation 28:

$$k_{cat_{obs}} = \frac{k_{c_1}[EHS] + k_{c_2}[EH_2S]}{[EHS] + [EH_2S]} \qquad \text{(Eq. 28)}$$

106

From Equation 28 one can more clearly see that the observed k_{cat} arises as the sum of k_{c1} times its fractional contribution, $[EHS]/([EHS] + [EH_2S])$, and k_{c2} times its fractional contribution, $[EH_2S]/([EHS] + [EH_2S])$.

It is clear from Equation 24 that the proton concentration affects the relative contribution of each of the catalytic rate constants. Changes in pH of the reaction were minimized by adjusting the temperature of the buffer before adjusting the pH of the buffer thereby eliminating a temperature dependent change in the proton concentration. However, changes in the concentration of EH and EH_2 as a function of temperature-dependent changes in the pK_{a2} value can not be eliminated as a possible source for the non-linearity of the pH 7.5 Arrhenius and Eyring plots.

Since Scheme 2 assumes that there is no acid dissociation between EHS and EH_2S, we used Equation 5 to determine k_c/K_m values at different proton concentrations and at different temperatures. The pH curves of k_c/K_m that were generated with NFF3, did not show the extreme difference in amplitude between the putative $(k_c/K_m)_1$ and $(k_c/K_m)_2$ peaks that had been shown previously (Harrison et al. 1992). A possible reason for the difference in relative peak amplitudes will be discussed later. Taking advantage of the comparable amplitudes, Equation 29 is then applied to determine K_{a1} and K_{a3}.

$$(k_c/K_m)_{obs} = \frac{k_c/K_m}{\dfrac{K_{a1}}{[H]} + 1 + \dfrac{[H]}{K_{a3}}} \quad \text{(Eq. 29)}$$

This Equation assumes a simple mechanism with a bell shaped curve for k_c/K_m as a function of pH. Although the equation assumes only two K_a values are involved, for continuity we

107

have maintained the nomenclature that is used for a three K_a mechanism. The values of K_{a1} and K_{a3} estimated from Equation 29 are assumed to be in the range of those that would be estimated using Equation 1, if the pH dependent behavior of the k_c/K_m is representative of the behavior of k_c and because there is not a large difference between the two apparent rates, $(k_c/K_m)_1$ and $(k_c/K_m)_2$.

Once K_{a1} and K_{a3} were estimated at five temperatures, Equation 1 was used to estimate K_{a2}. Equation 1, like Equation 24 has 7 variables. However, having already estimated the values of K_{a1} and K_{a3} leaves only 3 of the variables unknown: $(k_c/K_m)_1$, $(k_c/K_m)_2$ and K_{a2}. The resultant K_a values are presented in a Van't Hoff plot in Figure 48.

While the Van't Hoff plots of K_{a1} and K_{a3} show only slight temperature dependencies, this was not true with K_{a2}. Although the same value, 10^{-7}, was entered into the Grafit program as an initial estimate of K_{a2} at each temperature, the final computer-estimated values show strong, non-linear temperature dependence. Table 6 lists the pK_a values estimated by this method with their corresponding temperature.

Figure 48
Van't Hoff plots of acid dissociation
constants, K_{a1}(squares), K_{a2}
(triangles) and K_{a3} (circles).
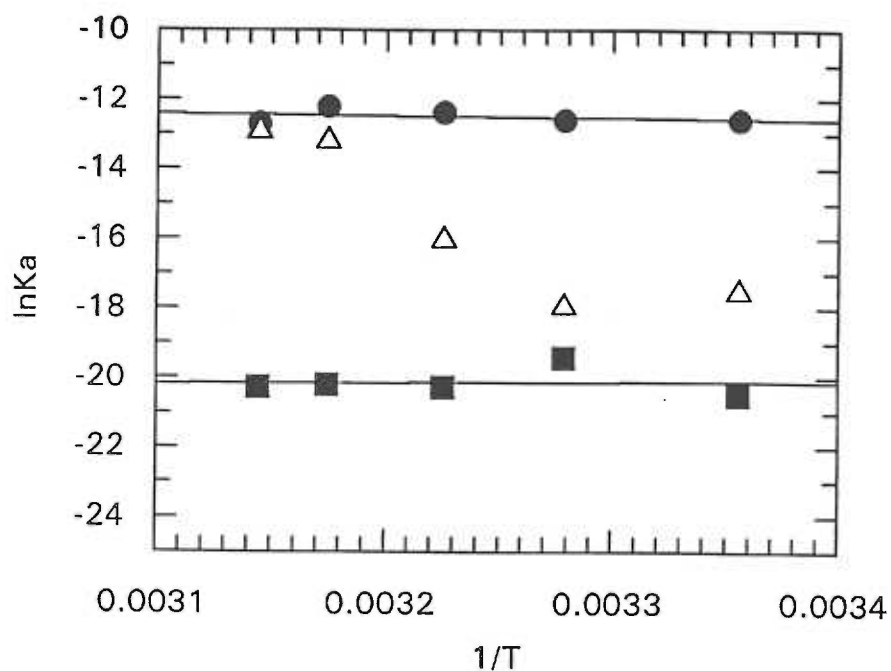
Table 6

pK$_a$ values determined from pH dependence of k_c/K_m using Equations 1 and 29.

Temp (°C)	25	32	37	40	45
pK$_{a1}$	8.91	8.44	8.81	8.78	8.8
pK$_{a2}$	7.62	7.80	6.97	5.74	5.62
pK$_{a3}$	5.48	5.48	5.38	5.31	5.52

109

Using these pK_a values and the individual rate constants, it should be possible to generate theoretical pH 7.5 observed k_{cat} values that approximate the experimental pH 7.5 values if the mechanism resembles that of Scheme 2 from which the equations have been derived. In order to use the estimated k_{c1} and k_{c2} to generate theoretical k_{cat} values at a pH where almost all of the enzyme is in one of the two active forms, as it would be at pH 7.5, the k_{c1} and k_{c2} values must be estimated taking the inactivation due to pK_{a1} and pK_{a3} into account. This would not be necessary if the amount of inactive enzyme at pH 6.0 and 8.0 was not significant. However, the k_{c1} and k_{c2} estimates come from activity measured at proton concentrations where a significant amount of the enzyme is in the inactive form, so the first step toward a theoretical approximation of the k_{cat} at pH 7.5 is to account for the E and the EH_3 forms of the enzyme that were present in the reactions conducted at pH 6.0 and pH 8.0.

Values of k_{cat} are estimated by dividing V_{max} by the concentration of enzyme that was added to the reaction solution. However, the k_{c1} and k_{c2} calculated this way at pH 8.0 and 6.0 can not be used to give a theoretical k_{cat} at pH 7.5 until the inactive enzyme at these proton concentrations is accounted for. Since the pK_{a3} and pK_{a1} are within one pH unit of pH 6.0 and 8.0 respectively, the active enzyme concentration under these two conditions was calculated at each temperature using the respective slopes and intercepts of the K_a Van't Hoff plots. The consequence of this calculation is sets of k_{cat} values which have taken inactivation (conversion to the EH_3 and E enzyme forms) into account for the pH 6.0 and 8.0 reactions and can be used to calculate theoretical estimates of k_{cat} to pH 7.5 where almost all of the enzyme in the reaction is in one of the two active forms.

110

Plotting the theoretical and the experimental pH 7.5 Eyring curves on the same graph,

Figure 49, shows how the plots relate to one another. We find that at higher temperatures,

the two sets of data are almost superimposed on one another. At lower temperatures

however, this is not the case.
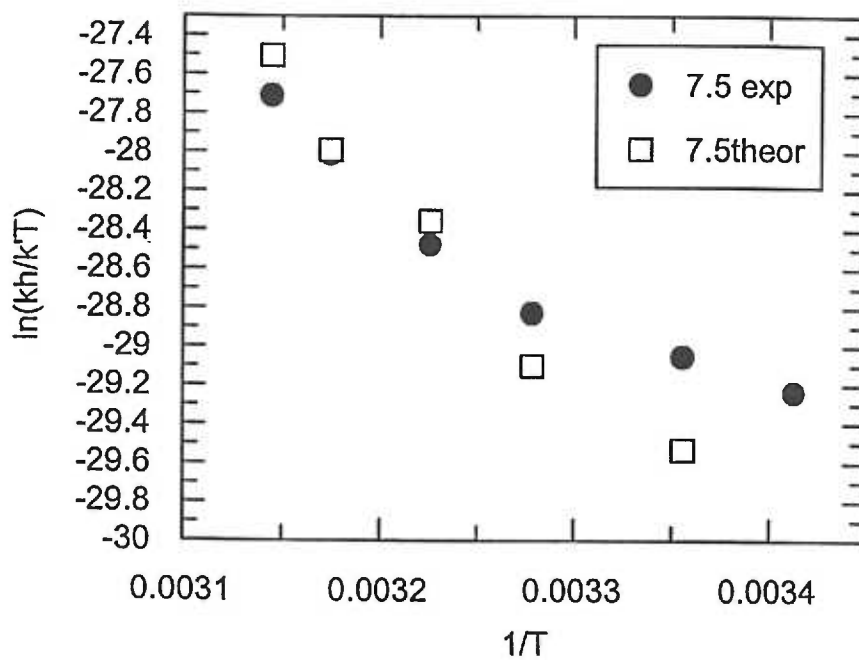
Figure 49
Theoretical pH 7.5 Eyring data generated as
described above (open circles) and pH 7.5 data
measured experimentally (filled circles) showing
divergence at low temperatures.

To understand why this may be, in Figure 50 the Eyring plots of pH 7.5 experimental data, and Eyring plots of pH 6.0 and 8.0 are plotted on one graph, where the rates at pH 6.0 and 8.0 are estimated for active enzyme only, to allow a comparison of their relative values. At higher temperatures, the pH 7.5 and 8.0 data are almost superimposed. At lower temperatures, the pH 6.0 and 7.5 data run almost parallel to each other. The slope (which corresponds to the enthalpy) of the pH 6.0 Eyring, and the slope of the three lower temperatures of the pH 7.5 Eyring are extremely close at $-4,185$ and $-4,339$, respectively. Thus it does appear that the pH 7.5 curve may be composed of the two enthalpy values corresponding to the two rate constants as they appear in Scheme 2. An explanation for why the theoretical pH 7.5 k_{cat} data did not approximate the experimental data at lower temperatures is offered below.
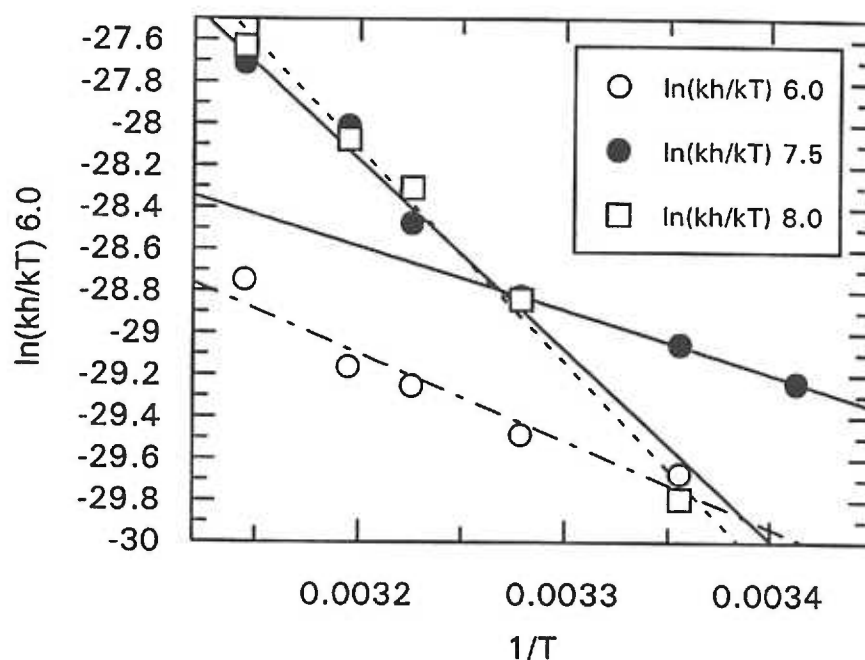
Figure 50
Eyring plot of pH 7.5 experimental data (solid circles), pH 6.0 (open circles) and pH 8.0 (open squares) with rates calculated for active enzyme only.

112

If the observed k_{cat} at pH 7.5 contains contributions from the pH 6.0 and pH 8.0 k_{cat} values, then it would be expected that the values at pH 7.5 on an Eyring plot of k_{cat} should never be greater than the Eyring values of pH 6.0 and pH 8.0 values (once those values have been adjusted for inactivated enzyme). If Scheme 2 is correct, then one explanation for the pH 6.0 Eyring plot to be less than that of pH 7.5 would be that there is less of the EH_2 form of the enzyme at pH 6.0 than there is at pH 7.5.

One possible reason this may occur is that the value for pK_{a3} is actually higher than that estimated from our experiments. For our determination of the pK_a values, we employed Equation 5 and estimated k_c/K_m from the initial velocities. From those data, we determined the pK_a values as previously described, however, it is possible that the pH dependence of the k_{cat} may be different than that of k_c/K_m (Denu and Dixon 1995).

Another possible explanation is that the maleate present in the pH 6.0 but not the pH 7.5 reactions has an inhibitor-like effect. However, MES and sodium acetate buffers at pH 6.0 also yielded lower activity than buffers at pH 7.5 at high substrate concentrations.

Given that the activity of the enzyme at pH 6.0 is consistently lower than that seen at pH 7.5 at high substrate concentrations, suggesting that the k_{cat} is also likely to follow this pattern, it seems more likely that the lower values seen in the pH 6.0 Eyring plot compared with the pH 7.5 Eyring plot is due to a pK_{a3} value that is closer to pH 6.0 than that determined from the k_c/K_m data. Determination of the pK_{a3} of the k_{cat} reaction would require that reactions be performed at a minimum of 5 additional proton concentrations each studied at 5 temperatures. Before making such an investment of resources, the hypothesis that (with

nothing else changed) pK_{a3} values closer to pH 6.0 than those listed in Table 6 could yield theoretical pH 7.5 data that would approximate the experimental data was tested mathematically.

The theoretical pH 7.5 data was generated once again using the slopes and intercepts of the K_{a1} van't Hoff and of the estimated K_{a2} values listed in Table 6. However, for the pK_{a3} values, the slope of the K_{a3} van't Hoff plot was used, but with an intercept that would put the pK_{a3} values closer to pH 6.0. In doing this, we have not manipulated the slope of the temperature dependence, but only its position on the van't Hoff plot.

Figure 51 shows the Eyring plot of the theoretical pH 7.5 data, generated according to the above description, together with the experimental data. This figure shows that the theoretical data closely approximates the experimental data, suggesting that if the pK_{a3} values for k_{cat} were closer to pH 6.0 causing a decrease in $[EH_2]$ at pH 6.0, our data is in agreement with Scheme 2.

While we offer this as a possible explanation for the lower activity seen at pH 6.0, we do not exclude other possible reasons. It is important to note that the selection of pH 6.0 as the pH at which to conduct reactions was guided by the proposed Scheme 2 and with the hope that this pH would give rise to a significantly high proportion of EH_2 over EH. It was not known whether this pH would give rise to the greatest activity.

114
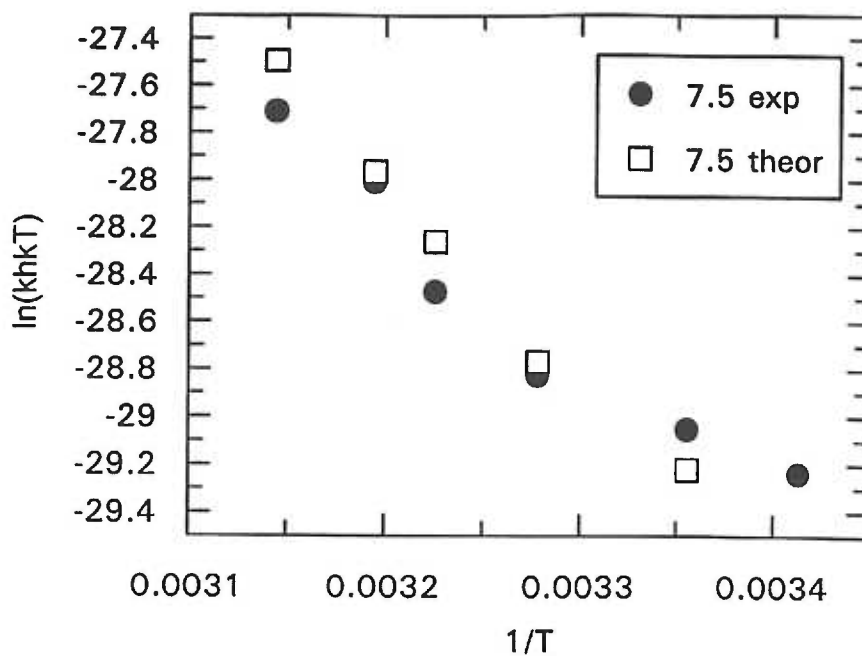
Figure 51
Revised theoretical plot of pH 7.5 Eyring (open
circles) and the pH 7.5 experimental Eyring plot
(filled circles).

The experiments conducted here with NFF3 do not allow us to exclude protonating

groups that are present on the substrate as the cause of one of the pK_a values. Without

deviating from the parallel mechanism these results would be equally possible with only one

active form of the enzyme. Shown below is Scheme 3:

Scheme 3

$$EH_2$$

$$K_{a3} \updownarrow \quad K_{m2}$$
$$\longrightarrow EH{:}SH \rightarrow EH + PH$$
$$SH$$

$$EH \quad K_{a2} \updownarrow$$
$$S$$

$$K_{a1} \updownarrow \quad K_{m1} \longrightarrow EH{:}S \rightarrow EH + P$$

$$E$$

115
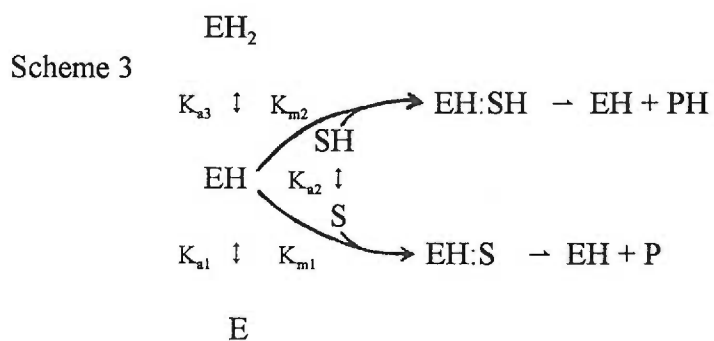
Scheme 3 shows a single active enzyme form interacting with substrate in one of two states of protonation, SH or S. The equilibrium between these two states is represented by K_{a2}. As one can see, there still exist two K_m and two k_{cat} constants in the mechanism. As with Scheme 2, the number of enzyme molecules progressing via one or the other pathway will be largely dependent upon pK_{a2} and the pH of the reaction. Below, possible substrate residues are discussed.

Beginning at the amino terminus, the first two residues capable of protonation are the acetylated arginine and the lysine in position P_4. The arginine has been previously eliminated as being responsible for any of the pK_a values seen in Scheme 1 (Harrison et al. 1992). Although the arginine was part of a different substrate, it occupied the same position, P_6, as it does in NFF3. The lysine is a basic amino acid with a pK_a of 10 when it is free and not part of a polypeptide. The temperature dependent values of pK_{a2} that we have measured fall between 7.62 and 5.62. Therefore we feel that neither of these two residues can account for pK_{a2}.

The next candidate residue would be the glutamate which occupies the P_1 site. The pK_a of free glutamic acid is estimated at 4.2. Acid dissociation values can be affected and changed by their environment (Liu et al. 1997) however, this glutamate was not present in peptide used in the previous study which supported the parallel mechanism of Scheme 1. If this glutamate was responsible for pK_{a2}, it would had to have been present not only in NFF3 but in the substrate of Harrison et. al. as well. Therefore, it seems unlikely that this glutamate is the source of pK_{a2}. It is possible, however, that this glutamate is responsible for the bell

116

shaped pH curve of k_c/K_m. The previous report of a large peak at approximately pH 6.0 and a shoulder at approximately pH 8.0 was performed with a substrate that contained a glutamine in place of this glutamate.

It seems very unlikely that pK_{a2} is due to protonation of a substrate residue. We must therefore look carefully at candidate residues on stromelysin. Although we have no reason to exclude long range effects, without structural data that addresses pH effects, we have no direct evidence for such effects and speculation of long range effects can be unlimited. Therefore we will restrict our discussion to residues in or near the active site. To do this, we use tertiary structure information that has been reported for stromelysin in conjunction with structure and mechanism information reported for a related proteinase.

Thermolysin, a bacterial metalloproteinase, has been more extensively characterized than any of the MMPs and it shares many structural characteristics with MMPs. For this reason, it has been used as a reference molecule for structural comparison with MMPs (Becker et al. 1995, Borkakoti et al. 1994, Gooley et al. 1994). The thermolysin Glu[143] has been proposed to catalyze the hydrolysis of a peptide bond by general base catalysis (Tronrud et al. 1992). In a zinc metalloproteinase from Bacillus subtilis that has high homology with thermolysin, the Glu[143] equivalent is proposed to hydrolyze a peptide bond by general acid catalysis (Tsuru et al. 1993). By structural analysis Glu[202] appears to be analogous to Glu[143] in thermolysin (Becker et al. 1995). It is also the only charged residue that is in close proximity to the active site zinc, positioned adjacent to His[201] which is one of the zinc coordinating histidines. This glutamate is conserved throughout the MMP family as a part of the conserved zinc binding domain HEXXHXXXXH.

117

It is possible that a single residue that is capable of catalytic activity in both its protonated and de-protonated states is responsible for pK_{a2}. Given that the Glu[202] equivalent in two related metalloproteinases has been proposed to have a role as a general acid and a general base catalyst, it seems plausible that in stromelysin it may be capable of either. In order for this to be the case, the pK_a of Glu[202] would have to be shifted to between 5.62-7.62 according to the k_c/K_m data. Although the pK_a of glutamate is generally more acidic, a pK_a as high as 8.5 has been reported for glutamate in lysozyme complexed with substrate compared to a pK_a of approximately 6.5 when complexed with inhibitor. (Parsons and Raftery 1972). Since there appear to be no other charged groups in the vicinity of Glu[202], it may be possible that deprotonation is disfavored and that the pK_a would be elevated.

Another residue near the active site is Tyr[155], whose ionizing proton has been reported in one of the NMR structures to be just over 3 Å away from the active site zinc (Van Doren et al. 1995b). The pK_a of tyrosine is generally about 10. At that pK_a Tyr[155] would have remained protonated and uncharged in all of our experiments. It may be possible, therefore, for the tyrosine to act as a proton donor. It is also possible that a more distant residue undergoes ionization and has an effect on the kinetic constants. This might be the case if the residue causes even a small conformational change such that the position of some of the residues or side groups that are involved in either binding of the substrate, or cleavage of the substrate have been perturbed enough to alter their effectiveness.

118

CONCLUSIONS

We have shown that stromelysin proteolysis of peptide substrate NFF3 yields non-linear Arrhenius and Eyring plots of k_{cat} at pH 7.5. This would suggest either a simple mechanism with a temperature dependent change in the heat capacity of the transition state or a complex mechanism. Testing for the former explanation indicated that if the mechanism was simple and non-linearity observed at pH 7.5 was due to a temperature dependent change in the heat capacity of the transition state, then there would have to be a corresponding, very large conformational change. To date, the possibility of a conformational change has not been addressed by structural studies. We can not therefore exclude the possibility, nor can we exclude the possibility that a conformational change accompanies a change in pH. However, the data indicate that the conformational change would have to be on the order of that seen in protein folding/unfolding reactions, decreasing the likelihood of this explanation. It is also difficult to explain the decrease in non-linearity seen at pH 6.0 and 8.0 without invoking a more complex mechanism. Therefore, we feel that a simple mechanism with a temperature dependent change in the heat capacity of the transition state is a less likely explanation.

We feel that a more likely explanation is that the non-linearity seen at pH 7.5 is due to a mechanism that is more complex than a simple Michaelis-Menten mechanism. We have shown that the degree of non-linearity is significantly decreased at pH 6.0 and 8.0 and that linear regression of the Arrhenius plots results in two different slopes, suggesting two different activation energies, and in turn, two different mechanistic pathways. Further, linear regression of the thermodynamic plots of pH 6.0 and the three lower temperatures of the pH 7.5 plot yield nearly parallel slopes, while linear regression of the pH 8.0 data and the three

119

higher temperatures of pH 7.5 are almost superimposable. These data together seem to suggest that the non-linearity of the Arrhenius and Eyring plots of k_{cat} at pH 7.5 is due to a conversion from the pathway corresponding to the activation energy of the pH 6.0 reaction to that of pH 8.0 with increasing temperature. Since the two pathways are associated with two different proton concentrations, it would seem reasonable to interpret the break in the thermodynamic plots at pH 7.5 as the result of de-protonation of some group that affects the rate limiting step of the reaction.

These data are supporting evidence for a parallel mechanism involving at least three acid dissociation constants. The simplest mechanism that the data is in agreement with is Scheme 2. According to this mechanism, the data suggests that at pH 7.5 there is a shift from k_{c2} as the major contributing rate constant to k_{c1} as the major contributing rate constant as temperature increases. The data also shows that as the pH of the reaction is shifted away from pH 7.5, the Arrhenius and Eyring plots become more linear. This is also consistent with a parallel mechanism.

Scheme 3 shows that the central pK_a is attributed to ionization of a substrate proton. While Scheme 3 could be consistent with our data alone, our data in conjunction with that of Harrison et. al. (Harrison et al. 1992) allow us to eliminate Scheme 3 as the mechanism. This leads us to conclude that the mechanism more closely resembles that of Scheme 2. While the mechanism may be more complex than Scheme 2, Scheme 2 is the simplest mechanism that fits the data.

REFERENCES

Acott, T., P. Kingsley, J. Samples, and E. Van Buskirk. 1988. Human trabecular meshwork organ culture: Morphology and glycosaminoglycan synthesis. *Investigative Ophthalmology and Visual Science* 29: 90-100.

Acott, T. S., and M. K. Wirtz. 1996. Biochemistry of aqueous outflow. Pages 281-305 in R. Ritch, M. B. Shields, and T. Krupin, eds. *The Glaucomas*. Mosby, St. Louis.

Agren, M. S., C. J. Taplin, J. F. J. Woessner, W. H. Eaglstein, and P. M. Mertz. 1992. - Collagenase in wound healing: effect of wound age and type. *Journal of Investigative Dermatology* 99: 709-14.

Alexander, J. P., J. R. Samples, E. M. Van Buskirk, and T. S. Acott. 1991. Expression of matrix metalloproteinases and inhibitor by human trabecular meshwork. *Investigative Ophthalmology & Visual Science* 32: 172-80.

Allingham, R., A. de Kater, and C. Ethier. 1996. Schlemm's canal and primary open angle glaucoma correlation between Schlemm's canal dimensions and outflow facility. *Experimental Eye Research* 62: 101-9.

Ando, H., S. S. Twining, B. Y. Yue, X. Zhou, M. E. Fini, T. Kaiya, E. J. Higginbotham, and J. Sugar. 1993. MMPs and proteinase inhibitors in the human aqueous humor. *Investigative Ophthalmology & Visual Science* 34: 3541-8.

Apte, S. S., B. R. Olsen, and G. Murphy. 1995. The gene structure of tissue inhibitor of metalloproteinases (TIMP)-3 and its inhibitory activities define the distinct TIMP gene family. *Journal Biological Chemistry* 270: 14313-8.

Baragi, V. M., C. J. Fliszar, M. C. Conroy, Q. Z. Ye, J. M. Shipley, and H. G. Welgus. 1994. Contribution of the C-terminal domain of metalloproteinases to binding by Tissue inhibitor of Metalloproteinases. *Journal of Biological Chemistry* 269: 12692-12697.

Bayne, E. K., N. I. Hutchinson, L. A. Walakovits, S. Donatelli, K. L. MacNaul, C. F. Harper, P. Cameron, V. L. Moore, and M. W. Lark. 1992. Production, purification and characterization of canine prostromelysin. *Matrix* 12: 173-84.

Becker, J., A. Marcy, L. Rokosz, M. Axel, J. Burbaum, P. Fitzgerald, P. Cameron, C. Esser, W. Hagmann, J. Hermes, and J. Springer. 1995. Stromelysin-1: Three-dimensional structure of the inhibited catalytic domain and of the C-truncated proenzyme. *Protein Science* 4: 1966-1976.

Benbow, U., G. Buttice, H. Nagase, and M. Kurkinen. 1996. Characterization of the 46-kD Intermediates of Matrix Metalloproteinase 3 (Stromelysin 1) Obtained by Site-directed Mutation of Phenylalanine 83. *Journal of Biological Chemistry* 271: 10715-10722.

Bigg, H., Y. Shi, Y. Liu, B. Steffensen, and C. Overall. 1997. Specific, High Affinity Binding of Tissue Inhibitor of Metalloproteinases-4 (TIMP-4) to the COOH-terminal Hemopexin-like Domain of Human Gelatinase A: TIMP-4 binds progelatinase A and the COOH-terminal domain in a similar manner to TIMP-2. *Journal of Biological Chemistry* 272: 15496-500.

Blandamer, M., J. Bergess, R. Robertson, and J. Scott. 1982. Dependence of Equilibrium and Rate Constants on Temperature and Pressure. *Chemical Reviews* 82: 259-86.

Bodden, M. K., G. J. Harber, B. Birkedal-Hansen, L. J. Windsor, N. C. Caterina, J. A. Engler, and H. Birkedal-Hansen. 1994. Functional domains of human TIMP-1 (tissue inhibitor of metalloproteinases). *Journal of Biological Chemistry* 269: 18943-52.

Bode, W., P. Reinemer, R. Huber, T. Kleine, S. Schnierer, and H. Tschesche. 1994. The X-ray crystal structure of the catalytic domain of human neutrophil collagenase inhibited by a substrate analogue reveals the essentials for catalysis and specificity. *EMBO Journal* 13: 1263-9.

Borkakoti, N., F. Winkler, D. Williams, A. D'Arcy, M. Broadhurst, P. Brown, W. Johnson, and E. Murray. 1994. Structure of the catalytic domain of human fibroblast collagenase complexed with an inhibitor. *Structural Biology* 1: 106-110.

Boudreau, N., C. Sympson, Z. Werb, and M. Bissell. 1995. Suppression of ICE and Apoptosis in Mammary Epithelial Cells by Extracellular Matrix. *Science* 267: 891-93.

Brubaker, R. 1991. Flow of Aqueous Humor in Humans. *Investigative Ophthalmology & Visual Science* 32: 3145-66.

Burnette, W. 1981. "Western blotting": Electrophoretic transfer of proteins from sodium dodecyl sulfate-polyacrylamide gels to unmodified nitrocellulose and radiographic detection with antibody and radioiodinated protein A. *Anals of Biochemistry* 112: 195.

Cao, J., A. Rehemtulla, W. Bahou, and S. Zucker. 1996. Membrane type matrix metalloproteinase 1 activates pro-gelatinase A without Furin cleavage of the N-terminal domain. *Journal of Biological Chemistry* 271: 30174-80.

Carmichael, D., A. Sommer, R. Thompson, D. Anderson, C. Smith, H. Welgus, and G. Stricklin. 1986. Primary structure and cDNA cloning of human fibroblast collagenase inhibitor. *Proceedings of the National Academy of Science USA* 83: 2407-11.

Cawston, T., G. Murphy, E. Mercer, W. Galloway, B. Hazleman, and J. Reynolds. 1983. The interaction of purified rabbit bone collagenase with puirified rabbit bone metalloproteinase inhibitor. *Biochemical Journal* 211: 313-318.

Chen, L. C., M. E. Noelken, and H. Nagase. 1993. Disruption of the cysteine-75 and zinc ion coordination is not sufficient to activate the precursor of human matrix metalloproteinase 3 (stromelysin 1). *Biochemistry* 32: 10289-95.

Chen, W.-T. 1992. Membrane proteases: roles in tissue remodeling and tumor invasion. *Current Opinion in Cell Biology* 4: 802-9.

Clark, A., K. Wilson, A. de Kater, R. Allingham, and M. McCartney. 1995. Dexamethasone-induced ocular hypertension in perfusion-cultured human eyes. *Investigative Ophthalmology and Visual Science* 36: 478-89.

Denu, J., and J. Dixon. 1995. A catalytic mechanism for the dual-specific phosphatases. *Proceedings of the National Academy of Science USA* 92: 5910-14.

Dielemans, I., J. Vingerling, R. Wolfs, A. Hofman, D. Grobbee, and P. de Jong. 1994. The prevalence of primary open-angle glaucoma in a population-based study in the Netherlands - The Rotterdam study. *Ophthalmology* 101: 1851-1855.

Engler, J. A., L. J. Windsor, B. Birkedal-Hansen, and H. Birkedal-Hansen. 1992. The latency of the human fibroblast collagenase precursor depends on on an internal cysteine residue. *Matrix Supplement* 1: 231-6.

Erickson-Lamy, K. 1992. The perfused human ocular anterior segment as a model for aqueous outflow physiology. *Journal of Glaucoma* 1: 44-53.

Erickson-Lamy, K., J. Rohen, and W. Grant. 1988. Outflow facility studies in the perfused bovine aqueous outflow pathways. *Current Eye Research* 7: 799-807.

Erikson-Lamy, K., and J. Rohen, Grant, WM. 1991. Outflow facility studies in perfulsed human ocular anterior segment. *Experimental Eye Research* 52: 723-31.

Farmer, W. H., and Z. Yuan. 1991. A Continuous Fluorescent Assay for Measuring Protease activity using Natural Protein Substrate. *Analytical Biochemistry* 197: 347-352.

Fife, R. S., and G. W. Sledge Jr. 1995. Effects of doxycycline on in vitro growth, migration, and gelatinase activity of breat carcinoma cells. *Journal of Laboratory and Clinical Medicine* : 407-410.

Fosang, A. J., P. J. Neame, T. E. Hardingham, G. Murphy, and J. A. Hamilton . 1991. Cleavage of cartilage proteoglycan between G1 and G2 domains by stromelysins. *Journal of Biological Chemistry* 266: 15579-82.

Fosang, A. J., P. J. Neame, K. Last, T. E. Hardingham, G. Murphy, and J. A. Hamilton. 1992. The interglobular domain of cartilage aggrecan is cleaved by PUMP, gelatinases, and cathepsin B. *Journal of Biological Chemistry* 267: 19470-4.

Fotouhi, N., A. Lugo, M. Visnick, L. Lusch, R. Walsky, J. W. Coffey, and A. C. Hanglow. 1994. Potent peptide inhibitors of stromelysin based on the prodomain region of matrix metalloproteinases. *Journal of Biological Chemistry* 269: 30227-31.

Freimark, B. D., W. S. Feeser, and S. A. Rosenfeld. 1994. Multiple sites of the propeptide region of human stromelysin-1 are required for maintaining a latent form of the enzyme. *Journal of Biological Chemistry* 269: 26982-26987.

Galazka, G., L. Windsor, H. Birkedal-Hansen, and J. Engler. 1996. APMA (4-Aminophenylmercuric Acetate) Activation of Stromelysin-1 Involves Protein Interactions in Addition to Those with Cysteine-75 in the Propeptide. *Biochemistry* 35: 11221-11227.

Gijbels, K., R. Galardy, and L. Steinman. 1994. Reversal of Experimental Autoimmune Encephalomyelitis with Hydroxamate Inihibitor of Matrix Metalloproteases. *Journal of Clinical Investigation* 94: 2177-82.

Gooley, P., J. O'Connell, A. Marcy, G. Cuca, S. Salowe, B. Bush, J. Hermes, C. Esser, W. Hagmann, J. Springer, and B. Johnson. 1994. The NMR structure of the inhibited catalytic domain of human stromelysin-1. *Structural Biology* 1: 111-118.

Gooley, P. R., B. A. Johnson, A. I. Marcy, G. C. Cuca, S. P. Salowe, W. K. Hagmann, C. K. Esser, and J. P. Springer. 1993. Secondary structure and zinc ligation of human recombinant short-form stromelysin by multidimensional heteronuclear NMR. *Biochemistry* 32: 13098-108.

Grant, G. A., G. I. Goldberg, S. M. Wilhelm, C. He, and A. Z. Eisen. 1992. Activation of extracellular matrix metalloproteases by proteases and organomercurials. *Matrix Supplement* 1: 217-23.

Greene, j., M. Wang, Y. E. Liu, L. A. Raymond, C. Rosen, and Y. E. Shi. 1996. Molecular Cloning and Characterization of Human Tissue Inhibitor of Metalloproteinase 4. *Journal of Biological Chemistry* 271: 30375-30380.

Guerin, C., J. Laterra, T. Masnyk, L. M. Golub, and H. Brem. 1992. Selective Endothelial Growth Inhibition by Tetracyclines that Inhibit Collagenase. *Biochemical and Biophysical Research Communications* 188: 740-745.

Gunja-Smith, Z., and J. F. J. Woessner. 1993. - Activation of cartilage stromelysin-1 at acid pH and its relation to. *Agents & Actions* 40: 228-31.

Hanglow, A. C., A. Lugo, R. Walsky, M. Finch-Arietta, L. Lusch, M. Visnick, and N. Fotouhi. 1993. Peptides based on the conserved predomain sequence of matrix metalloproteinases inhibit human stromelysin and collagenase. *Agents & Actions* 39: C148-50.

Hanglow, A. C., A. Lugo, R. Walsky, M. Visnick, J. W. Coffey, and N. Fotouhi. 1994. Inhibition of human stromelysin by peptides based on the N-terminal domain of tissue inhibitor of metalloproteinases-1. *Biochemical Biophysical Research Communications* 205: 1156-63.

Harrison, R. K., B. Chang, L. Niedzwiecki, and R. L. Stein. 1992. Mechanistic studies on the human matrix metalloproteinase stromelysin. *Biochemistry* 31: 10757-62.

He, C., S. Wilhelm, A. Pentalnd, B. Marmer, G. Grant, A. Eisen, and G. Goldberg. 1989. Tissue cooperation in a proteolytic cascade activating human interstitial collagenase. *Proceedings of the National Academy of Science, USA* 86: 2632-36.

Heussen, C., and E. Dowdle. 1980. Electrophoretic Analysis of Plasminogen Activators in polyacrylamide Gels containing sodium dodecyl sulfate and Copolymerized substrates. *Analytical Chemistry* 102: 196-202.

Hiraoka, K., Y. Sasaguri, S. Komiya, A. Inoue, and M. Morimatsu. 1992. Cell Proliferation-related production of matrix metalloproteinases 1 (Tissue collagenase) and 3 (stromelysin) by cultured human rheumatoid synovial fibroblasts. *Biochemistry International* 27: 1083-91.

Housley, T. J., A. P. Baumann, I. D. Braun, G. Davis, P. K. Seperack, and S. M. Wilhelm. 1993. Recombinant Chinese Hamster Ovary Cell maTris metalloprotease-3 (MMP-3, Stromelysin-1): Role of calcium in promatrix metalloprotease-3 activation and thermostability of the low mass catalytic domain of MMP-3. *Journal of Biological Chemistry* 268: 4481-4487.

Imai, K., Y. Yokohama, I. Nakanishi, E. Ohuchi, Y. Fujii, N. Nakai, and Y. Okada. 1995. Matrix Metalloproteinase 7 (Matrilysin) from Human Rectal Carcinoma Cells. *Journal of Biological Chemistry* 270: 6691-97.

Ingman, T., T. Sorsa, J. Michaelis, and Y. Konttinen. 1994. Immunohistochemical study of neutrophil- and fibroblast-type collagenases and stromelysin-1 in adult periodontitis. *Scandinavian Journal of Dental Research* 102: 342-9.

Ishiguro, N., T. Ito, K. Obata, N. Fujimoto, and H. Iwata. 1996. Determination of stromelysin-1, 72 and 92 kDa type IV collagenase, tissue inhibitor of metalloproteinase-1 (TIMP-1), and TIMP-2 in synovial fluid and serum from patients with rheumatoid arthritis. *Journal of Rheumatology* 23: 1599-604.

Izquierdo, M. C., and R. L. Stein. 1990. Mechanistic Studies of Thermolysin. *Journal of the American Chemical Society* 112: 6054-6062.

Johnson, D. 1996. Human trabecular meshwork cell survival is dependent on perfusion rate. *Investigative Ophthalmology and Visual Science* 37: 1204-1208.

Johnson, D., J. Bradley, and T. Acott. 1990. The effect of dexamethasone on glycosaminoglycans of human trabecular meshwork in perfusion organ culture. *Investigative Ophthalmology and Visual Science* 31: 2568-71.

Johnson, D., and P. Knepper. 1994. Microscale analysis of the glycosaminoglycans of human trabecular meshwork: a study in perfusion cultured eyes. *Journal of Glaucoma* 3: 58-69.

Johnson, D., and R. Tschumper. 1987. Human trabecular meshwork organ culture. *Ivestigative Ophthalmology & Visual Science* 28: 945-53.

Johnson, D., and R. Tschumper. 1989. The effect of organ culture on human trabecular meshwork. *Experimental Eye Research* 49: 113-27.

Kaufman, P. 1988. *Clinical Ophthalmology*. J.B. Lippincott, Philadelphia.

Kaufman, P., and T. Mittag. 1994. Medical Therapy of Glaucoma. Pages 9.7-9.30 in S. Podos, M. Yanoff, P. Kaufman, and T. Mittag, eds. *Textbook of Ophthalmology*. Mosby, St. Louis.

Kleiner, D. E. J., A. Tuuttila, K. Tryggvason, and W. G. Stetler-Stevenson. 1993. Stability analysis of latent and active 72-kDa type IV collagenase: the role of tissue inhibitor of metalloproteinases-2 (TIMP-2). *Biochemistry* 32: 1583-92.

Knauper, V., S. M. Wilhelm, P. K. Seperack, Y. A. DeClerck, K. E. Langley, A. Osthues, and H. Tschesche. 1993. Direct activation of human neutrophil procollagenase by recombinant stromelysin. *Biochemical Journal* 295: 581-6.

Knepper, P., W. Goossens, and P. Palmberg. 1996. Glycosaminoglycon stratification of the juxtacanalicular tissue in normal and primary open-angle glaucoma. *Investigative Ophthalmology & Visual Science* 37: 2414-25.

Koklitis, P. A., G. Murphy, C. Sutton, and S. Angal. 1991. Purification of recombinant human prostromelysin. Studies on heat activation to give high-Mr and low-Mr active forms, and a comparison of recombinant with natural stromelysin activities. *Biochemical Journal* 276: 217-21.

Lakowicz, J. 1983. *Principles of Fluorescence Spectroscopy.* Plenum Press, New York.

Laemmli, U. K. 1970. Cleavage of structural proteins during the assembly of the head of bacteriophage T4. *Nature* 227, 680-685.

Larsson, L.-I., E. Rettig, and R. Brubaker. 1995. Aqueous flow in open-angle glaucoma. *Archives of Ophthalmology* 113: 283-86.

Leske, M., A. Connell, A. Schachat, and L. Hyman. 1994. The Barbados eye study - Prevalence of open angle glaucoma. *Archives of Ophthalmology* 112: 821-9.

Li, J., P. Brick, M. O'Hare, T. Skarzynski, L. Lloyd, V. Curry, I. Clark, H. Bigg, B. Hazleman, T. Cawston, and D. Blow. 1995. Structure of full-length porcine synovial collagenase reveals a C-terminal domain containing a calcium-linked, four-bladed beta-propeller. *Structure* 3: 541-549.

Libson, A., A. Gittis, I. Collier, B. Marmer, G. Goldberg, and E. Lattman. 1995. Crystal structure of the haemopexin-like C-terminal domain of gelatinase A. *Nature Structural Biology* 2: 938-942.

Lin, C.-Y., J.-K. Wang, J. Torri, L. Dou, Q. Sang, and R. Dickson. 1997. Characterization of a Novel, Membrane-bound, 80-kDa Matrix-degrading Protease from Human Breast Cancer Cells: Monoclonal antibody production, isolation, and localization. *Journal of Biological Chemistry* 272: 9147-52.

Liu, T., M. Ryan, F. Dahlquist, and O. Griffith. 1997. Determination of pKa values of the histidine side chains of phosphatidylinositol-specific phospholipase C from Bacillus cereus by NMR spectroscopy and site-directed mutagenesis. *Protein Science* 6: 1937-44.

Lochter, A., A. Srebrow, C. Sympson, N. Terracio, Z. Werb, and M. Bissell. 1997. Misregulation of Stromelysin-1 Expression in Mouse Mammary Tumor Cells Accompanies Acquisition of Stromelysin-1-dependent Invasive Properties. *Journal of Biological Chemistry* 272: 5007-15.

Lohmander, L. S., L. A. Hoerrner, and M. W. Lark. 1993. Metalloproteinases, tissue inhibitor, and proteoglycan fragments in knee synovial fluid in human osteoarthritis. *Arthritis & Rheumatism* 36: 181-9.

Lovejoy, B., A. Cleasby, A. Hassell, K. Longley, M. Luther, D. Weigl, G. McGeehan, A. McElroy, D. Drewry, M. Lambert, and S. Jordan. 1994. Structure of the catalytic domain of fibroblast collagenase complexed with an inhibitor. *Science* 263: 375-377.

Mathews, C., and K. van Holde. 1990. *Biochemistry*. The Benjamin/Cummings Publishing Company, Redwood City.

Miyazaki, K., K. Funahashi, Y. Numata, N. Koshikawa, K. Akaogi, Y. Kikkawa, H. Yasumitsu, and M. Umeda. 1993. Purification and Characterization of a Two-Chain Form of Tissue Inhibitor of Metalloproteinases (TIMP) Type 2 and a Low Molecular Weight TIMP-like protein. *Journal of Biological Chemistry* 268: 14387-93.

Mort, J., G. Dodge, P. Roughley, J. Liu, S. Finch, G. Dipasquale, and A. Poole. 1993. Direct evidence for active metalloproteinases mediating matrix degradation in interleukin 1-stimulated human articular cartilage. *Matrix* 13: 95-102.

Murphy, G., J. A. Allan, F. Willenbrock, M. I. Cockett, J. P. O. Connell, and A. J. Docherty. 1992a. The role of the C-terminal domain in collagenase and stromelysin specificity. *Journal of Biological Chemistry* 267: 9612-8.

Murphy, G., S. Atkinson, R. Ward, J. Gavrilovic, and J. J. Reynolds. 1992b. The role of plasminogen activators in the regulation of connective tissue metalloproteinases. [Review]. *Annals of the New York Academy of Sciences* 667: 1-12.

Murphy, G., M. Cockett, P. Stephens, B. Smith, and A. Docherty. 1987. Stromelysin is an activator of procollagenase. *Biochem. J.* 248: 265-268.

Murphy, G., M. I. Cockett, R. V. Ward, and A. J. Docherty. 1991a. Matrix metalloproteinase degradation of elastin, type IV collagen and proteoglycan. A quantitative comparison of the activities of 95 kDa and 72 kDa gelatinases, stromelysins-1 and -2 and punctuated metalloproteinase (PUMP). *Biochemical Journal* 277: 277-9.

Murphy, G., A. Houbrechts, M. I. Cockett, R. A. Williamson, M. O. Shea, and A. J. Docherty. 1991b. The N-terminal domain of tissue inhibitor of metalloproteinases retains metalloproteinase inhibitory activity. *Biochemistry* 30: 8097-102.

Murphy, G., R. Ward, J. Gavrilovic, and S. Atkinson. 1992c. Physiological mechanisms for metalloproteinase activation. *Matrix Supplement* 1: 224-30.

Murphy, G., F. Willenbrock, R. V. Ward, M. I. Cockett, D. Eaton, and A. J. Docherty. 1992d. The C-terminal domain of 72 kDa gelatinase A is not required for catalysis, but is essential for membrane activation and modulates interactions with tissue inhibitors of metalloproteinases [published erratum appears in Biochem J 1992 Jun 15;284(Pt 3):935]. *Biochemical Journal* 283: 637-41.

Nagase, H. 1995. Human stromelysins 1 and 2. *Methods in Enzymology* 248: 449-470.

Nagase, H., J. Enghild, K. Suzuki, and G. Salvesen. 1990. Stepwise Activation Mechanism of the Precursor of Matrix Metalloproteinase 3 (Stromelysin) by Proteinases and (4-Aminophenyl)mercuric Acetate. *Biochemistry* 29: 5783-89.

Nagase, H., C. G. Fields, and G. B. Fields. 1994. Design and characterization of a fluorogenic substrate selectively hydrolyzed by stromelysin 1 (matrix metalloproteinase-3). *Journal of Biological Chemistry* 269: 20952-7.

Nagase, H., K. Suzuki, T. Morodomi, J. J. Enghild, and G. Salvesen. 1992. Activation mechanisms of the precursors of matrix metalloproteinases 1, 2 and 3. *Matrix Supplement* 1: 237-44.

Newell, F. W. 1982. *Ophthalmology Principles and Concepts*. C.V. Mosby Company, St. Louis.

Nguyen, Q., F. Willenbrock, M. I. Cockett, M. O. Shea, A. J. Docherty, and G. Murphy. 1994. Different domain interactions are involved in the binding of tissue inhibitors of metalloproteinases to stromelysin-1 and gelatinase A. *Biochemistry* 33: 2089-95.

Okada, Y., E. J. Harris, and H. Nagase. 1988. The precursor of a metalloendopeptidase from human rheumatoid synovial fibrobasts. Purification and mechanisms of activation by endopeptidases and 4-aminophenylmercuric acetate. *Biochemical Journal* 254: 731-41.

Okada, Y., H. Nagase, and E. D. Harris Jr. 1986. A Metalloproteinase from Human Rheumatoid Synovial Fibroblasts that Digests Connective Tissue Matrix Components. *Journal of Biological Chemistry* 261 No. 30: 14245-13255.

129

Park, A. J., L. M. Matrisian, A. F. Kells, R. Pearson, Z. Y. Yuan, and M. Navre. 1991. - Mutational analysis of the transin (rat stromelysin) autoinhibitor region demonstrates a role for residues surrounding the "cysteine switch". *Journal of Biological Chemistry* 266: 1584-1590.

Parshley, D., J. Bradley, A. Fisk, A. Hadaegh, J. Samples, E. Van Buskirk, and T. Acott. 1996. Laser trabeculoplasty induces stromelysin expression by trabecular juxtacanalicular cells. *Investigative Ophthalmology & Visual Sciences* 37: 795-804.

Parshley, D. E., J. M. B. Bradley, J. R. Samples, E. M. Van Buskirk, and T. S. Acott. 1995. Early changes in matrix metalloproteinases and inhibitors after in vivo laser treatment to the trabecular meshwork. *Current Eye Research* 14: 537-44.

Parsons, S., and M. Raftery. 1972. Ionization behabior of the cleft carboxyls in lysozyme-substrate complexes. *Biochemistry* 11: 1633-38.

Polette, M., C. Clavel, M. Cockett, S. Girod de Bentzmann, G. Murphy, and P. Birembaut. 1993. Detection and localization of mRNAs encoding matrix metalloproteinases and their tissue inhibitor in human breast pathology. *Invasion & Metastasis* 13: 31-7.

Quigley, H. 1993. Open-Angle Glaucoma. *New England Journal of Medicine* 328: 1097-1106.

Quigley, H. 1996. Number of People with Glaucoma Worldwide. *British Journal of Ophthalmology* 80: 389-393.

Quigley, H., and S. Vitale. 1997. Models of Open-Angle Glaucoma Prevalence and Incidence in the United States. *Investigative Ophthalmology and Visual Science* 38: 83-91.

Reinemer, P., F. Grams, R. Huber, T. Kleine, S. Schnierer, M. Piper, H. Tschesche, and W. Bode. 1994. Structural implications for the role of the N terminus in the 'superactivation' of collagenases. A crystallographic study. *FEBS Letters* 338: 227-33.

Reynolds, J., R. Hembry, and N. Meikle. 1994. Connective tissue degradation in health and periodontal disease and the roles of matricx metalloproteinases and their natural inhibitors. *Advances in Dental Research* 8: 312-9.

Salowe, S. P., A. I. Marcy, G. C. Cuca, C. K. Smith, I. E. Kopka, W. K. Hagmann, and J. D. Hermes. 1992. Characterization of zinc-binding sites in human stromelysin-1: stoichiometry of the catalytic domain and identification of a cysteine ligand in the proenzyme. *Biochemistry* 31: 4535-40.

Sambrook, J., E. F. Fritsch, and T. Maniatis. 1989. *Molecular Cloning: A Laboratory Manual*. Cold Spring Harbor Laboratory Press, Cold Spring Harbor.

Samples, J. R., J. P. Alexander, and T. S. Acott. 1993. Regulation of the levels of human trabecular matrix metalloproteinases and inhibitor by interleukin-1 and dexamethasone. *Investigative Ophthalmology & Visual Science* 34: 3386-95.

Sato H., and M. Seiki. 1996. Membrane-Type Matrix Metalloproteinases (MT-MMPs) in Tumor Metastasis. *Journal of Biochemistry* 119: 209-215.

Sato H., T. Takino, Y. Okada, J. Cao, A. Shinagawa, E. Yamamoto, and M. Seiki. 1994. A Matrix Metalloproteinase expressed on the surface of invasive tumor cells. *Nature* 370: 61-65.

Schper, H. W., D. S. Grant, W. G. Stetler-Stevenson, R. Fridman, G. D. Orazi, A. N. Murphy, R. E. Bird, M. Hoythya, t. T. R. Fuers, D. L. French, and et al. 1993. Type IV collagenase(s) and TIMPs modulate endothelial cell morphogenesis in vitro. *Journal of Cellular Physiology* 156: 235-46.

Schler, B. S., J. Maimon, L. M. Golub, N. S. Ramamurthy, and R. A. Greenwald. 1992. Tetracyclines Inhibit Intracellular Muscle Proteolysis in vitro. *Biochemical and Biophysical Research Communications* 188: 767-772.

Sch G. S., S. Strelow, G. A. Stern, N. Chegini, M. B. Grant, R. E. Galardy, D. Grobelny, . J. Rowsey, r. K. Stoneciphe, V. Parmley, and et al. 1992. - Treatment of alkali-injured rabbit corneas with a synthetic inhibitor of matrix metalloproteinases. *Investigative Ophthalmology & Visual Science* 33: 3325-31.

Sha S. D., C. J. Fliszar, T. J. Broekelmann, R. P. Mecham, R. M. Senior, and H. G. Welgus. 1995. - Activation of the 92-kDa gelatinase by stromelysin and 4-aminophenylmercuric acetate: differential processing and stabilization of the carboxyl-terminal domain by tissue inhibitor of metalloproteases (TIMP). *Journal of Biological Chemistry* 270: 6351-6.

Snyd W. Daniel, T. Kramer, and R. Seftor. 1993. Corticosteroid Treatment and ...ecular Meshwork Proteases in Cell and Organ Culture Supernatants. ...rimental Eye Research* 57: 461-68.

Sout ..., M. Davies, R. Booth, and A. Newby. 1992. Involvement of extracellular-...-degrading metalloproteinases in rabbit aortic smooth-muscle cell proliferacion. *...em. J.* 288: 93-99.

Umihira, J., S. Nagata, M. Nohara, T. Hanai, N. Usuda, and K. Segawa. 1994. Localization of elastin in the normal and glaucomatous human trabecular meshwork. *Investigative Ophthalmology & Visual Science* 35: 486-94.

Van Doren, S., A. Kurochkin, W. Hu, Q.-Z. Ye, L. Johnson, D. Hupe, and E. Zuiderweg. 1995a. Solution structure of the catalytic domain of human stromelysin complexed with a hydrophobic inhibitor. *Protein Science* 4: 2487-2498.

Van Doren, S., A. Kurochkin, W. Hu, Q.-Z. Ye, L. Johnson, D. Hupe, and E. Zuiderweg. 1995b. Stromelysin-1 Catalytic Domain with Hydorphobic INhibitor Bound, Ph 7.0, 32c, 20mM CaCl, 15% Acetonitrile, NMR average of 20 structures minimized with restraints. Protein Data Bank.

Van Doren, S., A. Kurochkin, Q.-Z. Ye, L. Johnson, D. Hupe, and E. Zuiderweg. 1993. Assignments for main-chain nuclear magnetic resonances and delineation of the secondary structure of the catalytic domain of human stromelysin-1 as obtained from triple-resonance 3D NMR experiments. *Biochemistry* 32: 13109-13122.

Van Meurs, J., P. Van Lent, L. Joosten, P. Van der Kraan, and W. Van den Berg. 1997. Quantification of mRNA levels in joint capsule and artricular cartilage of the murine knee joint by TR-PCR: kinetics of stromelysin and IL-1 mRNA levels during arthritis. *Rheumatology International* 16: 197-205.

Vranka, J. 1997. The characterization of gelatinase inhibition and the involvement of the matrix metalloproteinases and their inhibitors in glaucoma and a retinal degeneration. Pages 227. *Department of Biochemistry and Molecular Biology*. Oregon Health Sciences University, Portland.

Wallon, U., and C. Overall. 1997. The Hemopexin-like Domain (C Domain) of Human Gelatinase A (Matrix Metalloproteinase-2) Requires Ca2+ for Fibronectin and Heparin Binding: Binding properties of recombinant gelatinase A C Domain to extracellular matrix and basement membrane components. *Journal of Biological Chemistry* 272: 7473-81.

Wetmore, D., and K. Hardman. 1996. Roles of the Propeptide and Metal Ions in the Folding and Stability of the Catalytic Domain of Stromelysin (Matrix Metalloproteinase 3). *Biochemistry* 35: 6549-58.

Wilhelm, S. M., Z. H. Shao, T. J. Housley, P. K. Seperack, A. P. Baumann, Z. Gunja-Smith, and J. F. J. Woessner. 1993. - Matrix metalloproteinase-3 (stromelysin-1). Identification as the cartilage acid metalloprotease and effect of ph on catalytic properties and calcium affinity. *Journal of Biological Chemistry* 268: 21906-13.

Willenbrock, F., T. Crabbe, P. M. Slocombe, C. W. Sutton, A. J. Docherty, M. I. Cockett, M. O. Shea, K. Brocklehurst, I. R. Phillips, and G. Murphy. 1993. The activity of the tissue inhibitors of metalloproteinases is regulated by C-terminal domain interactions: a kinetic analysis of the inhibition of gelatinase A. *Biochemistry* 32: 4330-7.

Willenbrock, F., G. Murphy, I. R. Phillips, and K. Brocklehurst. 1995. The second zinc atom in the matrix metalloproteinase catalytic domain is absent in the full-length enzymes: a possible role for the C-terminal domain. *FEBS Letters* 358: 189-92.

Williamson, R. A., B. J. Smith, S. Angal, G. Murphy, and R. B. Freedman. 1993. Structural analysis of tissue inhibitor of metalloproteinases-1 (TIMP-1) by tryptic peptide mapping. *Biochimica et Biophysica Acta* 1164: 8-16.

Wysocki, A., L. Staiano-Coico, and F. Grinnell. 1993. Wound fluid from chronic leg ulcers contains elevated levels of metalloproteinases MMP-2 and MMP-9. *Journal of Investigative Dermatology* 101: 64-68.